

# Theoretical Physics Implications of the Binary Black-Hole Merger GW150914

Nicolás Yunes,<sup>1</sup> Kent Yagi,<sup>2</sup> and Frans Pretorius<sup>2</sup>

<sup>1</sup>*eXtreme Gravity Institute, Department of Physics,  
Montana State University, Bozeman, MT 59717, USA.*

<sup>2</sup>*Department of Physics, Princeton University, Princeton, New Jersey 08544, USA.*

(Dated: April 2, 2022)

The gravitational-wave observation GW150914 by Advanced LIGO provides the first opportunity to learn about physics in the extreme gravity of coalescing binary black holes. The LIGO/Virgo collaboration has verified that this observation is consistent with General Relativity, constraining the presence of parametric anomalies in the signal. This paper expands this analysis to a larger class of anomalies, highlighting the inferences that can be drawn on non-standard theoretical physics mechanisms that would affect the signal. We find that GW150914 constrains a plethora of mechanisms associated with the generation and propagation of gravitational waves, including the activation of scalar fields, gravitational leakage into large extra dimensions, the variability of Newton’s constant, the speed of gravity, a modified dispersion relation, gravitational Lorentz violation and the strong equivalence principle. Unlike other observations that limit these mechanisms, GW150914 is a direct probe of dynamical strong-field gravity and gravitational wave propagation. We also show that GW150914 constrains the properties of exotic compact object alternatives to Kerr black holes. The true potential for GW150914 to both constrain exotic objects and physics beyond General Relativity is limited by the lack of understanding of the dynamical strong field in almost all modified gravity theories. GW150914 thus raises the bar that these theories must pass, both in terms of having a sound theoretical underpinning, and the minimal level to which the corresponding equations of motion must be solved in binary coalescences. We conclude with a discussion of additional inferences that can be drawn from smaller-confidence observations, such as the LVT151012 trigger and electromagnetic counterparts to GW150914, the latter of which would produce dramatic constraints on the speed of gravity and gravitational Lorentz violation.

PACS numbers: 04.30.Db,04.50Kd,04.25.Nx,97.60.Jd

## I. INTRODUCTION

The Laser Interferometer Gravitational-Wave Observatory (LIGO)/Virgo collaboration has recently announced the first direct detection of gravitational waves (GWs) [1]. With a signal-to-noise ratio (SNR) of  $\sim 24$ , and associated statistical  $\sigma > 5.1$ , there is little doubt that GW150914, as it has been named, is a true GW observation. The details of the signal indicate the GWs were produced during the late quasi-circular inspiral, merger and ringdown of a binary black hole (BH) system. The loudness of the event is due to a combination of Advanced LIGO’s (aLIGO) remarkable sensitivity (dimensionless strains of  $h \sim 10^{-21}$ ), the source’s proximity to Earth ( $410_{-180}^{+160}$  Mpc) and how massive the binary was (source-frame component masses  $(m_1, m_2) = (36_{-4}^{+5}, 29_{-4}^{+4})M_\odot$ ), the latter property fortuitously leading to the intrinsically loudest part of the signal lying in aLIGO’s most sensitive frequency band. This is thus an ideal event to learn about theoretical physics in extreme gravity.

The social scientist and epistemologist Karl Popper argued that scientists can never truly “prove” that a theory is correct, but rather that all we can do is disprove, or more accurately constrain, alternative hypothesis [2]. The theory that remains and cannot be disproven by observations becomes the *status quo*. Indeed, this was the case for Newtonian gravity before the 1900s, and it is the case today for Einstein’s theory of General Relativity (GR). The latter has been subjected to a battery of tests with Solar System [3], binary pulsar [4, 5] and cosmological observations [6–10], with no signs of failure<sup>1</sup>. These tests, however, cannot effectively probe the *extreme gravity regime*: where the gravitational field is strong and dynamical, where the curvature of spacetime is large, and where characteristic velocities are comparable to the speed of light [11].

The event GW150914 allows for just that. The putative BHs that generated this GW are intrinsically strong-field sources, they reached speeds  $\sim 0.5$  times the speed of light prior to merger, and the GW luminosity peaked at  $\sim 10^{56}$  ergs/s, within 3 orders of magnitude of the Planck luminosity. Consequently, the gravitational field was not only immense, but it changed violently and rapidly during the 0.2 second duration of the event. GW150914 is then perfect to learn about the extreme gravity regime. The LIGO/Virgo collaboration began this study, showing that the residual after subtracting the best-fit GR template is consistent with noise [12]. Moreover, the collaboration searched for the presence of certain anomalies, i.e. features in the signal that deviate from the GR predic-

tion. The latter has been subjected to a battery of tests with Solar System [3], binary pulsar [4, 5] and cosmological observations [6–10], with no signs of failure<sup>1</sup>. These tests, however, cannot effectively probe the *extreme gravity regime*: where the gravitational field is strong and dynamical, where the curvature of spacetime is large, and where characteristic velocities are comparable to the speed of light [11].

The event GW150914 allows for just that. The putative BHs that generated this GW are intrinsically strong-field sources, they reached speeds  $\sim 0.5$  times the speed of light prior to merger, and the GW luminosity peaked at  $\sim 10^{56}$  ergs/s, within 3 orders of magnitude of the Planck luminosity. Consequently, the gravitational field was not only immense, but it changed violently and rapidly during the 0.2 second duration of the event. GW150914 is then perfect to learn about the extreme gravity regime. The LIGO/Virgo collaboration began this study, showing that the residual after subtracting the best-fit GR template is consistent with noise [12]. Moreover, the collaboration searched for the presence of certain anomalies, i.e. features in the signal that deviate from the GR predic-

<sup>1</sup> Some have argued dark matter or dark energy could be explained by modified gravity theories, though the observational evidence does not favor this over a simple cosmological constant or as-of-yet undiscovered dark matter particles.

tion, using a parameterized model and found no evidence for any.

Having established GR as the status quo in the extreme gravity regime, one can now follow Popper and study the theoretical physics implications of the event. More specifically, one can examine what the verification of GR with event GW150914 and the absence of anomalies in the data imply for theoretical physics (see [3, 11, 13–15] for reviews on modified theories of gravity and testing them in the extreme gravity regime with GWs). For example, GW150914 has the potential to constrain new radiative channels, such as dipole scalar field emission or GW polarizations beyond the plus and cross polarizations predicted by GR, BH mass leakage into extra dimensions, and any temporal variability of Newton’s gravitational constant during the coalescence. These implications, in turn, affect the viability of theoretical physics mechanisms that play an important role in quantum gravitational phenomenology and high-energy model-building [16].

Before summarizing our results, we would like to discuss what is perhaps the most important consequence of GW150914 with regards to the state of modified gravity theories relevant to this event: what should be an exquisite piece of data providing powerful constraints is weakened by our woeful lack of understanding of how gravity can, in principle, differ from GR in this regime. Most<sup>2</sup> of the existing studies of the coalescence of compact binaries that could be alternatives to binary BH mergers in GR are limited to two regimes:

- (i) the early inspiral where post-Newtonian (PN) expansions<sup>3</sup> (to some order) have been computed, or
- (ii) isolated stationary compact object alternatives to BHs in GR, where their quasi-normal mode (QNM) structure is putatively relevant to the late-time dynamics of the post-merger remnant.

Prior to GW150914 the mainstream consensus was that binary BH mergers aLIGO would likely hear would be lower mass; hence, a significant portion of the earlier inspiral would contribute to the SNR where the perturbative calculations in (i) have more discriminating power, and the plunge/merger regime is less crucial. Similarly, regarding (ii), stationary solutions are adequate for electromagnetic wave tests [22–25] that e.g. the Event Horizon Telescope [26] could make by looking at the “shadows” of SgA\* and M87; the knowledge of the QNM struc-

ture of alternative stationary solutions could be applied to future space-based measurements of the ringdown phase of supermassive BH mergers [27, 28]. GW150914 has now presented us with data where most of the SNR is coming from a regime where the assumptions that both (i) and (ii) rest on are questionable.

Assuming GW150914 is a binary compact object coalescence driven by radiation reaction, and being agnostic to the nature of the pre-merger constituents and theory governing the merger, the most striking feature of the observed signal is the following: after reaching peak amplitude, the GW wave emission drops to below the noise threshold within the light-crossing time of the length-scale implied by the chirp mass of the binary. This is of course entirely as expected in GR, though the vacuum physics within the brief transition is extremely rich:

- (a) cosmic censorship is respected, and hence, the no-bifurcation theorem requires the horizons merge into a single structure,
- (b) the BH uniqueness (“no-hair”) results together with the apparent stability of the Kerr family of solutions implies the end-state must be a Kerr BH<sup>4</sup>, and
- (c) numerical solutions show that the time post-formation of a common dynamical horizon to when a linearly perturbed Kerr solution adequately describes the waveform is remarkably short.

That it has taken over half a century of dedicated research by the GR community to allow us to make this short itemized summary of the physics of a BH merger is a testament to how non-trivial this feature of the signal of GW150914 is. It also highlights how poor our understanding of the nature of *conceivable* theories of gravity in this regime is, and going forward, it now no longer suffices for alternatives to claim viability based solely on consistency with weak-field tests of GR.

“Exotic” compact object alternatives to BHs within GR can also no longer claim viability based solely on weak-field tests or constraints from electromagnetic observations of accretion disks. The LIGO/Virgo collaboration claimed that GW150914 cannot rule out exotic compact objects such as boson stars or gravastars [12]. We argue (and expand more upon this in Section IV) that this is only true if the exotic alternatives either promptly collapse to a BH (hence, at the very least, GW150914 is an observation of BH formation from a coalescing exotic binary), or the properties of the matter comprising the exotic star must allow for damping of highly non-linear *matter* oscillations on the light-crossing time of the remnant. We are not aware of any theoretically self-consistent model of a compact object star in GR that has this latter property.

<sup>2</sup> The only exceptions within the broader scope of compact object coalescence are scalar-tensor theories; here several numerical studies have given information on the full non-linear merger dynamics, where one or both of the compact objects are neutron stars (NSs) [17–19], and where both are BHs with a prescribed scalar field background [20, 21].

<sup>3</sup> This approximation solves the field equations using an expansion in small velocities (relative to the speed of light) and weak gravitational fields. A term proportional to  $(v/c)^{2N}$  relative to its leading-order term expression is said to be of NPN order.

<sup>4</sup> The non-linear stability of Kerr has not yet been proven in a strict mathematical sense, see e.g. [29] and the discussion therein.

The GW150914 event, moreover, exposes the shortcomings in the non-GR theories behind several exotic compact object models, and the caveats that must be kept in mind attempting to draw conclusions about what GW150914 might say about such exotica. For example, take gravastars and traversable wormholes, recently studied in this context [30, 31]. There are no self-consistent theories that describe how these objects can form, let alone their dynamics in the highly non-linear, violent regime of a collision. Hence it must be somehow assumed not only that such theories exist, but also that when solved they will (as smoothly as measured in the waveform and as rapidly as a binary BH collision occurs in GR) lead to an isolated remnant whose GW ringdown modes dominate the post-merger signal. This does not happen in known matter compact object mergers in GR. Case-in-point are binary NS mergers, where if prompt collapse to a BH does not occur, the post-merger hypermassive remnant is not close to being well-described as an isolated stationary NS perturbed by linear oscillations (see [32–38] for some recent studies).

As then with modified gravity vacuum mergers mentioned previously, GW150914 has significantly raised the bar that exotic matter alternatives to BHs must pass to be considered viable. To restate the obvious, at “zeroth-order” both vacuum mergers in modified gravity theories and exotic compact objects mergers in GR must arise from mathematically well-posed equations of motion (at least at an effective field theory level) that can be solved to describe such mergers. This must be true *before* addressing questions of whether details of the post-merger observed with GW150914 are consistent or ruled out by modified gravity theories and exotic spacetimes.

### A. Summary of Key Results

With the limitations and caveats just discussed in mind, the main goal of this paper is to study what GW150914 implies about the theoretical nature of extreme gravity. Even though earlier experiments and observations in the weak field have placed bounds on mechanisms we will discuss, and in some cases these will be stronger than what we extract from GW150914 at present, we emphasize again the latter bounds are for the first time coming directly from the extreme (dynamical *and* strong field) gravity regime. Also, many existing bounds are plagued by systematics associated with models of non-gravitational physics required to interpret observations; for GW150914 the errors in the analytic and numerical GR waveforms used to interpret the LIGO signal are a small part of the error budget [65]. We now summarize our main findings, with details described in subsequent sections.

**GW150914 constrains a plethora of emission mechanisms beyond GW radiation reaction.**

The first half of Table I presents a summary of the GW emission or generation mechanisms that can be constrained. In particular, GW150914 constrains the presence of dipole radiation in the signal due to e.g. the activation or growth of a scalar field, the presence of BH mass leakage due to large extra dimensions, a time-varying gravitational constant due to e.g. the existence of a time-varying scalar field, and the presence of Lorentz-violating effects in the production of GWs.

We arrive at these conclusions through a Fisher parameter estimation study, which we show agrees with the Bayesian analysis of [12] to 30–50%, wherever we can compare our results (i.e. for corrections at positive PN orders). We use the same (parametrically-deformed) inspiral-merger-ringdown waveform model (so-called gIMR) employed by the LIGO collaboration [12], but without precession. As there seems to be some confusion in the literature about the scope of these models, we show mathematically that gIMR is a subset of the parameterized post-Einsteinian (ppE) framework of [66] when the baseline GR waveform is taken to be the phenomenological waveform model of [67–69]. We also illustrate that ignorance of the higher-order PN corrections to the inspiral waveform in modified gravity does not necessarily weaken the constraints to the leading order physics obtained with a model that only uses the corresponding leading-order PN deformation. Specifically, using Jordan-Fierz-Brans-Dicke theory (Brans-Dicke or BD for short) [70–75] as the test-case, we estimate that a higher PN order modified waveform model would only correct the constraints by  $\mathcal{O}(10\%)$  at most<sup>5</sup>.

The fact that the gIMR model is a subset of the ppE framework allows us to use the many years of work on ppE theory and modified gravity theory to draw theoretical physics implications from the absence of ppE-like anomalies in the GW150914 data. In particular, each ppE exponent (or equivalently, the relative PN order shown in the third column of Table I) describing how the frequency response of a chirping binary is altered can be related to a set of physical mechanisms that are responsible for the effect. This allows us to test some of the fundamental pillars of GR, which typically are related to tests of the Strong Equivalence Principle (SEP) [3]:

- (I) The trajectories of freely-falling test bodies, including self-gravitating ones, are independent of their internal structure and composition (the weak equivalence principle (WEP) extended to self-gravitating bodies).
- (II) Results of any local experiment, including gravitational ones, are independent of when and

<sup>5</sup> Such a correction would be important if one is attempting to characterize a measured anomaly, but is less of an issue when constraining its existence, as explained e.g. in [76].

Theoretical Mechanism	GR Pillar	PN	$\beta$	Example Theory Constraints		
				Repr. Parameters	GW150914	Current Bounds
Scalar Field Activation	SEP	-1	$1.6 \times 10^{-4}$	$\sqrt{ \alpha_{\text{EdGB}} }$ [km]	—	$10^7$ [39], 2 [40–42]
	SEP, No BH Hair	-1	$1.6 \times 10^{-4}$	$ \dot{\phi} $ [1/sec]	—	$10^{-6}$ [43]
	SEP, Parity Invariance	+2	$1.3 \times 10^1$	$\sqrt{ \alpha_{\text{CS}} }$ [km]	—	$10^8$ [44, 45]
Vector Field Activation	SEP, Lorentz Invariance	0	$7.2 \times 10^{-3}$	$(c_+, c_-)$	(0.9, 2.1)	(0.03, 0.003) [46, 47]
Extra Dimension Mass Leakage	4D spacetime	-4	$9.1 \times 10^{-9}$	$\ell$ [ $\mu\text{m}$ ]	$5.4 \times 10^{10}$	$10$ – $10^3$ [48–52]
Time-Varying $G$	SEP	-4	$9.1 \times 10^{-9}$	$ \dot{G} $ [ $10^{-12}/\text{yr}$ ]	$5.4 \times 10^{18}$	0.1–1 [53–57]
Massive graviton	massless graviton	+1	$1.3 \times 10^{-1}$	$m_g$ [eV]	$1.2 \times 10^{-22}$ [12]	$10^{-29}$ – $10^{-18}$ [58–62]
Modified Dispersion Relation ( <i>Modified Special Relativity</i> )	$v_g = c$	+5.5	$2.3 \times 10^2$	$\mathbb{A} > 0$ [1/eV]	$1.6 \times 10^{-7}$	—
		+5.5	$2.3 \times 10^2$	$\mathbb{A} < 0$ [1/eV]	$1.6 \times 10^{-7}$	$2.7 \times 10^{-36}$ [63]
Modified Dispersion Relation ( <i>Extra Dimensions</i> )	$v_g = c$	+7	$8.7 \times 10^2$	$\mathbb{A} > 0$ [1/eV <sup>2</sup> ]	$9.3 \times 10^4$	—
		+7	$8.7 \times 10^2$	$\mathbb{A} < 0$ [1/eV <sup>2</sup> ]	$9.3 \times 10^4$	$4.6 \times 10^{-56}$ [63]
Modified Dispersion Relation ( <i>Lorentz Violation</i> )	SEP, Lorentz Invariance	—	—	$c_+$	0.7 [64]	(0.03, 0.003) [46, 47]

TABLE I. Theoretical mechanisms (first column) that arise in modified theories of gravity and how they violate fundamental pillars of GR (second column). The numbers in boldface show the approximate, 90%-confidence upper bounds placed by GW150914 on ppE parameters (fourth column) and on parameters (sixth column) representing specific theoretical mechanisms realized in a set of gravitational theories (fifth column) that enter at different PN order (third column) relative to GR, and current constraints on such example theories (last column). The top section of the table shows constraints on modifications to GW generation, while the bottom corresponds to constraints on GW propagation. Constraints on scalar field activation, which violates the SEP or gravitational parity invariance, are exemplified through realizations in Einstein-dilaton Gauss-Bonnet (EdGB) gravity, dynamical Chern-Simons (dCS) gravity and scalar-tensor theories, controlled by the coupling constants  $\alpha_{\text{EdGB}}$ ,  $\alpha_{\text{CS}}$  and the scalar field growth rate  $\dot{\phi}$  respectively. GW150914 cannot constrain these theories from the leading PN order correction in the waveform phase within the small coupling approximation, which assumes that the deformation away from GR is small. Constraints on the activation of vector fields, which violates Lorentz invariance and SEP by breaking LPI and LLI, are exemplified in Einstein-Æther (EA) theory with dimensionless coupling constants  $(c_+, c_-)$ . Constraints on BH mass leakage into extra dimensions are exemplified through the realization of a RS-II braneworld model, where  $\ell$  is the size of the large extra dimension. Constraints on the time variation of the gravitational constant, which also violates SEP by breaking LPI, are characterized by limits on  $\dot{G}$ . Constraints on massive gravity are exemplified with a kinematical realization in terms of modifications to the GW dispersion relation, whose magnitude is controlled by the graviton mass  $m_g$ . We also present constraints on the group velocity of GWs  $v_g$  for both super-luminal (positive  $\mathbb{A}$ ) and subluminal propagation (negative  $\mathbb{A}$ ) in two different well-motivated cases. For comparison, we present the constraint on violations of gravitational Lorentz invariance from the arrival time delay of GWs between Hanford and Livingston detectors.

where they are performed (local position invariance (LPI)), and of the velocity of the experimental apparatus (local Lorentz invariance (LLI)).

Dipole gravitational radiation due to the activation of additional dynamical fields can violate item (I). The time variation of Newton’s gravitational constant violates LPI. The presence of Lorentz-violating effects due to, for example the presence of dynamical vector fields, breaks both LPI and LLI. GW150914 is therefore much more than a probe into the structure of spacetime of a binary BH merger; it further allows for checks of some of the most important pillars of Einstein’s theory.

**GW150914 constrains a number of theoretical mechanisms that modify GW propagation.**

The second half of Table I presents a summary of the propagation mechanisms that can be constrained. GW150914 not only constrains the mass of the graviton, as first calculated by the LIGO/Virgo collaboration [12], but it more generically constrains the dispersion relation

of GWs, both super- and sub-luminal GW propagation, and the presence of Lorentz violation in the propagation of GWs.

As with effects active during the generation of GWs, we arrive at these conclusions with a Fisher analysis, which we have also checked is consistent with the Bayesian study of [12] wherever possible. For example, we have verified that the Fisher constraint on the graviton mass  $m_g$  with a simple massive graviton dispersion relation is consistent with the Bayesian bound of [12], both of which are a few times more stringent than the current Solar System bound [58]. All of the inferences on the propagation of GWs that we draw from GW150914 come from information on the phasing of the GW, a much more powerful tool than information derived solely from the difference in GW time of arrival between the Hanford and Livingston detectors. In particular, the bound presented here and in [12] is twenty orders of magnitude stronger than that based on a time delay argument [64].

Notice, however, that unlike in the GW generation case, the constraints on GW propagation mechanisms are often significantly stronger than other current con-

straints from binary pulsar and Solar System observations (in particular the  $A > 0$  modified dispersion relation restrictions listed in Table I, and lower PN cases illustrated in Fig. 9); the current strongest bounds on the modified dispersion relation of the graviton listed in Table I typically come from observations of galaxy clusters [60] and cosmic rays [63]. Although theories that predict modifications to GW propagation also typically modify the GW generation mechanism, the former typically dominate the latter. This is because modifications to GW propagation accumulate on the propagation time scale (ie. the distance), while modifications to GW generation accumulate while the system is generating GWs in band. The latter will never be comparable to the former for aLIGO sources, unless the binary happens to coalesce in the Solar System.

**GW150914 allows inferences to be made regarding the validity of the Kerr hypothesis, and likewise it constrains properties of exotic compact object alternatives to Kerr BHs.**

GW150914 was a *golden* event [77], which allows a measurement of the amount of energy and angular momentum carried away by GWs during coalescence [12]. This information can be used to infer properties of the geometry of the compact objects, and in particular the innermost-stable circular orbit (ISCO) of the remnant. We use the fact that in GR the spin of the final BH, which was measured in GW150914, is a function of the spins of the individual BHs before merger and the orbital angular momentum of a “test particle” at the ISCO radius of the final Kerr BH [78]. Inferences about the location of the ISCO can then be used to constrain string-inspired BH solutions [45, 79] and parametrically deformed Kerr metrics [80]. The observed energy loss could also be used to limit the amount of exotic “hair” (e.g. [81, 82]) the BHs in this event have. If a sizable fraction of the initial mass of each BH is attributable to hair, presumably a correspondingly large fraction could be radiated during merger (exactly how much would need to be calculated via numerical simulations). Although the SNR of GW150914 is not high enough to allow for interesting constraints on the above spacetimes, future louder signals would allow for tighter bounds via this analysis.

As discussed earlier in the introduction, the dramatic drop in the observed signal within a few ms after reaching peak amplitude is consistent with the rapid hair-loss experienced by the Kerr remnant in GR. On the flip side, this observation is a severe constraint on the properties of hypothesized exotic alternatives to Kerr BHs. Assuming the collision is violent enough to excite oscillations in the remnant that are large enough to produce observable GW emission, we can place bounds on an effective viscosity that the exotic matter must have to be consistent with the observed signal. Alternatively, lack of observed damped normal-mode oscillations of such exotic matter

can be used to place restrictions on the initial amplitude and damping time-scales of these putative modes.

Finally, we discuss the theoretical physics implications if the LVT151012 trigger is indeed a GW observation [83], and if the Fermi Gamma-ray Burst Monitor (GBM) signal observed in near coincidence with GW150914 [84] is an actual counterpart to the merger event. If LVT151012 was generated by a binary BH merger with source-frame component masses  $(m_1, m_2) = (23_{-5}^{+18}, 13_{-3}^{+4})M_\odot$ , then certain low-frequency theoretical mechanisms (such as the time variation of Newton’s gravitational constant or the BH mass leakage into extra dimensions) could be constrained a factor of 5 more stringently than with event GW150914. If the GBM signal was a short gamma-ray burst (GRB) counterpart to event GW150914, then the speed of GWs could be constrained in a model-independent fashion. The strength of this constraint depends on the intrinsic time delay between the gamma-ray and GW emission [85], which is currently uncertain due to our ignorance of the gamma-ray emission mechanism. If one assumes that the Fermi event was a prompt emission counterpart to GW150914 and GWs do not propagate sub-luminally, the speed of GWs can be constrained to be equal to the speed of light to one part in  $10^{17}$  [86–88]. This, in turn, would impose dramatic constraints on gravitational Lorentz violation [89–92], restricting the latter ten orders of magnitude more stringently than current binary pulsar constraints [46, 47], as predicted in [93]. However these conclusions are premature at this stage, given the large false-alarm rate of the LVT151012 trigger and the low-confidence of the GBM event, but they ought to be kept in mind for future GW observations.

The remainder of this paper presents the details of the calculations that allowed us to arrive at the conclusions presented above. Section II describes the main properties of the different coalescence phases of GW150914, together with the GW model typically employed in GR and parametric extensions that model deformations from GR. Section III discusses the theoretical implications that can be derived from the observation of event GW150914. This section begins with a description of the physical mechanisms that can and cannot be constrained, then derives bounds, separately focusing on mechanisms related to the generation of GWs and those associated with the propagation of GWs. Section IV focuses on implications for the existence of exotic spacetimes, concentrating on properties of the ISCO of the remnant and on effective material properties and additional oscillation modes of compact object alternatives to Kerr BHs. Section V discusses implications derived from less confident observations, in particular the GW trigger LVT151012, and the GRB observation by the Fermi GBM. Section VI concludes and points to future work. Certain ancillary details and supporting calculations are included in appendices. All throughout, we follow the conventions of Misner, Thorne and Wheeler [94], and unless otherwise stated use geometric units where  $G = 1 = c$ .

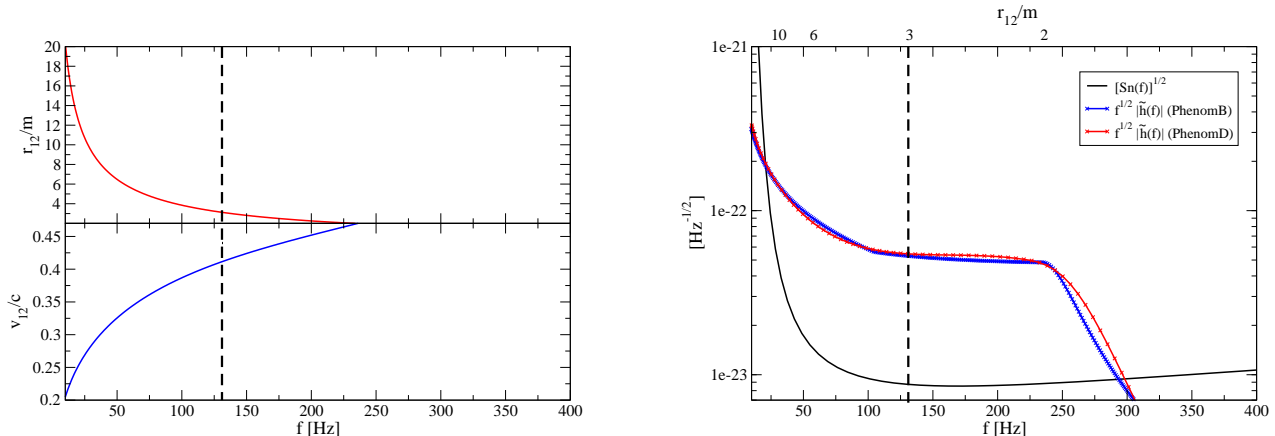


FIG. 1. (Color online) (Left) Third-order PN estimates of the orbital separation and velocity as a function of the GW frequency. (Right) Estimate of the (square root of the) spectral noise density curve of aLIGO when GW150914 was detected (as interpolated from the data made publicly available by the LIGO Collaboration [95] as described in Appendix A) as a function of frequency, as well as the product of the square root of the frequency and the Fourier GW amplitude, also as a function of frequency for two commonly used waveform models (PhenomB [67] and PhenomD [69, 96]), with an SNR of 24. The top axis shows the binary separation using its relation to the GW frequency shown in the top left panel. In both plots, the vertical dashed line at 132 Hz roughly indicates what we will call the end of the inspiral phase and the beginning of the merger and ringdown phase.

## II. BH COALESCENCE AS A PROBE OF EXTREME GRAVITY

This section begins by describing the different phases of the GW150914 event in detail and how they can probe extreme gravity. The section then describes the GW models used in GR to describe the phases of coalescence, as well as the parametric models that capture deformations from GR. When discussing the latter, we show that the parametrically-deformed model used by the LIGO/Virgo collaboration in [12] is an implementation of the ppE framework [66] for a particular GR model. This implies that one can work in the ppE framework to interpret constraints on departures from GR as constraints on different physical mechanisms, the mapping between which is summarized at the end of this section.

### A. Description of Coalescence

The coalescence of a binary system can be divided into 3 phases:

- **Inspiral.** The compact objects are well-separated with respect to the total mass ( $r_{12}/m \gg 1$ ) and the characteristic orbital velocity is much smaller than the speed of light ( $v/c \ll 1$ ), so that they inspiral adiabatically.
- **Plunge and Merger.** The compact objects are so close to each other that they do not spiral in adiabatically any longer, but instead plunge toward

one other and merge with characteristic velocities comparable to the speed of light.

- **Ringdown.** The highly-distorted remnant formed after merger oscillates, radiating away any deformations and relaxes to a stationary state.

Even though this classification is clean in concept, in reality the transition from one phase to another is not abrupt, and there is no stark demarcation in the waveform when one ends and the next begins.

Event GW150914 entered the aLIGO sensitivity band when the compact objects were already quite close. The left panel of Fig. 1 shows the orbital velocity as a function of GW frequency, estimated here via  $v_{12} = (\pi m f)^{1/3}$ , with  $m$  the total mass and  $f$  the GW frequency. At 10 Hz the compact objects were traveling at  $v_{12}/c \sim 0.2$  and the initial orbital separation<sup>6</sup> was about  $r_{12} \sim 20m$ , approximately 1960 km for GW150914. When the frequency reached 132 Hz, the binary's orbital velocity was roughly  $v_{12}/c \sim 0.4$  and the orbital separation approached  $r_{12} \sim 3m \sim 300$  km; the latter is close to the light-ring of a test particle in the Schwarzschild spacetime of a BH with mass equal to the total mass of GW150914. Beyond 132 Hz, the binary rapidly plunged, merging at approximately 230 Hz as the orbital separation decreased to  $r_{12} \sim 2m$  where two Schwarzschild BHs would have

<sup>6</sup> The mapping between orbital separation and frequency  $r_{12} = r_{12}(f)$  is gauge dependent, but for estimate purposes only, we use in this section the 3PN accurate relation reviewed in [97].

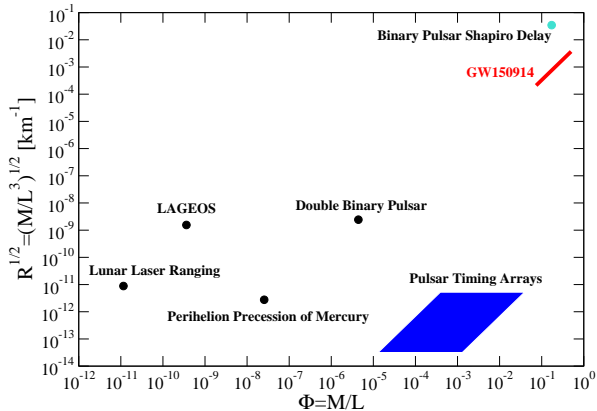


FIG. 2. (Color online) Schematic diagram of the curvature-potential phase space sampled by various experiments that test GR. The y-axis shows the inverse of the characteristic curvature length scale, while the x-axis shows the characteristic gravitational potential. The characteristic mass and length scale for each system plotted is summarized in Table II. The lighter (blue) dot shows that the Shapiro time delay from binary pulsars does probe strong curvature, though as illustrated in Fig. 3 it does not give information on the dynamical regime. GW150914 samples a regime where the curvature and the potential are both simultaneously large, and dynamical, as it sweeps a finite range in the potential and curvature length. The finite area of pulsar timing arrays is due to the range in the GW frequency and the total mass of supermassive BH binaries that such arrays may detect in the future.

touched. This frequency also roughly coincides with the start of the ringdown, as the Fourier amplitude of the signal shows a break at around this frequency (see the right panel of Fig. 1). Although all of these phases cannot be sharply defined, we will here follow the LIGO/Virgo collaboration and refer to  $f \in (10, 132)$  Hz as the inspiral phase, and  $f \in (132, 300)$  as the merger and ringdown phase.

The previous observations make it very clear that the binary BH coalescence that generated event GW150914 is in the extreme gravity regime. One way to quantify this is to compute the characteristic curvature  $\mathcal{R} = M/\mathcal{L}^3$  and the characteristic gravitational potential  $\Phi = M/\mathcal{L}$ , where  $M$  and  $\mathcal{L}$  are the characteristic mass and size of the system. Following [22, 98], Fig. 2 shows these quantities evaluated from  $f = 20$  Hz to merger with event GW150914 (for illustrative purposes, we take  $\mathcal{L} = r_{12}$  and  $M = m$ ). For comparison purposes, we also show the curvature and the gravitational potential for the LAGEOS satellites [99], the Earth-Moon System used in lunar laser ranging [100], the Mercury-Sun system used in perihelion precession observations, pulsar timing observations [101], and the double binary pulsar [102]; the mass and length scale of each system is summarized in Table II.

	$\mathcal{M}$	$\mathcal{L}$
GW150914	$64.8 M_{\odot}$	190–1300 km
Pulsar Shapiro Delay	$1.34 M_{\odot}$	12 km
Pulsar Timing Arrays	$10^6 - 10^9 M_{\odot}$	$10^{9.6} - 10^{12}$ km
Double Binary Pulsar	$2.59 M_{\odot}$	$8.7 \times 10^5$ km
LAGEOS	$1 M_{\oplus}$	$1 R_{\oplus}$
Lunar Laser Ranging	$1 M_{\oplus}$	$3.8 \times 10^5$ km
Pericenter Precession of Mercury	$1 M_{\odot}$	$5.8 \times 10^7$ km

TABLE II. The characteristic mass and length scale chosen to compute the characteristic curvature and potential in Fig. 2. For event GW150914 and for pulsar timing arrays, we extract the length scale from the observed frequency via  $\mathcal{L} = [M/(\pi f)^2]^{1/3}$ , where for the former we choose  $f = 20$  Hz up to contact, while for the latter we choose  $f = 3 \times 10^{-9} - 5 \times 10^{-7}$  Hz.

Of course, binary pulsar observations can also sample strong (but non-dynamical) gravitational fields through observations of the Shapiro time delay (as the photons emitted by one binary component graze the surface of the companion), which is shown with a blue-shaded dot.

GW150914 lands in the far top right corner of the phase space of Fig. 2, precisely where gravity is extreme, but what this figure does not show very clearly is how *dynamical* the gravitational field for each observation is. Some of this can be inferred from the fact that GW150914 in Fig. 2 is shown as a line instead of a point (since it probes a range of curvatures and potentials), but this depiction does not convey how dynamic event GW150914 is. This is shown in the left panel of Fig. 3, which is similar to Fig. 2, except that the x-axis shows the radiation-reaction time-scale sampled by each observation. We model the latter via  $|T| = |E_b/\dot{E}_b|$ , where  $E_b$  is the characteristic gravitational binding energy and  $\dot{E}_b$  is the rate of change of this energy, which for a binary system we approximate as the GW energy flux at spatial infinity, i.e.  $|T| = (5/64)(m/\eta)v_{12}^{-8}$ , where  $v_{12}$  is the binary’s orbital velocity,  $m$  is the total mass and  $\eta = m_1 m_2 / m^2$  is the symmetric mass ratio. For a binary system, this quantity is exactly the same as  $\Phi/\dot{\Phi}$  and (up to factors of order unity)  $\mathcal{R}/\dot{\mathcal{R}}$ . Thus,  $T$  is a measure of how long it takes the system, and in particular the gravitational field and the curvature, to change appreciably. Observe that GW150914 lands on the top left of the left panel of Fig. 3, at least four orders of magnitude away from the double binary pulsar; note that the Shapiro time delay observation does not appear in this figure, as it is not a dynamical constraint. For GW150914, how rapidly the curvature and the potential sweep through the detector’s sensitivity band is explicitly shown on the right panel of Fig. 3.

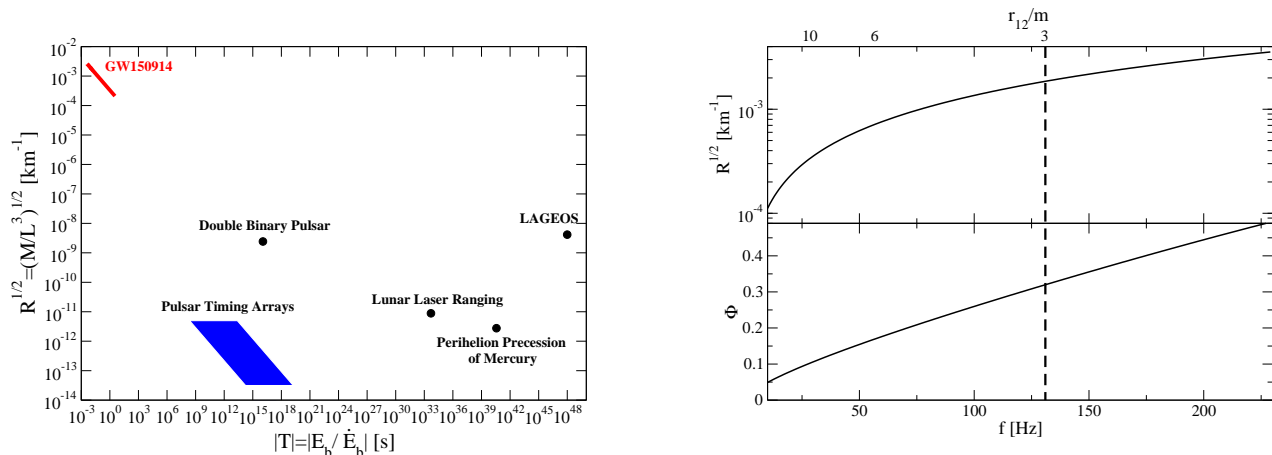


FIG. 3. (Color online) (Left) Schematic diagram of the curvature-radiation reaction time-scale phase space sampled by relevant experiments shown in Fig. 2. As evident GW150914 samples a regime of dynamic gravity where the radiation-reaction timescale is the shortest by many orders of magnitude. (Right) Characteristic curvature and strength of the Newtonian gravitational potential as a function of GW frequency.

## B. GW Model in GR and outside GR

### 1. IMRPhenom Model in GR

The LIGO/Virgo collaboration employed two main waveform models (both calculated within GR) to reconstruct the signal in [12]. One of these, the so-called *IMRPhenom* model [67–69], was heavily used to validate GR. This phenomenological approach models the Fourier transform of the response function as a piecewise function with 3 distinct pieces or phases, where each phase  $i$  takes the following form:

$$\tilde{h}_i(f) = A_i(f) e^{i\Phi_i(f)}. \quad (1)$$

The three phases that are distinguished are the inspiral, an intermediate phase and the merger-ringdown phase. In [12], the LIGO/Virgo collaboration employed the most recent IMRPhenom model [69], also called PhenomD, but modified to include precession by rotating the spin-aligned waveform to a precessing frame [103]. In this paper, we will ignore precession effects, since event GW150914 is so short that precession is unimportant<sup>7</sup>. We therefore describe below the PhenomD model of [69]. The differences in the constraints on non-GR effects obtained with PhenomB and PhenomD waveforms are discussed in Appendix B.

In the inspiral phase, the waveform is modeled as follows. The amplitude is treated in PN theory, including

terms up to 3PN order that are known analytically, and higher-order functionals (up to 4.5PN order) fitted to numerical simulations. The phase is decomposed into two contributions

$$\Phi_I(f) = \Phi_{\text{EI}}(f) + \Phi_{\text{LI}}(f), \quad (2)$$

where the early-inspiral part is simply

$$\Phi_{\text{EI}}(f) = 2\pi f t_c - \phi_c - \frac{\pi}{4} + \frac{3}{128\eta} (\pi m f)^{-5/3} \sum_{i=0}^7 \phi_i (\pi m f)^{i/3}, \quad (3)$$

and the late inspiral part is given by

$$\Phi_{\text{LI}}(f) = \frac{1}{\eta} \left[ \sigma_0 + \sigma_1(mf) + \frac{3}{4}\sigma_2(mf)^{4/3} + \frac{3}{5}\sigma_3(mf)^{5/3} + \frac{1}{2}\sigma_4(mf)^2 \right]. \quad (4)$$

The early inspiral parameters ( $t_c, \phi_c$ ) correspond to a constant time and phase offset,  $\eta = m_1 m_2 / m^2$  is the symmetric mass ratio with  $m = m_1 + m_2$  the total mass, and the  $\phi_i$  coefficients are functions of the component masses and the component spins (see e.g. Appendix A in [69]). The late inspiral parameters  $\sigma_0$  and  $\sigma_1$  can be absorbed into  $\phi_c$  and  $t_c$  respectively, while  $\sigma_2, \sigma_3$  and  $\sigma_4$  are in principle functions of the system parameters that represent (unknown) higher PN order corrections; these are fitted to polynomials of these system parameters by comparing to numerical simulations.

In the intermediate phase, the waveform is modeled as follows. The amplitude is a fourth-order polynomial in frequency, with coefficients fitted to numerical simula-

<sup>7</sup> In fact, the LIGO/Virgo collaboration was unable to accurately extract the individual spin components of the BH binary in event GW150914, nor the spin parameter combination that characterizes the amount of precession.

tions. The phase is modeled via the function:

$$\Phi_{\text{Int}}(f) = \frac{1}{\eta} \left[ \beta_0 + \beta_1(mf) + \beta_2 \ln(mf) - \frac{1}{3}\beta_3(mf)^{-3} \right], \quad (5)$$

where the coefficients  $\beta_0$  and  $\beta_1$  are fixed by requiring a smooth connection to the inspiral phase, while  $\beta_2$  and  $\beta_3$  are given in polynomial fits to numerical data in terms of  $\eta$  and an effective spin parameter.

Finally, the merger-ringdown phase is modeled as follows. The amplitude is treated as the product of a Lorentzian and an exponentially decaying function of frequency (see Eq. (58)), shifted by the real part of the ringdown frequency. The phase is modeled through the function

$$\Phi_{\text{MR}}(f) = \frac{1}{\eta} \left[ \alpha_0 + \alpha_1(mf) - \alpha_2(mf)^{-1} + \frac{4}{3}\alpha_3(mf)^{3/4} + \alpha_4 \arctan \left( \frac{f - \alpha_5 f_{\text{RD}}}{f_{\text{damp}}} \right) \right], \quad (6)$$

where  $f_{\text{RD}}$  is the real part of the ringdown frequency and  $f_{\text{damp}}$  is an approximation to the inverse damping time. As done for the  $\beta_i$  coefficients,  $\alpha_0$  and  $\alpha_1$  are determined by requiring a smooth connection to the intermediate phase, while the remaining parameters are polynomial fits to numerical data.

## 2. Parametrically Deformed Models

The IMRPhenom model is constructed within GR, and thus, it must be generalized in order to account for modified gravity effects. The LIGO/Virgo collaboration decided to introduce a generalized IMRPhenom (gIMR) model through the substitution rule

$$\vec{p} \rightarrow \vec{p}(1 + \delta p), \quad (7)$$

where  $\vec{p}$  is either  $\phi_i$ ,  $\sigma_i$ ,  $\beta_i$  or  $\alpha_i$ . For example, when the modification is introduced in the early inspiral, then  $\phi_i \rightarrow \phi_i(1 + \delta\phi_i)$  and the gIMR model is schematically

$$\tilde{h}_{\text{gIMR}}(f) = \begin{cases} A_{\text{I}}(f)e^{i\Phi_{\text{I}}(f)}e^{i\delta\Phi_{\text{I,gIMR}}} & f \leq f_{\text{Int}}, \\ A_{\text{Int}}(f)e^{i\Phi_{\text{Int}}(f)} & f_{\text{Int}} \leq f \leq f_{\text{MR}}, \\ A_{\text{MR}}(f)e^{i\Phi_{\text{MR}}(f)} & f_{\text{MR}} \leq f, \end{cases} \quad (8)$$

where  $(f_{\text{Int}}, f_{\text{MR}})$  are the frequencies where the waveforms transition from the inspiral to the intermediate phase and from the intermediate to merger-ringdown phase<sup>8</sup> [69]

<sup>8</sup> The PhenomB waveform model can indeed be expressed as a piecewise function. Its updated version, PhenomD, which is what the gIMR model is based on, cannot technically be written as a piecewise function because the transition frequencies for the amplitudes and phases are not exactly the same. Nonetheless, the arguments we present next continue to hold if one considers each phase of the coalescence (inspiral, intermediate, merger-ringdown) separately.

and where we have defined

$$\delta\Phi_{\text{I,gIMR}} = \frac{3}{128\eta} \sum_{i=0}^7 \phi_i \delta\phi_i (\pi mf)^{(i-5)/3}. \quad (9)$$

The term proportional to  $\delta\phi_1$  does not follow the definition in Eq. (7) as  $\phi_1 = 0$  in GR. Rather, it shows the absolute correction at 0.5PN order. In principle, there could also be GR modifications that are proportional to  $\ln f$  in Eq. (9), but in practice, there are no known theories that predict such a behavior; nonetheless, the arguments we present below continue to hold for such high-PN order modifications when the ppE framework is also extended to higher-PN order [104].

As we now show mathematically, the gIMR model is an implementation of the ppE framework [66] applied to the IMRPhenom waveform. This may seem obvious, though there has been some debate in the literature as to the overlap of the various methods of deforming GR waveforms; we thus thought it would be instructive to describe this in more detail here. The ppE framework was devised to capture how theoretical mechanisms that deviate from GR impact the waveform. The general idea was to introduce amplitude and phase deformations to the best GR waveform model available. Back when [66] was written, the IMRPhenom model had not yet been developed, so [66] used its predecessor [105] to model the GR waveform. Thus, one of the first (and simplest because of the use of a single ppE phase deformation) IMR ppE model proposed in [66] (see Eq. (1) in that paper) was

$$\tilde{h}_{\text{ppE}}(f) = \begin{cases} A_{\text{I}}(f)e^{i\Phi_{\text{I}}(f)}e^{i\delta\Phi_{\text{I,ppE}}} & f \leq f_{\text{Int}}, \\ A_{\text{Int}}(f)e^{i\Phi_{\text{Int}}(f)} & f_{\text{Int}} \leq f \leq f_{\text{MR}}, \\ A_{\text{MR}}(f)e^{i\Phi_{\text{MR}}(f)} & f_{\text{MR}} \leq f, \end{cases} \quad (10)$$

where back then the amplitudes did not include PN corrections and the ringdown was modeled with a Lorentzian, following the PhenomB model (i.e. the predecessor of the PhenomD model). Neglecting negative PN terms which were included in [66], the ppE inspiral phase deformation took the form (see Eq. (45) of [66])

$$\delta\Phi_{\text{I,ppE}}(f) = \frac{3}{128} (\pi \mathcal{M} f)^{-5/3} \sum_{i=0}^7 \phi_i^{\text{ppE}} (\pi \mathcal{M} f)^{i/3}, \quad (11)$$

where the coefficients  $\phi_i^{\text{ppE}}$  are ppE parameters and  $\mathcal{M} = \eta^{3/5} m$  is the chirp mass. We recognize immediately that the gIMR phase deformation in Eqs. (8), (9) are mathematically identical to the ppE phase deformation in Eqs. (10), (11) with the mapping  $\phi_i^{\text{ppE}} = \phi_i \delta\phi_i \eta^{-i/5}$ .

One can of course introduce ppE parameters at every PN order, thus greatly enlarging the parameter space, but a much more informative test is to consider one deformation at a time. Indeed, [104] first showed and [12] verified that using many GR deformations in the phase greatly dilutes the amount of information that can be

extracted from the signal, without a noticeable gain in the ability to detect an anomaly. Furthermore, there is no reason to expect an alternative theory will respect (or even allow) the GR PN sequence of rational exponents, and limiting to these thus weakens the scope of the test. Considering then a single deformation at a time, the inspiral ppE phase takes the form (see Eq. (1) in [66])

$$\delta\Phi_{1,\text{ppE}}(f) = \beta (\pi\mathcal{M}f)^{b/3}, \quad (12)$$

where  $\beta$  is called the amplitude coefficient and  $b$  is the exponent coefficient. The former controls the magnitude of the deformation to GR, while the latter controls the type of physical mechanism that is responsible for the modification. If one considers the gIMR model with only a single PN coefficient modification that enters at  $(n/2)$ -PN order with  $n \in \mathbb{N}$  (as also done in [12]), then the mapping between gIMR and ppE is simply

$$b = n - 5, \quad (13)$$

and

$$\beta = \frac{3}{128} \phi_n \delta\phi_n \eta^{-n/5}, \quad \text{if } \phi_n \neq 0, \quad (14)$$

or

$$\beta = \frac{3}{128} \delta\phi_n \eta^{-n/5}, \quad \text{if } \phi_n = 0, \quad (15)$$

(no summed implied over  $n$  in these equations). Evaluating the first few terms, for example,

$$\beta = \frac{3}{128} \delta\phi_0, \quad \text{at 0PN order}, \quad (16)$$

$$\beta = \frac{3}{128} \delta\phi_1 \eta^{-1/5}, \quad \text{at 0.5PN order}, \quad (17)$$

$$\beta = \frac{3}{128} \phi_2 \delta\phi_2 \eta^{-2/5}, \quad \text{at 1PN order}, \quad (18)$$

where we used  $\phi_0 = 1$  in Eq. (16), while  $\phi_2 = 3715/756 + (55/9)\eta$ , and the other inspiral phase coefficients of GR can be found in Appendix A of [69].

The gIMR waveforms are then a restricted subset of the ppE waveforms presented in [66]. This is because the gIMR waveforms only consider positive PN deformations to the waveform phase and no deformations to the amplitude. The ppE framework allows for both of these, the former of which (the negative PN order deformations) is particularly important when extracting information about theoretical physics, as discussed in the introduction.

### 3. From Parametric Deformations to Theoretical Physics

Now that we have established that the gIMR model is a subset of the ppE framework applied to the IMRPhenom waveform family, we can use all of the machinery of

the ppE formalism to connect GR deformations to specific theoretical mechanisms. The latter can be classified into *generation mechanisms* and *propagation mechanisms*. The mapping between these mechanisms and ppE parameters  $\beta$  or  $\delta\phi_i$  has been developed over the past several years in [45, 66, 76, 93, 106–119] and it is summarized in the review paper [11]. For completeness, we present this mapping here, updated with recent results.

#### 3.1 Generation Mechanisms

Generation mechanisms refer to those that are active close to the binary system, where the GWs are being generated. Typically, one refers to this region as the near-zone in the PN formalism, and the inner-zone in BH perturbation theory. One can think of generation mechanisms as modification to the Poisson equation in the weak-field limit of the Einstein equations, i.e. modifications to the structure of the fields in terms of the source multipole moments. Such modifications then propagate into corrections to the binding energy and angular momentum of a binary, and thus to the equations of motion. The character of the modification depends sensitively on the particular mechanism that activates. For example, when a scalar field activates in the near zone, it typically leads to dipolar energy loss in the binary system, and thus, to a faster rate of orbital decay than predicted in GR.

Table III summarizes the theoretical effects and mechanisms in the generation of GWs that can be constrained given the observation of GWs emitted in the coalescence of a BH binary, as in the case of GW150914. By “theoretical effect” we mean the type of modification that is induced on the GW observable, while “theoretical mechanism” refers to the process that produces the aforementioned modification. The table also provides examples of theories where these effects and mechanism arise, together with the relative PN order at which they enter the Fourier GW phase. Finally, the table provides the mapping between the ppE coefficient  $\beta$  (or alternatively  $\delta\phi_i$ ) and the system parameters and coupling constants that control the magnitude of the modification, where we have defined

$$\beta_{\text{EdGB}} = -\frac{5}{7168} \zeta_{\text{EdGB}} \frac{(m_1^2 s_2^{\text{EdGB}} - m_2^2 s_1^{\text{EdGB}})^2}{m^4 \eta^{18/5}}, \quad (19)$$

$$\beta_{\text{ST}} = -\frac{5}{1792} \dot{\phi}^2 \eta^{2/5} (m_1 s_1^{\text{ST}} - m_2 s_2^{\text{ST}})^2, \quad (20)$$

$$\beta_{\text{ED}} = \frac{25}{851968} \left( \frac{dm}{dt} \right) \frac{3 - 26\eta + 34\eta^2}{\eta^{2/5}(1 - 2\eta)}, \quad (21)$$

$$\beta_{\dot{G}} = -\frac{25}{65536} \dot{G}\mathcal{M}, \quad (22)$$

$$\beta_{\text{acs}} = \frac{1549225}{11812864} \frac{\zeta_{\text{CS}}}{\eta^{14/5}} \left[ \left( 1 - \frac{231808}{61969} \eta \right) \chi_s^2 + \left( 1 - \frac{16068}{61969} \eta \right) \chi_a^2 - 2\delta_m \chi_s \chi_a \right], \quad (23)$$

Theoretical Effect	Theoretical Mechanism	Theories	ppE $b$	Order	Mapping
Scalar Dipolar Radiation	Scalar Monopole Field Activation BH Hair Growth	EdGB [110, 112, 120, 121]	-7	-1PN	$\beta_{\text{EdGB}}$ [110]
		Scalar-Tensor Theories [43, 122]	-7	-1PN	$\beta_{\text{ST}}$ [43, 122]
Anomalous Acceleration	Extra Dimension Mass Leakage Time-Variation of $G$	RS-II Braneworld [123, 124]	-13	-4PN	$\beta_{\text{ED}}$ [111]
		Phenomenological [107, 125]	-13	-4PN	$\beta_G$ [107]
Scalar Quadrupolar Radiation Scalar Dipole Force Quadrupole Moment Deformation	Scalar Dipole Field Activation due to Gravitational Parity Violation	dCS [110, 126]	-1	+2PN	$\beta_{\text{dCS}}$ [116]
Scalar/Vector Dipolar Radiation Modified Quadrupolar Radiation	Vector Field Activation due to Lorentz Violation	EA [89, 90], khronometric [91, 92]	-7	-1PN	$\beta_{\text{EA}}^{(-1)}$ [93]
			-5	0PN	$\beta_{\text{EA}}^{(0)}$ [93]
Modified Dispersion Relation	GW Propagation/Kinematics	Massive Gravity [127–130]	-3	+1PN	$\beta_{\text{MDR}}$ [115, 127]
		Double Special Relativity [131–134]	+6	+5.5PN	
		Extra Dim. [135], Horava-Lifshitz [136–138]	+9	+7PN	

TABLE III. Theoretical effects introduced into the GW observable due to various theoretical mechanisms, together with example theories where such mechanisms arise. For each effect and mechanism, we specify the ppE exponent which would signal its appearance, the relative PN order at which these effects enter the Fourier GW phase, and the mapping to the ppE magnitude coefficient  $\beta$ .

$$\beta_{\mathcal{E}}^{(0PN)} = -\frac{3}{128} \left(1 - \frac{c_{14}}{2}\right) \left(\frac{1}{w_2} + \frac{2c_{14}c_+^2}{(2c_1 - c_-c_+)^2w_1} + \frac{3c_{14}}{2w_0(2 - c_{14})}\right) - 1. \quad (24)$$

The system parameters that enter these equations are the symmetric and antisymmetric dimensionless spin combinations  $\chi_{s,a} = (a_{\parallel 1}/m_1 \pm a_{\parallel 2}/m_2)/2$  with  $a_{\parallel A}$  representing the projection of the (dimensional) spin vector  $\vec{a}_A$  onto the unit orbital angular momentum vector, the dimensionless mass difference  $\delta_m = (m_1 - m_2)/m$ , the co-moving distance to the source  $D$ , and the redshift  $z$ . We have not included in this table any effect or mechanism that can only be constrained with binary systems where at least one component is a NS (for those mappings refer to the review paper [11]).

The ppE parameter  $\beta$  controls the magnitude of the modifications introduced by mechanisms that activate in the generation of GWs, and thus, it depends on the coupling constants of the theory where these mechanisms are realized. In EdGB gravity and in dCS gravity, BHs have scalar hair as sourced by the Kretschmann curvature and the Pontryagin invariant. These scalar monopole and dipole fields induce scalar dipolar and quadrupolar radiation, which then speeds up the rate at which the binary inspirals. The magnitude of this modification is proportional to the dimensionless EdGB and dCS coupling parameters  $\zeta_{\text{EdGB}}$  and  $\zeta_{\text{CS}}$ , which depend on a dimensional coupling parameter divided by the BH mass to the fourth power, as we will show explicitly in Sec. III A. The quantities  $s_A^{\text{EdGB}}$  in Eq. (19) are the spin-dependent factors of BH scalar charges in EdGB gravity given by  $s_A^{\text{EdGB}} \equiv 2(\sqrt{1 - \chi_A^2} - 1 + \chi_A^2)/\chi_A^2$  [139]. In scalar-tensor theories, a BH can acquire a scalar charge if the scalar field is evolving in time with a growth rate  $\dot{\phi}$  due to e.g. a cosmological background [21, 43, 122]. The quantities  $s_A^{\text{ST}} \equiv [1 + (1 - \chi_A^2)^{1/2}]/2$  in Eq. (20) are the spin-dependent, BH scalar charges in scalar-tensor theories with BH hair growth [43]. In braneworld models, leakage

of gravitons into extra dimensions induces an anomalous acceleration that is proportional to the rate of leakage into the bulk  $dm/dt$ , which in turn is proportional to the square of the ratio of the size of the extra dimension to the total mass<sup>9</sup>. Phenomenological models where Newton’s gravitational constant  $G$  has a small time-variation also induce an anomalous acceleration, and thus modifications to the Fourier waveform phase scale with  $\dot{G}$ . EA theory generically predicts gravitational Lorentz violation, where the magnitude of the latter is controlled by the dimensionless coupling parameters  $(c_+, c_-)$ . The parameters  $c_1$  and  $c_{14}$  are also dimensionless coupling parameters that can be written in terms of  $(c_+, c_-)$ , while  $w_0$ ,  $w_1$  and  $w_2$  are the propagation speeds of the spin-0, spin-1 and spin-2 modes, which also depend on  $(c_+, c_-)$ . The ppE parameter  $\beta_{\mathcal{E}}^{(0PN)}$  also contains terms that depend on the BH sensitivities, which are currently unknown. We neglect such terms in this paper because Ref. [93] showed that they are subdominant for NS binaries. We do not present the ppE parameter  $\beta_{\mathcal{E}}^{(-1PN)}$  that enters at -1PN order, since it is proportional to the square of the difference in the individual BH sensitivities.

### 3.2 Propagation Mechanisms

Propagation mechanisms refer to those that activate while the wave is propagating away from the source in a regime at least several GW wavelengths away from the binary’s center of mass (in the so-called far-zone, radiation zone or wave-zone). One can think of propagation mechanisms as modifications to the plane-wave propagator in field theory, i.e. modifications to the inverse of the wave operator. The latter can introduce modifications to the amplitude of the waves, such as amplitude mixing generated by gravitational parity violation [108], or they can

<sup>9</sup> This corrects a small typo in the review paper [11], and recasts the constraint in terms of the rate of change of the total mass.

introduce modifications to the phase of the waves, due to real corrections to the wave's dispersion relation [115]. Modifications to the dispersion relation are typically also associated with either modifications to the Lorentz group or to its action in real or momentum space. Because of this, such modifications are associated with gravitational Lorentz-violating effects, which are typically found in quantum-gravitational models, such as loop quantum gravity [140] and string theory [141, 142].

Table III also summarizes the theoretical mechanisms that can be constrained in the propagation of GWs using GWs from BH binaries. As in the generation case, the table provides the mapping between the ppE coefficient  $\beta$  and the system parameters and coupling constants of particular theories with modified dispersion relation. For a generic modified dispersion relation of the form

$$E^2 = (pc)^2 + \mathbb{A} (pc)^\alpha, \quad (25)$$

the modification to the Fourier GW phase takes on the ppE form of Eq. (12) with

$$\beta_{\text{MDR}} = \frac{\pi^{2-\alpha}}{(1-\alpha)} \frac{D_\alpha}{\lambda_{\mathbb{A}}^{2-\alpha}} \frac{\mathcal{M}^{1-\alpha}}{(1+z)^{1-\alpha}}, \quad (26)$$

$$b = 3\alpha - 3. \quad (27)$$

In these equations,  $E$  and  $p$  are the energy and momentum of the graviton respectively, while  $\mathbb{A}$  is the strength of the dispersion modification (that depends on the coupling constants of the particular theory) and  $\lambda_{\mathbb{A}} \equiv h \mathbb{A}^{1/(\alpha-2)}$  is similar to a Compton wavelength. For events at small redshift, the distance measure

$$D_\alpha = \frac{z}{H_0 \sqrt{\Omega_M + \Omega_\Lambda}} \left[ 1 - \frac{z}{4} \left( \frac{3\Omega_M}{\Omega_M + \Omega_\Lambda} + 2\alpha \right) + \mathcal{O}(z^2) \right], \quad (28)$$

with  $z$  the redshift and  $H_0$  the current value of the Hubble constant. This modification to the Fourier phase is independent of the generation mechanism, and in particular, independent of the particular waveform model used for the inspiral, merger and ringdown. Thus, one can add this modification onto any waveform model, if one is interested in studying the implications a GW observation has on Lorentz-violating modified dispersion relations.

A GW that obeys a modified dispersion relation will also travel at a speed different from that of light. Using Eq. (25) we can calculate the group velocity  $v_g$  to find

$$\frac{v_g^2}{c^2} = \frac{1}{c^2} \frac{d\omega}{dk} = 1 + (\alpha - 1) \mathbb{A} E^{\alpha-2}. \quad (29)$$

Notice that for  $\alpha > 1$  and  $\mathbb{A} < 0$ , GWs travel slower than the speed of light. When this is the case, high energy massive particles may travel faster than GWs and emit gravitational Cherenkov radiation [143, 144]. The fact that observed high energy cosmic ray particles have traveled extragalactic distances without losing energy to this type of radiation places a stringent constraint on the magnitude of  $\mathbb{A}$  in the  $\mathbb{A} < 0$  sector, in particular when  $\alpha \geq 2$  [63].

The dimensionless constant  $\alpha$  controls the type of dispersion modification. In the limit where  $E$  and  $p$  are large compared to  $(\mathbb{A}p^\alpha)^{1/2}$ , but small compared to the Planck energy  $E_p$ , this generic parameterization can capture the following theories or phenomenological models:

- *Double Special Relativity* [131–134]:  $\mathbb{A} = \eta_{\text{dsrt}}$  and  $\alpha = 3$ , where  $\eta_{\text{dsrt}}$  is a parameter of the order of the Planck length,
- *Extra-Dimensional Theories* [135]:  $\mathbb{A} = -\alpha_{\text{edt}}$  and  $\alpha = 4$ , where  $\alpha_{\text{edt}}$  is a constant related to the square of the Planck length,
- *Hořava-Lifshitz Gravity* [136–138, 145]:  $\mathbb{A} = \kappa_{\text{hl}}^4 \mu_{\text{hl}}^2 / 16$  and  $\alpha = 4$ , where  $\kappa_{\text{hl}}$  and  $\mu_{\text{hl}}$  are constants of the theory,
- *Massive Graviton* [127–130]:  $\mathbb{A} = (m_g c^2)^2$  and  $\alpha = 0$ , where  $m_g$  is the mass of the graviton.
- *Gravitational Standard Model Extension (SME)* [146]:  $\mathbb{A} = -2\mathring{k}_{(V)}^{(d)}$  for even  $d \geq 4$  and  $\mathbb{A} = \pm 2\mathring{k}_{(V)}^{(d)}$  for odd  $d \geq 5$  with  $\alpha = d - 2$  in the rotation-invariant limit to linear order in  $\mathring{k}_{(V)}^{(d)}$ , where  $\mathring{k}_{(V)}^{(d)}$  are constant coefficients that control the Lorentz-violation operators. The modified dispersion relation without rotation invariance is given by Eq. (5) in [146].

The first two also typically predict a constant (massive graviton) term, but we have left this term out of the list above. Notice also that the modifications to the dispersion relation need not be automatically Planck suppressed [147, 148]. This is because Planck suppression typically arises because of Lorentz-invariance; in theories that lack this symmetry, modifications to the dispersion relation can be dramatically enhanced upon regularization and renormalization [149].

The models described above predict modifications to the dispersion relation that enter at rather high PN order (5.5PN when  $\alpha = 3$  and 7PN when  $\alpha = 4$ ). Such very high PN order modifications only play an important role in the late inspiral or the intermediate region between inspiral and merger. However, propagation mechanisms induce modifications in the observable that also build up with distance travelled. One then expects that the best instruments to constrain such effects would be space-based detectors, that could in principle see events to high redshift ( $z \sim 10$ ). Event GW150914, nonetheless, was generated 1.3 billion light-years away from Earth, and this is a sufficiently large baseline to consider possible constraints on propagation mechanisms.

Theories that predict modified dispersion relations for the graviton are also likely to modify GWs in the generation phase, so which one dominates? Let us show that the former typically dominates the latter due to the accumulation of the modified gravity effect with distance, using massive gravity as an example. Reference [59] showed that the fractional correction to the radiated GW en-

ergy flux from a binary in massive gravity is given by  $\sim 1/(\lambda_g^2 f^2)$ . Therefore, the ppE parameter due to GW generation is roughly given by  $\beta_{\text{MG}}^{(\text{gen})} \sim (3/128)\pi^2 \mathcal{M}^2/\lambda_g^2$  with  $b = -11$ , namely a  $-3\text{PN}$  correction. Comparing this with the ppE parameter for the modified propagation,  $\beta_{\text{MG}}^{(\text{prop})} \sim \pi^2 D_0 \mathcal{M}/\lambda_g^2$  with  $b = -3$  [see Eq. (26) with  $\alpha = 0$ ], one finds

$$\frac{\beta_{\text{MG}}^{(\text{prop})} u^{-1}}{\beta_{\text{MG}}^{(\text{gen})} u^{-11/3}} \sim 10^{18} \left( \frac{\mathcal{M}}{28M_\odot} \right)^{5/3} \times \left( \frac{D_0}{381\text{Mpc}} \right) \left( \frac{f}{100\text{Hz}} \right)^{8/3}. \quad (30)$$

This clearly shows that the propagation effect dominates the generation effect, even when the former is of higher PN order relative to the latter. Therefore, when we consider modifications to the propagation of GWs, we neglect modifications to GW generation.

### III. THEORETICAL IMPLICATIONS OF EVENT GW150914

This section discusses the theoretical implications of event GW150914. We begin by discussing, in general, the mechanisms that can and cannot be constrained by this event due to its assumed vacuum nature. This leads to a generic prediction of the strength of future constraints on higher-curvature models from events like GW150914. The section then continues by classifying theoretical implications into those that affect the generation of GWs and those that affect the propagation of GWs, and determining the precise implications of GW150914 for each class. In both cases, we relate Bayesian as well as Fisher estimates on parameter constraints to different physical mechanisms. We show that our ignorance of very high PN order effects in the GW phase do not limit our ability to constrain theoretical mechanisms.

When we carry out Fisher analyses [150] in Secs. III B and III C, the parameter vector that determines our IMRPhenom waveform is  $\theta = (\ln \mathcal{M}_z, \ln \eta, \chi_s, \chi_a, t_c, \phi_c, \ln A_0, \beta)$ , where  $A_0$  is an overall amplitude factor proportional to  $\mathcal{M}_z^{5/6}/D_L$ , with  $\mathcal{M}_z$  and  $D_L$  the redshifted chirp mass and luminosity distance respectively. The parameter values for the injection are  $(m_1, m_2) = (35.7, 29.1)M_\odot$  in the source frame with  $z \approx 0.088$  and  $\chi_s = \chi_a = t_c = \phi_c = \beta = 0$ , while  $A_0$  is determined by requiring that the total (network) SNR=24. These injected parameters are consistent with the GW150914 measurement [1]. We start the integration of the Fisher matrix at 20Hz to be consistent with the aLIGO sensitivity curve during the O1 observation period and we use a fit to the spectral noise sensitivity curve during O1 (see Appendix A). We follow [150–152] and impose a physical Gaussian prior on  $\chi_s$  and  $\chi_a$  that corresponds to  $|\chi_s| \leq 1$  and  $|\chi_a| \leq 1$ .

#### A. (Im)possible Theoretical Implications

Event GW150914 is a fantastic probe of theoretical physics that has important implications for certain aspects of strong-field gravity, but unfortunately not all. The prime example of the latter are theoretical models where gravity is described by a metric tensor with evolution equations that differ from the Einstein equations only through a modified “right-hand side” that depends on the matter stress-energy tensor. An example of such a theoretical model is Eddington-inspired Born-Infeld (EiBI) gravity [153] and certain  $f(R)$  theories. Since in vacuum spacetimes these theories reduce exactly to GR, GW150914 cannot say anything about them<sup>10</sup>.

A theoretical mechanism that for a similar reason evades probing with GW150914 is the activation of certain scalar or pseudo-scalar fields in the strong gravity regime sourced by dense matter. The idea here is that gravity is not just described by a metric tensor, but also by a scalar or pseudo-scalar field that affects its evolution. When the scalar field is not excited, the theory reduces to GR; but when the scalar field is excited, it typically transports energy away from the binary, which leads to dipolar energy loss, and in turn, to an acceleration in the rate at which the binary inspirals. Examples of such theories include BD theory [70–75], the scalar-tensor theory extension of Damour and Esposito-Farèse [157, 158], and  $f(R)$  models as they can be mapped to scalar tensor theories [159].

As a concrete example, consider a scalar field  $\phi$  with the following model-dependent evolution equation

$$\square\phi = S, \quad (31)$$

where  $\square$  is the D’Alembertian operator and  $S$  is a source term that depends on the particular theoretical model. If the source term depends only on a scalar combination of the stress-energy tensor, the Ricci tensor or the Ricci scalar, then it will vanish in any BH spacetime (vacuum and Ricci-flat). Thus if there is no background or cosmological field present, a binary BH merger cannot excite the field. To constrain such theoretical models one thus needs at least one of the binary components to be a NS. A non-trivial cosmological [43, 122] or background component to the field would interact with a BH merger leading to scalar radiation [20, 21], however the energy in a cosmological scalar field would be insignificant on the scales relevant to a compact object merger, and have a negligible effect on the inspiral [11].

Consider now a scalar field  $\phi$  that evolves according to Eq. (31), but where the source  $S$  is a scalar functional of the Riemann tensor. If so,  $S$  will typically not vanish for

<sup>10</sup> In the presence of matter, however, these theories do predict large modifications, that in principle do not allow for the construction of regular, stellar configurations [154–156].

BH spacetimes<sup>11</sup>, thus sourcing the scalar field and providing a new channel to transport energy away from the binary, accelerating its inspiral<sup>12</sup>. Generically, quadratic curvature effective<sup>13</sup> theories [110, 119], such as dCS gravity [116, 126, 169] and EdGB gravity [112], will lead to such source terms (see also the discussion in [170]). In these theories, the scalar field is sourced by (second-order) curvature invariants  $\mathcal{R}^2$ , such that  $S \propto \alpha \mathcal{R}^2$ , with  $\alpha$  a coupling constant (with dimensions of [length]<sup>2</sup> in geometric units if  $\phi$  is dimensionless). The scalar field will then transport energy away from the system, as given by the integral of the field's stress-energy tensor over a 2-sphere:  $\dot{E}^{(\phi)} \propto r^2 (\partial\phi)^2$ , where  $r$  is the field point distance. Solving for the scalar field in the small coupling approximation and through Green's functions, one generically finds that  $\dot{E}^{(\phi)} \sim (\alpha^2/m^4)(m/r_{12})^p$ , where  $p$  is an integer that determines the PN order of the effect, and is in turn determined by the precise functional form of  $\mathcal{R}^2$ . For example, in EdGB gravity,  $\mathcal{R}^2$  is the Gauss-Bonnet invariant, which then leads to (electric) dipole scalar radiation for which  $p = 4$  (a  $-1$ PN order effect relative to the GR quadrupolar energy flux) [116].

Such a modification to the energy emission modifies binary inspirals by changing the chirping rate  $\dot{f}$ , affecting both the gravitational waveform phase and amplitude evolution. The verification of GR by event GW150914 then implies that such a modification is not present at a level above the noise, which should yield a constraint of the form  $\delta \gtrsim (\alpha^2/m^4)(m/r_{12})^{p-5}$ , where  $\delta$  is a fractional number tallying all the sources of noise and uncertainty in the observation and analysis of GW150914; obviously, one such source will be statistical uncertainty, which will scale inversely with the SNR. Solving for  $\sqrt{\alpha}$  leads to an estimate of generic constraints on the generation of scalar field emission

$$\sqrt{\alpha} \lesssim m \delta^{1/4} \left(\frac{r_{12}}{m}\right)^{\frac{p-5}{4}}. \quad (32)$$

Observe that the smaller the separation that is reached, the more stringent the constraint, which saturates roughly at merger. The sum of systematic and statistical error  $\delta$  plays a minor role in the constraint on the characteristic length scale of the theory  $\sqrt{\alpha}$ , as it is raised to the one-fourth power (though such an error plays an important role in constraining the deformation in e.g. the energy flux which scales as  $\alpha^2/m^4$ ). The constraint is then essentially dominated by the total mass of the system, or equivalently by the radius of curvature of the merged BH.

Clearly then, the smaller the total mass of the binary, the stronger the constraint. For event GW150914<sup>14</sup>, using a fractional error of 4% (consistent with a 96% verification of GR [12]) and setting  $r_{12} = 2m$ , we find a constraint on scalar field emission of roughly  $\sqrt{\alpha} \lesssim 35\text{km}$ . As shown in Table I, such a constraint is roughly an order of magnitude weaker than current bounds using low-mass X-ray binaries [41] or those using the existence of NS solutions [171], but the latter are much more astrophysical-model dependent, relying on assumptions on the mass transfer rate and the properties of stellar winds [73, 172], and the equation of state.

## B. Implications on the Generation of GWs

### 1. Constraining Generation Mechanisms

As described in Sec. II B 3, constraints on a plethora of mechanisms that may be active in the generation of GWs can be captured within the ppE formalism. Therefore, constraints on the ppE amplitude coefficients  $\beta$  (or  $\delta\phi_i$ ) as a function of PN order provide constraints on physical mechanisms as well. This is one of the benefits and power of the ppE framework.

The LIGO/Virgo collaboration in [12] performed a Bayesian analysis of the constraints that event GW150914 places on the ppE coefficients  $\delta\phi_i$  (at 90% confidence), using the IMRPhenom model with precessing spins. Figure 4 plots these constraints mapped to constraints on  $\beta$  as a function of relative PN order in the Fourier GW phase (green crosses). For example, a constraint on  $\beta$  at 0PN order means a constraint on a ppE term in the Fourier GW phase that is proportional to  $(\pi\mathcal{M}f)^{-5/3}$ .

Another way to estimate constraints on  $\beta$  given event GW150914 is to carry out a Fisher analysis [174, 175]. We have done this using IMRPhenom waveforms without precessing spins (as these have a minimal effect on the waveforms [65]) and a spectral noise density that is constructed by fitting the aLIGO data (see Appendix A). The results are plotted in Fig. 4 as a function of PN order (red solid line). Observe that the Fisher estimate is a very good approximation to the more complete Bayesian analysis of [65], overestimating the constraint by roughly 15–50%. A Fisher estimate, thus, is still a valid tool that typically leads to *conservative* constraints on deviations from GR. We do not show constraints at 2.5PN order as such a correction is degenerate with a constant phase shift. Observe also the Fisher analysis here includes negative PN order effects, since many theoretical implications require such constraints; the Bayesian anal-

<sup>11</sup> Vector and tensor fields can also be sourced in BH spacetimes in e.g. Lorentz violating theories of gravity [160–164] and bimetric gravity theories [165, 166].

<sup>12</sup> The scalar field also modifies the binding energy of the system, but this typically occurs at a higher PN order [110].

<sup>13</sup> Such theories can, in principle, lead to Ostrogradski instabilities, but only when they are treated as exact. They are well-posed within the effective field theory framework [167, 168].

<sup>14</sup> Notice that with this constraint, the quantity  $\zeta = \alpha^2/m^4$  is much smaller than unity, which then justifies the use of the small coupling approximation.

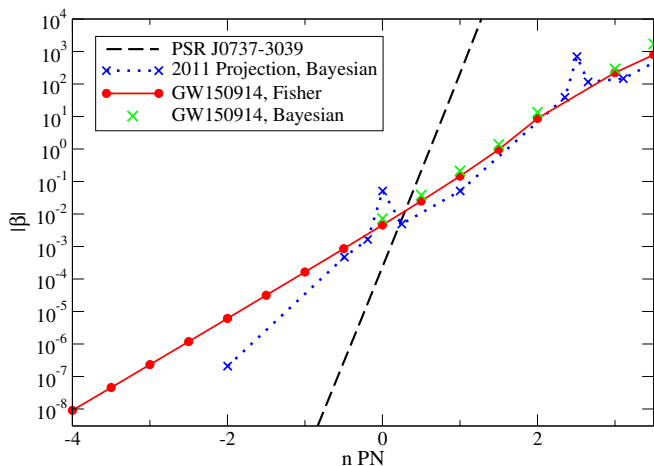


FIG. 4. (Color online) 90%-confidence constraints on the ppE parameter  $|\beta|$  at  $n$ th PN order. The green crosses represent the bounds reported in [12] through a Bayesian analysis of event GW150914, mapped to constraints on  $\beta$ . The red dots and line represent bounds estimated with a Fisher analysis, using the IMRPhenom waveform (without spin precession) and a fit to the aLIGO spectral noise density. The blue dotted line shows projected constraints predicted in 2011 by [109] for a similar system to that which generated GW150914. The dashed black line is a rough estimate on the constraints that the double binary pulsar PSR J0737-3039 [102] can place on the ppE  $\beta$  parameter [173]. Observe that the constraints obtained with a Fisher analysis agree very well with the Bayesian constraint reported in [12]. Also note that binary pulsar observations can constrain negative PN order deviations better than aLIGO, while aLIGO does better than binary pulsar observations at higher PN order, as first calculated in [173].

ysis of [12] does not report on these negative PN order constraints, which is why they are not shown in Fig. 4.

Our analysis and the study of the LIGO collaboration in [12] differ in many ways, and yet, the two yield similar constraints on  $\beta$ . The main differences between these studies are that the former (latter) uses

- (i) a Fisher (Bayesian) analysis,
- (ii) non-precessing (precessing) waveform templates,
- (iii) a fit (real data) for the noise curve,
- (iv) a simulated waveform injection compatible with the real signal (the real signal), and
- (v) includes only statistical (both statistical and systematic) errors.

Probably, differences (i)–(iii) do not have a large impact on the  $\beta$  constraints for the following reasons. The difference between Fisher and Bayesian studies scales as  $\mathcal{O}(1/\text{SNR})$  [176], which is only  $\sim \mathcal{O}(4\%)$  for the large SNR of GW150914. Precession is a small effect for GW150914, which the LIGO collaboration found to not be measurable [65]. The real noise spectral density contains many spikes, but these are very thin, and thus, for

the same SNR, they affect constraints on  $\beta$  by only a few % (see Appendix A). On the other hand, differences (iv) and (v) are probably more important. For example, in our Fisher analysis we set the spin magnitudes of the injection to zero, but the posteriors found by the LIGO collaboration [65] are quite wide, and a different choice of spin magnitude can affect our Fisher estimates by a factor of  $\sim 2$ . Even using the Bayesian analysis of [65], the mapping between  $\delta\phi_i$  and  $\beta$  [see Eqs. (14) and (15)] depends on the posterior distribution of other parameters, and different choices can affect constraints on  $\beta$  at high PN order by also a factor of  $\sim 2$ . As another example, consider the systematic errors on the measurement of  $\delta\phi_i$  (or  $\beta$ ) reported in [12], i.e. the distance from the peak of the posterior to zero; these systematic errors are comparable to the statistical error, the former of which is not included in the Fisher bound. In spite of these differences, the constraints on  $\beta$  that we found through our analysis are very close to those reported by the LIGO collaboration, whenever we can compare them directly.

Interestingly, Ref. [109] had already estimated the accuracy to which the ppE parameter  $\beta$  could be constrained, using a detailed Bayesian analysis and inspiral-only waveforms. For comparison, we have taken the results of [109] directly and plotted them in Fig. 4 (dotted blue line) without modification, i.e. for a system with an SNR of 20, (source) component masses  $(m_1, m_2) = (12, 6)M_\odot$  ( $\eta = 0.222$ ) and luminosity distance  $D_L = 462$  Mpc. It is quite a coincidence that the SNR and the luminosity distance used in [109] in 2011 are so close to those of event GW150914, except that the latter is a much higher-mass system. Observe that the projected constraints predicted in 2011 are in good agreement with the actual constraints placed by aLIGO. The spikes in the constraints of [109] arise due to degeneracies with the chirp mass and the phase of coalescence, the former of which is partially broken when one incorporates the merger-ringdown phase, as done in [12]. Differences in the component masses (relative to the GW150914 event) also introduce differences in the amount of degeneracy between ppE parameters and the chirp mass.

For comparison, Fig. 4 also includes an estimate of the bounds that the double binary pulsar PSR J0737-3039 [102] can place on the ppE  $\beta$  parameter (black dashed line) [173]. These estimates are rough, since they do not take into account possible covariances between  $\beta$  and other pulsar parameters. Nonetheless, they are enough to illustrate that binary pulsars can do a much better job at constraining “negative PN” order effects, while aLIGO (and in particular event GW150914) can beat binary pulsar constraints above Newtonian (0PN) order, as first suggested in [173]. One must keep in mind, however, that a *direct* comparison of bounds on  $\beta$  from binary pulsar observations to those obtained with GWs is misleading, since the former cannot probe gravity when compact objects merge.

Let us now map the constraints on the ppE parameter

$\beta$  to specific theoretical mechanisms, some of which we already summarized in Table I (see also Table III). Constraints listed in the top part of this table are obtained from modifications to GW generation, while those in the bottom part come from modifications to GW propagation; here we focus on the former, and defer a discussion of the latter to Sec. III C. For reference, we also present current constraints obtained from other observations, such as table-top experiments and observations with low-mass X-ray binaries. We find the following theoretical implications of GW150914 on GW generation:

- *EdGB gravity*: GW150914 cannot place constraints on EdGB gravity due to degeneracies between the spin magnitudes, the component masses and the EdGB coupling constant in the leading-order (dipole) EdGB waveform correction. If one were to assume *a priori* that the spins of the binary constituents of GW150914 are zero and the component masses are given by their posterior peaks, then one would be able to constrain  $\sqrt{|\alpha_{\text{EdGB}}|} \lesssim 22\text{km}$ , which is consistent with the estimate of Sec. III A. Without this a-priori information and using spin combinations within the 90% posterior distribution measured by aLIGO [65], the constraint on the EdGB coupling constant weakens dramatically (see Appendix C). Saturating this weakened constraint leads to a large value of  $\zeta_{\text{EdGB}}$ , which violates the small-coupling approximation used to derive the waveform correction in the first place [Eq. (19)]. GW150914 may still be able to place meaningful constraints on EdGB gravity from higher PN order corrections, but these have not yet been calculated.
- *dCS gravity*: As in the EdGB case, GW150914 cannot place meaningful constraints on dCS gravity because of degeneracies between the spin magnitudes, the component masses and the dCS coupling constant in the leading-order dCS waveform correction. If one were to assume *a priori* that the spins of the BHs in GW150914 are zero, which is consistent with the 90% posterior distribution measured by aLIGO [65], then the leading-order dCS modification would vanish exactly, and the next-to-leading order correction would enter at very high PN order [110, 177]. This would lead to an extremely weak constraint on the dCS coupling constant, which if saturated would lead to a value of  $\zeta_{\text{dCS}}$  that violates the small coupling approximation adopted to derive Eq. (23) in the first place.
- *Scalar-tensor theories with BH scalar growth due to the excitation of a time-dependent scalar field* [43, 122]. GW150914 cannot place constraints on  $\dot{\phi}$  because of degeneracies between this quantity and the component masses and the spin magnitudes in the waveform correction. Choosing spin magnitudes that lead to the weakest (most conservative) constraint with masses fixed to the injected ones, one

then finds the bound  $\dot{\phi} < \mathcal{O}(10^4/\text{sec})$ . Saturating this constraint, however, leads to a dimensionless expansion parameter that violates the small coupling approximation  $m_A \dot{\phi} \ll 1$ , which was used to construct the waveform deformation in the first place [43, 122].

- *EA theory*: GW150914 can place constraints on EA theory, although these are weaker than the current binary pulsar bound. Since the bound on EA theory in Table I is derived from the bound on  $\beta_{\text{E}}^{(0PN)}$ , it corresponds to assuming that scalar and vector dipole radiation are suppressed *a priori*. This can be justified for NSs, but not for BHs, as their sensitivities in this theory have not yet been calculated. If one includes both  $\beta_{\text{E}}^{(-1PN)}$  and  $\beta_{\text{E}}^{(0PN)}$  in the parameter set, as done e.g. in the projected constraints of [93], the bound on  $\beta_{\text{E}}^{(0PN)}$  becomes weaker due to degeneracies. Observe, nonetheless, that although the GW150914 constraint is weaker than current bounds, it arises entirely from interactions that take place in BH spacetimes with extreme gravity, where one could have expected such effects to be enhanced.
- *Extra dimensions and temporal variation of G*: GW150914 can place constraints on the size of the extra dimension<sup>15</sup> and any time-variation in  $G$ , but these are worse than other current constraints, such as those imposed with binary pulsars. This is because these effects enter at  $-4\text{PN}$  order, which implies that binary pulsar observations (as shown in Fig. 4) and BH low-mass X-ray binaries lead to much stronger limits. Constraints that could be placed by space-borne detectors, such as eLISA and DECIGO, could be many orders of magnitude stronger than aLIGO (and competitive with current bounds) [107, 111]. Once more, nonetheless, notice that the GW150914 constraints are unique in that they use data from the extreme gravity regime.

## 2. Effect of higher PN order modifications

One may wonder whether these quantitative details of the theoretical implications of event GW150914 are robust, since we do not possess predictions for the GWs emitted during the entire inspiral-merger-ringdown coalescence that include modifications to Einstein's theory, such as the activation of a scalar field in a vacuum spacetime, or from the presence of large extra dimensions.

<sup>15</sup> The aLIGO constraint on the size of the extra dimension in the RS-II braneworld model is based on the conjecture that classical BHs evaporate [178, 179]. Given that static, brane-localized BH solutions have now been constructed, it is not clear whether classical BHs need to evaporate. If the latter is true, then BH observations cannot be used to constrain the size of extra dimensions in the way discussed here.

This section will demonstrate that it is not *a priori* necessary to have knowledge beyond the leading-order PN modification to derive meaningful implications from GW observations.

Consider the question of how accurately one can constrain a given modified gravity effect from an event like GW150914 that, to within observational uncertainties, appears consistent with GR. For a specific calculation, let us consider a  $-1$ PN deformation from GR, for example as induced by the activation of a scalar monopole charge in EdGB. Since the relevant higher-order PN corrections for EdGB gravity are not yet known, and to have a concrete example, we use the PN expansion computed in BD theory, which is known to 3.5PN order relative to the leading  $-1$ PN order term in the test-particle limit. To this order then, the inspiral Fourier phase is

$$\Phi_I^{\text{BD}}(f) = \Phi_I^{\text{GR}}(f) + \beta_{\text{BD}} (\pi \mathcal{M} f)^{b_{\text{BD}}} \left[ 1 + \sum_{i=2}^5 \delta\phi_i^{\text{BD}}(\eta) (\pi \mathcal{M} f)^{i/3} \right], \quad (33)$$

where  $b_{\text{BD}} = -7/3$  and [74]

$$\delta\phi_2^{\text{BD}} = -\frac{7}{2}\eta^{-2/5}, \quad (34)$$

$$\delta\phi_3^{\text{BD}} = 5\pi\eta^{-3/5}, \quad (35)$$

$$\delta\phi_4^{\text{BD}} = -\frac{350}{9}\eta^{-4/5}, \quad (36)$$

$$\delta\phi_5^{\text{BD}} = \frac{84}{5}\pi\eta^{-1}. \quad (37)$$

Although  $\beta_{\text{BD}} = 0$  for BH binaries even if the BD parameter is finite, one can still estimate the bound on  $\beta_{\text{BD}}$  with GW150914 to see if such a measurement is consistent with the BH no-hair theorem in BD theory. The subsequent coefficients present the familiar structure of the PN series: alternating signs, absence of a relative 0.5PN order modification in the Fourier phase, and growing coefficients as the PN order increases. Of course, this neglects mass-ratio corrections, as the modifications were calculated in the test-particle limit; however, in GR the PN series in the test-particle limit presents more (asymptotic) divergent features than in the comparable-mass limit, i.e. the coefficients of the series grow more rapidly with PN order in the test-particle limit. Thus, by using the  $\delta\phi_i$  above in the test-particle limit we are exaggerating the effect of higher PN terms in the waveform, which will suffice to make conservative statements.

With this in mind, we carried out five different Fisher analysis using the IMRPhenom waveform with the modified phase of Eq. (33): one analysis used only the leading order ( $-1$ PN) phase modification, while the others included higher PN corrections. Figure 5 shows Fisher estimates of the accuracy to which  $\beta_{\text{BD}}$  can be constrained from GW150914 as a function of the highest PN order included in the modified phase. For example,  $n = 0$  corresponds to Fisher studies where the correction to the waveform phase includes the leading-order ( $-1$ PN)

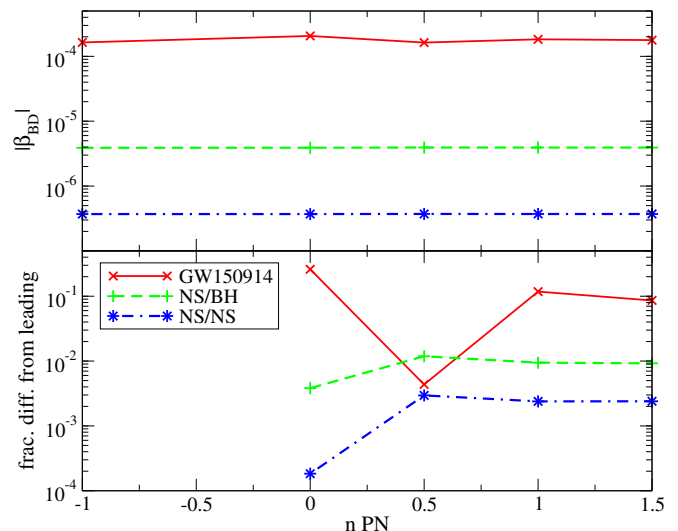


FIG. 5. (Color online) (Top) Fisher estimates of the accuracy one can constrain the ppE parameter  $\beta_{\text{BD}}$  at  $-1$ PN with GW150914, as a function of the highest PN order included in the modified waveform phase. The bound at  $-1$ PN order is the same as that in Fig. 4. For reference, we also show the bound from a NS/BH and NS/NS binary with  $\text{SNR}=24$ , and with masses  $(10, 1.4)M_{\odot}$  and  $(1.5, 1.3)M_{\odot}$  respectively. (Bottom) The absolute fractional difference of the bound on  $|\beta_{\text{BD}}|$  as a function of PN order. Observe that including higher order corrections only affects the bound obtained with only the leading PN order phase correction by at most  $\mathcal{O}(10\%)$  for GW150914. The fractional difference for the NS/BH and NS/NS binary is even smaller.

piece and its first PN-order correction (0PN). Observe that including higher-order PN terms barely modifies the strength of the constraint one can place on  $\beta_{\text{BD}}$ . If the event has already been shown to be consistent with GR and all one is trying to do is constrain deviations from Einstein's theory, then including only the leading-order PN term in the analysis suffices.

To show that the behavior described in the previous paragraph is not specific to BH binaries, we also present in Fig. 5 how higher PN corrections in BD affect the measurement accuracy of  $\beta_{\text{BD}}$  with a NS/BH and NS/NS binary, with masses  $(10, 1.4)M_{\odot}$  and  $(1.5, 1.3)M_{\odot}$  respectively. To compare with the GW150914 result, we set the SNR to 24. We still use the IMRPhenom waveform and neglect any finite size effects in NSs, which would first enter at 5PN order [180] and thus be weakly correlated with  $\beta_{\text{BD}}$ . We also neglect conservative corrections to the waveform phase, which are not included in Eqs. (34)–(37) and are absent for BH binaries in the test-particle limit [74]. Figure 5 shows that the higher PN order corrections in NS/BH and NS/NS binaries are even less important than in BH/BH binaries. This is because at a fixed frequency, the orbital velocity of the binary constituents is smaller for the former, which makes the higher order PN effects less important.

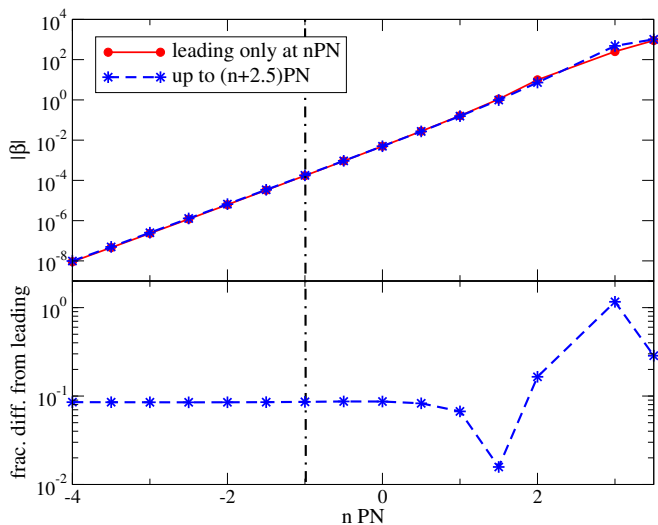


FIG. 6. (Color online) (Top) Upper bound on the leading ppE parameter  $|\beta|$  with only the leading PN correction at  $n$ PN order added (red solid) and with relative corrections the same as BD theory added up to  $(n + 2.5)$ PN order (blue dashed). The vertical dotted-dashed line shows  $n = -1$ , which corresponds to the case shown in Fig. 5. (Bottom) Fractional difference between the two curves in the top panel. Observe that such a difference generally becomes larger for high PN terms but is smaller than  $\sim 20\%$  in most cases.

How do higher PN order corrections affect constraints on ppE parameters in theories other than BD? To a limited extent, we can address this question by repeating the calculation presented above (for the GW150914 case), but varying  $b_{\text{BD}}$  in Eq. (33), instead of fixing it to  $-7/3$ . The top panel of Fig. 6 compares constraints on the ppE parameter  $\beta$  obtained with only the leading PN order correction (red solid) and with corrections up to 2.5PN order higher than the leading order term (blue dashed). To model the latter, we adopt the same relative corrections from the leading order term as in the BD case. The bottom panel shows the fractional difference of the two constraint curves. Observe that the difference remains around 10% for all  $n \leq 1$ . Although this difference generally grows with  $n$ , it typically remains smaller than  $\sim 20\%$  in most cases. When  $n = 3$ , a partial degeneracy with the phase of coalescence at 2.5PN order deteriorates the bound, but this can be ameliorated by removing  $\phi_c$  from the parameter list.

Given this analysis, we conclude that higher PN order corrections are typically subdominant, even if the leading-order correction enters at a PN order other than  $-1$ PN, provided the relative sizes of the terms are comparable or smaller than those in BD theory. On the other hand, if a theory contains more than a single coupling parameters (such as in EA theory), higher PN order corrections will not simply be proportional to the leading order term. In such cases, including more than the leading-order PN term in the waveform phase is critical

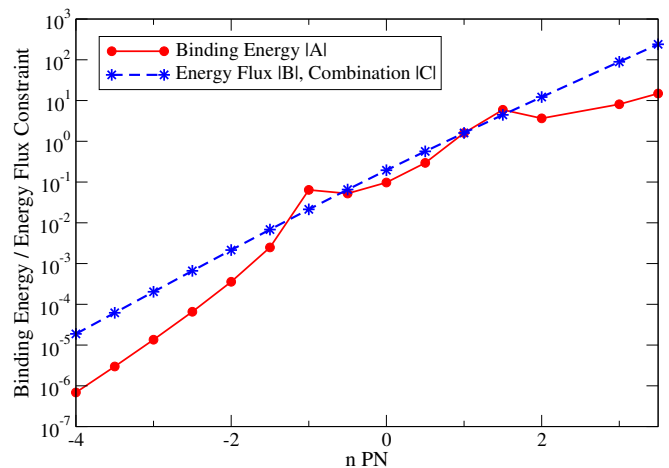


FIG. 7. (Color online) Upper bound on corrections to the binding energy  $|A|$ , energy flux  $|B|$  [see Eq. (38)] and a combination of these two  $|C|$  [see Eq. (39)] as a function of the PN order that they enter.

to break degeneracies between the coupling parameters. Moreover, if the modified gravity effect one is trying to constrain does not admit a PN expansion of Taylor form, as is the case during dynamical scalarization in scalar-tensor theories [118], then higher PN order terms would of course be intrinsically important to resolve the nonlinearities.

Whether one should include higher PN order terms in modified waveforms, of course, depends sensitively on whether the event in question has been shown to be consistent with GR or not. Let us imagine that a new GW observation is made. The first step should then be to determine whether this is consistent with GR or whether anomalies are present in the data. The verification of consistency can be made through the residual SNR argument suggested in [76, 109, 181] and performed for GW150914 by the LIGO/Virgo collaboration [12]. The search for anomalies could be done through a parameterized model, as the ppE framework<sup>16</sup>. Reference [104] has shown that using a single parametric deformation in the waveform phase is ideal to *detect* anomalies; the inclusion of simultaneous multiple deformations dilutes the power of such an analysis. However, it was further shown that if an anomaly is present, a single parametric deformation will not be able to pinpoint exactly what type of modification to GR is present in the data. It is only in such cases, i.e. when the data points to the presence of a statistically significant anomaly, that a higher PN order parametric deformation would be necessary to properly characterize it.

<sup>16</sup> Note that absence of a residual from the best-fit GR template does not necessarily imply the data is also consistent with the absence of anomalies, as in some cases a parameter bias in the GR template could “fit” the anomaly.

### 3. Generic Constraints in the Generation of GWs

What other generic features of GR in the generation phase can GW150914 constrain? To address this question, here we map the constraints on the ppE parameter  $|\beta|$  in Fig. 4 to those on generic corrections to the binding energy  $E_b$  of a binary and the radiated energy flux  $\dot{E}$ . We follow the ppE treatment of [114] and model such corrections as

$$E_b = E_{b,\text{GR}} (1 + Av^{2p}), \quad \dot{E} = \dot{E}_{\text{GR}} (1 + Bv^{2q}), \quad (38)$$

where  $v = (\pi m f)^{1/3}$  corresponds to the relative orbital velocity, while  $E_{b,\text{GR}}$  and  $\dot{E}_{\text{GR}}$  denote the binding energy and energy flux in GR. Non-GR fractional corrections to  $E_b$  and  $\dot{E}$  have a magnitude  $A$  and  $B$  that enter first at  $p$  and  $q$  PN order respectively. Such corrections propagate to those in the gravitational waveform phase. When  $p < q$ , the dominant non-GR effect comes from the correction to the binding energy; we do not know of any theory where this is the case. When  $p > q$ , the dominant effect comes from the correction to the energy flux; examples of this include BD, EdGB and EA theory. When  $p = q$ , both corrections to  $E_b$  and  $\dot{E}$  are of comparable PN order, as is the case in dCS gravity. The mapping between these parameters and  $\beta$  is given by [114]

$$\beta = \begin{cases} -\frac{5}{32} \frac{5p^2 - 2p - 6}{(4-p)(5-2p)} A & (p < q), \\ -\frac{15}{32} \frac{1}{(4-q)(5-2q)} \eta^{-2q/5} B & (p > q), \\ -\frac{15}{32} \frac{1}{(4-k)(5-2k)} \eta^{-2k/5} C & (p = k = q), \end{cases} \quad (39)$$

with  $C \equiv [(5k^2 - 2k - 6)A + 3B]/3$ .

Figure 7 presents the upper bound on  $|A|$ ,  $|B|$  and  $|C|$  obtained by mapping the bound on  $|\beta|$  in Fig. 4 via Eq. (39). This figure shows that GW150914 bounds the magnitude of corrections to  $E$  and  $\dot{E}$  to be significantly smaller than unity in the negative PN region. Since the mapping for  $p > q$  and  $p = k = q$  has the same structure, the bound on  $|B|$  and  $|C|$  coincide. Notice that  $\beta$  with  $p < q$  vanishes when  $p = (1 \pm \sqrt{31})/5 \sim -0.91$  and  $1.3$ , and hence, the constraint on  $|A|$  becomes significantly weaker close to these two values of  $p$ .

These generic constraints on the binding energy and energy flux can be used to place bounds on generic scalar field interactions in any theory. For example, if the BH components of a binary acquire scalar hair of  $\ell$ th multipole order (or  $\ell$ th scalar hair), the interaction of these hairs will produce a correction to the binding energy at  $2\ell$  PN order and a correction to the energy flux at  $(3\ell - 1)$  PN order [110]. The scalar field in EdGB gravity and in scalar-tensor theories gives rise to BH scalar hair of  $\ell = 0$  (monopole) multipole order, which modifies the binding energy and energy flux at 0PN and  $-1$ PN order respectively, with the latter being the well-known dipole radiation effect. On the other hand, in dCS gravity BHs acquire scalar hair of  $\ell = 1$  multipole order, and thus, the correction to the binding energy and en-

ergy flux enter both at 2PN order, with the latter being scalar quadrupolar radiation.

Another generic feature that GW150914 can constrain is the sudden activation or deactivation of dipole radiation at a given transition frequency  $f_*$  during BH binary inspirals. Such an abrupt activation and deactivation is known to arise in certain modified theories in the presence of matter. An example is *dynamical* scalarization in scalar-tensor theories [17–19, 118, 182, 183], during which the scalar charge of a NS in the binary grows suddenly at a given threshold binding energy or frequency, abruptly turning dipole radiation on. A similar mechanism arises in scalar-tensor theories without dynamical scalarization but with a massive scalar field [74, 184–186], during which the scalar dipole radiation activates at a transition frequency related to the mass of the scalar field. Scalar field deactivation occurs in scalar tensor theories that allow for *induced* scalarization [17, 18, 157, 158], during which the scalar charge of one of the NSs in the binary induces a scalar charge in its binary companion, suppressing scalar dipolar radiation since this is proportional to the square of the difference in scalar charge [17, 18].

Whether a sudden activation or deactivation of dipole radiation is possible in vacuum spacetimes has not been investigated in the theoretical realm. One possibility is to consider EdGB gravity with a massive scalar field, in which case one would expect scalar dipole radiation to turn on at a threshold frequency related to the scalar mass. A mass for the EdGB (dilaton) scalar field could arise due to super-symmetry breaking [187], in which case the mass would be of the order of the super-symmetry breaking scale. If one wishes for super-symmetry to resolve the hierarchy problem, then this scale must be larger or comparable to  $10^{12}$  eV, which then leads to a very massive dilaton, and thus, a very high threshold frequency that is well outside what can be probed with GW150914. Another possibility is to consider scalar-tensor theories with non-trivial initial data [20] for the scalar field, in which case the scalar field will evolve until it is absorbed by the BHs or it scatters to infinity, at which point dipole radiation will cease. The deactivation of dipole radiation in a vacuum spacetime could be present if Kerr BHs can acquire scalar hair and then lose it during the inspiral, which could occur in GR [81, 188–190] and in (complex-boson) scalar-tensor theories [191].

Observations of GWs with aLIGO can constrain such sudden scalar field activation, as first studied in [76]. This work showed through a Bayesian, model-hypothesis study that the simplest (one-parameter) ppE model is sensitive to a sudden turn on/off of dipole radiation if present in the data. Furthermore, a modification where this ppE model's phase term is multiplied by a Heaviside function with a new threshold frequency parameter was shown to be effective at detecting an abrupt activation or deactivation of dipole radiation anywhere in the aLIGO band.

GW150914 can thus place generic constraints on abrupt dipole-like changes to GW generation. The red

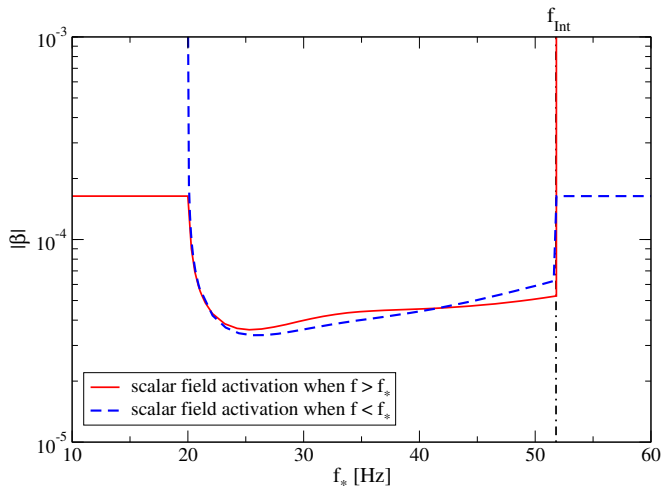


FIG. 8. (Color online) 90%-confidence upper bound on the ppE parameter  $|\beta|$  at  $-1$ PN as a function of the transition frequency  $f_*$ , for theories in which the scalar field only activates when  $f > f_*$  (red solid) and  $f < f_*$  (blue dashed). The vertical dotted-dashed line corresponds to the transition frequency  $f_{\text{Int}}$  between the inspiral and intermediate phase in the IMRPhenom waveform.

solid (blue dashed) curve in Fig. 8 presents the upper bound on  $|\beta|$  at  $-1$ PN versus  $f_*$ , assuming that the scalar field only activates when  $f > f_*$  ( $f < f_*$ ). Since the correction is included in the inspiral phase only, one cannot place constraints in the region  $f_* > f_{\text{Int}}$  ( $f_* < 20$ Hz) with this method, where  $f_* = f_{\text{Int}}$  is shown by the vertical dotted-dashed line. Observe that the constraint becomes stronger when the scalar field evolves during the observed inspiral phase ( $20\text{Hz} < f_* < f_{\text{Int}}$ ) compared to the case where the scalar field has already activated before the signal enters the aLIGO observation band ( $f_* < 20$ Hz) or deactivates in the post-inspiral phase ( $f_* > f_{\text{Int}}$ ). For example, when the scalar field activates at  $f > f_*$  (red solid curve), the constraints on  $|\beta|$  with  $f_* = 40$ Hz (the scalar field activates while the signal is in the observational frequency band of aLIGO) and  $f_* = 10$ Hz (the scalar field is already activated when the signal enters the band) are  $|\beta| < 4.5 \times 10^{-5}$  and  $|\beta| < 1.6 \times 10^{-4}$  respectively. This is because the former has a very distinct feature which helps break degeneracies between  $\beta$  and other parameters. Observe also that the constraint on  $|\beta|$  does not go smoothly to infinity at  $f_* = f_{\text{Int}}$ . This is because when  $f_* < f_{\text{Int}}$  ( $f_* > f_{\text{Int}}$ ), the correction introduced in the inspiral phase also propagates to intermediate and merger-ringdown phases through the smooth matching condition of the phase at interfaces, while such corrections disappear completely from the template when  $f_* > f_{\text{Int}}$  ( $f_* < f_{\text{Int}}$ ) (see Appendix B for a related discussion).

### C. Implications on the Propagation of GWs

We now study how strongly one can constrain the modified dispersion relation of the graviton using event GW150914 (see also [192, 193] for possible constraints on the equivalence principle with GW150914 through a Shapiro time delay measurement). As described in Sec. II B 3, we include  $\beta_{\text{MDR}}$  in Eq. (26) in the IMRPhenom waveform in all phases (inspiral, merger and ringdown). We then carry out a Fisher analysis and derive upper bounds on  $|\mathbb{A}|$  as a function of  $\alpha$ . Such an analysis corresponds to extending that in [115] by including also the merger and ringdown effects and using the specific parameters of event GW150914.

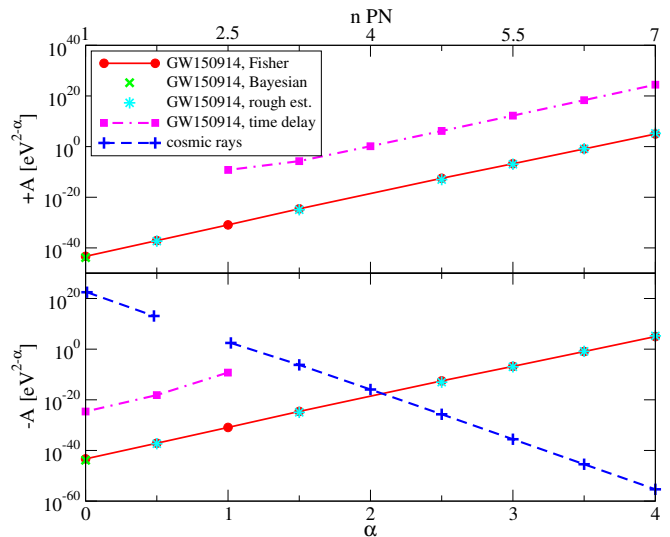


FIG. 9. (Color online) Upper bound on the amplitude of the correction to the graviton dispersion relation  $\mathbb{A}$  in Eq. (25) from GW150914 as a function of  $\alpha$  in the  $\mathbb{A} > 0$  (top) and  $\mathbb{A} < 0$  (bottom) obtained from 90-% confidence constraints on the ppE parameter  $\beta$ . The top axis shows the corresponding PN order at which the correction enters. The red circles are the Fisher estimates derived in this paper, while the green crosses are a mapping of the Bayesian bound in [12] on the graviton mass through  $m_g = \sqrt{\mathbb{A}}$  at  $\alpha = 0$ . Cyan stars are rough bounds on  $\mathbb{A}$  in Eq. (40) based on the Bayesian bound at  $\alpha = 0$ . The magenta squares correspond to a bound derived from the time of arrival of GW150914 at Hanford and Livingston [64]. Blue pluses present the bound on  $\mathbb{A}$  from the absence of gravitational Cherenkov radiation in cosmic ray observations [63], assuming that cosmic ray particles of  $p = 10^{11}$  GeV arrives from a distance of 100Mpc; these cannot constrain  $0.5 \leq \alpha \leq 1$ . The GW150914 observation constrains  $|\mathbb{A}|$ , while cosmic ray observations only constrain the negative sector of  $\mathbb{A}$ . Observe that the former places a stronger bound on the  $\mathbb{A} < 0$  region than the latter for  $\alpha \lesssim 2$ , while it places a unique bound on the  $\mathbb{A} > 0$  region.

The upper bound on  $|\mathbb{A}|$  from event GW150914 using a Fisher analysis is shown with red circles in Fig. 9. We do not show the bound at  $\alpha = 2$  as  $\beta_{\text{MDR}}$  is degenerate with  $t_c$  in this case. For reference, we also show the

bound on the super-luminal propagation of GWs with magenta squares, derived in [64] from the difference in arrival times at Hanford and Livingston. When mapping the bound in [64] to that on  $\mathbb{A}$  in Fig. 9, we assumed a GW frequency of  $f = 100\text{Hz}$ , corresponding to roughly the peak of the GW150914 signal. Observe that the new Fisher constraint is always stronger than the bound from the arrival time delay of GWs by roughly 20 orders of magnitude.

The constraints presented in Fig. 9 imply a constraint on the mass of the graviton (see also [194] for other constraints on the graviton screening mass from GW150914.) In massive gravity, assuming a simple dispersion relation,  $\mathbb{A} = m_g^2$  with  $\alpha = 0$ . Therefore, the GW150914 event places a bound of  $m_g < 2.2 \times 10^{-22}\text{eV}$  or a bound on the graviton Compton wavelength of  $\lambda_g > 5.8 \times 10^{12}\text{km}$ . Such bounds derived from a Fisher analysis are in good agreement with the bounds derived from a Bayesian analysis by the LIGO/Virgo collaboration [12], as summarized in Table I and shown in Fig. 9 with green crosses. This GW bound is a few times stronger than the current Solar System constraint [58] and more than two orders of magnitude stronger than the binary pulsar one [59], although comparable to the superradiance bound of [62]. On the other hand, it is weaker than the bound from galaxy cluster observations [60, 61], though the latter have larger systematic errors due to uncertainties in the dark matter distribution of the Universe.

The above GW bound on  $m_g$  can be applied to massive gravity theories, such as Fierz-Pauli theory [195] and Lorentz-violating massive gravity [128, 196, 197]. Although the former suffers from Boulware-Deser ghosts [198, 199], such ghosts are absent in the latter. Moreover, the latter can be extended into a UV completed theory [200]. On the other hand, the bound on the graviton mass presented above cannot be applied to theories like bigravity [201], as gravitons oscillate between physical and reference sectors and the dispersion relation becomes much more complicated [202, 203].

Let us now derive a simple, approximate expression for the GW150914 bound on  $\mathbb{A}$ . The Bayesian bound on  $m_g$  in [12] can be interpreted as a constraint on the propagation speed of GWs,  $|\delta_g| \equiv |1 - v_g/c| \lesssim 4.5 \times 10^{-20}$  assuming  $f = 100\text{Hz}$ . Reference [86] obtained the rough bound  $|\mathbb{A}| \lesssim 10^{-5}\text{eV}^{-1}$  for  $\alpha = 3$  from the constraint on  $\delta_g$  at  $\alpha = 0$  [12] by assuming that the latter is comparable to the bound on  $\delta_g$  when  $\alpha = 3$ . When one repeats the calculation with the dispersion relation presented above and the  $\alpha = 3$  case, one finds the constraint  $|\mathbb{A}| \lesssim 10^{-7}\text{eV}^{-1}$ , which is consistent with the Fisher analysis to roughly  $\sim 30\%$ . Applying the same assumption to arbitrary  $\alpha$ , one finds the rough bound

$$|\mathbb{A}| \lesssim \frac{1.5 \cdot 10^{-44}}{1 - \alpha} \left( \frac{10^{13}}{4.1} \right)^\alpha \left( \frac{f}{100\text{Hz}} \right)^{-\alpha} \quad (\alpha \neq 1). \quad (40)$$

These rough bounds are shown with cyan stars in Fig. 9, which give the correct order of magnitude estimate to

roughly 70%.

For reference, we also show the upper bound on  $-\mathbb{A}$  from the absence of gravitational Cherenkov radiation in cosmic ray observations [63] in Fig. 9. Notice that such an observation can only constrain the negative  $\mathbb{A}$  sector, i.e. when  $\mathbb{A} < 0$ . Observe that in this sector, the GW bound is stronger relative to the cosmic ray bound when  $\alpha \lesssim 2$ . On the other hand, in the positive  $\mathbb{A}$  sector, the GW event places a unique constraint. The GW bound, unfortunately, is very weak for high values of  $\alpha$ . For example, when  $\alpha = 3$  or 4, the bound on  $\mathbb{A}$  normalized to the Planck energy  $E_p$  becomes  $|\mathbb{A}E_p| < \mathcal{O}(10^{20})$  and  $|\mathbb{A}E_p^2| < \mathcal{O}(10^{60})$  respectively. The GW bound on  $\mathbb{A}$  when  $\alpha = 3$  and  $\alpha = 4$  is summarized in Table I.

One can easily map the constraint on  $\mathbb{A}$  in Fig. 9 to a generic gravitational Lorentz violation within the gravitational SME context. In fact, Kostelecky and Mewes [146] derived constraints on certain coefficients in this framework using the GW150914 event and its apparent lack of birefringence; the latter modifies the real part of the dispersion relation, which then modifies the propagation speeds of the plus and cross polarization modes<sup>17</sup>. Since the bound presented in Fig. 9 comes from the effect of a modified dispersion relation on the GW phase, it constrains a different aspect in the theory. Although the GW bound from Fig. 9 are likely to be weaker than the bound on SME parameters from gravitational Cherenkov radiation [204], the former are cleaner in the sense that they are bounds on the pure-gravity sector, whereas the latter is affected by the coupling between the matter and gravity sectors. In fact, gravitational Cherenkov radiation may even be forbidden for certain ranges of the coefficients and the bound from such radiation becomes invalid in such cases.

#### IV. THEORETICAL IMPLICATIONS ON EXOTIC SPACETIMES

The observation of the ringdown of GW150914 has been taken to mean that the object formed was a Kerr BH, a fact that can then be used to place stringent constraints on the existence of exotic compact objects. For example, Ref. [30] compared the measured ringdown frequency and damping time of GW150914 with the QNMs of a rotating gravastar, and found that the GW150914 remnant is unlikely to be such an object. Similarly, Ref. [205] compared the same frequency and damping time to the dominant QNM of a scalar field propagating

<sup>17</sup> The absence of the birefringence in GW150914 can either mean that Lorentz violation effects are too small that the delay in the arrival time between the two tensor modes were not detected, or such effects are too large that the slower mode arrived when the detector was offline or has not even arrived yet. Reference [146] assumed the former, but due to the possibility of the latter, one can only exclude a certain finite range in the parameter space of the Lorentz violation coefficients in gravitational SME.

in a parametrically deformed Kerr spacetime to place a constraint on the latter, which was naturally found to be degenerate with the spin of the deformed Kerr object. Such tests, and the overall line of reasoning, however, is much more nuanced than it would at first seem for the following three reasons.

First, such tests require that one chooses an exotic compact object or a specific Kerr deformation to compare GW150914 against, but there are many alternatives, most of which have severe theoretical problems from the start. The gravastars used in [30], for example, are “cut-and-paste” spacetimes where an interior de Sitter metric is glued to an exterior Schwarzschild metric through a boundary layer of exotic matter; such constructions are not realized naturally in GR or in any known modified theories of gravity. Moreover, all horizonless compact objects with stable circular photon orbits, including gravastars, are likely to be unstable due to ergoregion instabilities if they are spinning rapidly [206, 207]. The deformed Kerr metric used in [205] has an identical quadrupole moment to Kerr, but with a “shifted” event horizon. Yet, no known theory predicts such a deformed metric, and thus it is unclear what new physics this metric encodes.

Second, the observation of the beginning of the ringdown (right after merger) is not necessarily sufficient to distinguish between exotic compact objects that possess similar light rings. Recently, Refs. [31, 208, 209] argued that the frequency and damping time of the GWs emitted during the beginning of the ringdown are related to the orbital frequency and the instability timescale of circular null geodesics, associated in turn with the light ring of the spacetime. This is the case even if the GWs emitted at late times, when the QNMs dominate, are drastically dissimilar for different exotic compact objects, as is the case for gravastars or certain parametric deformations of the Kerr spacetime. GW150914 did not have a SNR large enough to measure the late-time, purely QNM-dominated phase of the signal if the amplitude of such QNMs is small, and so it cannot constrain all exotic BH alternatives.

Third, pure ringdown tests of the Kerr hypothesis – that the exterior metric of compact objects is given by the Kerr metric – do not address how the perturbed Kerr spacetime arose to begin with. For GW150914 the presumed Kerr remnant is clearly produced by the inspiral of two compact objects, each consistent with being Kerr BHs as well. That the properties of this phase (e.g. its duration, power spectrum, etc.) must match the binary merger problem in GR to a level consistent with the aLIGO observation places stringent constraints on the dynamics of the compact objects that merged. It is arguable then whether alternatives such as gravastars or parametrically deformed BHs, that do not have a sound theoretical underpinning to describe their dynamics during a collision, can be taken seriously in light of the data presented by GW150914; this is so even for use as an “in-principle” caveat to the evidence GW150914 provides for the existence of BHs.

With this in mind, this section explores the theoretical implications that one can infer from event GW150914 on the nature of exotic spacetimes from the combined late-inspiral, merger and ringdown. We begin by describing how the connection between the inspiral, merger and ringdown can provide information about the spacetime through the location of an effective ISCO, and how this could place constraints on modified gravity theories and on generic metric deformations. Unlike the prior study in [205], we use the entire late-inspiral, merger and ringdown phases of the GW150914 event, in a similar fashion to the consistency test carried out by the LIGO/Virgo Collaboration comparing the final mass and spin of the remnant extracted separately from the inspiral vs. post-inspiral segments of the data [12].

Next, we study what inferences one can draw from GW150914 on the nature of an exotic compact object remnant without appealing to any particular theory. We cast these inferences in the form of effective bulk and shear viscosities that would be required to explain the rapid damping time that aLIGO measured, assuming the bulk dynamics of the remnant can be characterized by viscous hydrodynamics (with appropriately exotic equation of state and transport properties). Even for non-material exotic alternatives this could still be a useful way to understand their dynamical behavior, akin to the membrane paradigm description of BHs in GR [210]. We then study how the GW150914 observation constrains the amplitude of a second oscillation mode, which can be either a higher-order, subleading BH QNM or a mode caused by additional matter oscillations of an exotic compact object. In contrast to other work [30], our analysis is model independent and we do not assume specific properties of such exotic compact objects. We conclude by discussing how our result can be used to constrain actual QNMs of exotic compact objects with a light ring [31, 208, 209].

### A. Implications on the ISCO Properties

GW150914 is a so-called golden binary merger event, defined as one that allows the accurate extraction of the total mass lost during the merger [77]. Using such binaries, one can, for example, first estimate the final mass  $m_f$  and the magnitude of the spin parameter vector  $a_f$  (where  $a_f = |\vec{a}_f| = |\vec{S}_f|/m_f$ , with  $\vec{S}_f$  the final spin angular momentum) of the remnant BH after merger from the inspiral part of the GWs using the phenomenological fit in [211, 212] and assuming GR is correct. One can then compare this fitted prediction to the posterior distribution of the mass and spin parameter of the remnant BH extracted using only the ringdown part of the waveform; the posterior then provides a set of best-fit parameters from its peak, and  $1\sigma$  errors  $\Delta m_f$  and  $\Delta a_f$ . The power of such a test was demonstrated using both Fisher [213] and Bayesian [214] methods very recently. The latter method was applied to the GW150914 data [12], demon-

strating consistency with GR, albeit with a relatively large 90% confidence contour about the GR value in the  $(\Delta m_f/m_f, \Delta a_f/a_f)$  plane, due to the low (for this test) SNR of the ringdown part of the event.

Inspired by these results, here we pursue a different approach to probe the extreme gravity nature of the compact objects that produced event GW150914. In GR, Refs. [78] proposed that the final spin angular momentum  $\vec{S}_f$  of a BH after merger with  $m_f \sim m$  (the difference between  $m_f$  and  $m$  is not significant in their analysis) is approximately given by the sum of the two individual spin angular momenta before merger and the orbital angular momentum of a “test particle” with mass  $\mu \equiv m\eta$  ( $m = m_1 + m_2$ ) at  $r_{\text{ISCO}}$  orbiting around a Kerr BH with this final spin:

$$\vec{S}_f = \vec{L}_{\text{orb}}(\mu, r_{\text{ISCO}}, a_f) + \vec{S}_1 + \vec{S}_2. \quad (41)$$

Indeed, this equation correctly reproduces numerical relativity simulations of the magnitude of the final BH spin after a merger of two non-spinning BHs within an error of  $\sim 3\%$  [78]; one could use a more accurate fit that includes precession, such as that in [212], but we leave such refinements to future work. Taking the projection of Eq. (41) along the unit orbital angular momentum vector  $\hat{L} = \vec{L}_{\text{orb}}/|\vec{L}_{\text{orb}}|$ , and substituting in that the spin angular momentum of BH  $A$  with mass  $m_A$  and (dimensional) spin vector  $\vec{a}_A$  is  $\vec{S}_A = m_A \vec{a}_A$ , we can re-arrange this equation to obtain

$$\frac{L_{\text{orb}}(\mu, r_{\text{ISCO}}, a_f)}{m^2} = \frac{a_{\parallel f}}{m} - \frac{a_{\parallel s}}{m} - \delta_m \frac{a_{\parallel a}}{m}, \quad (42)$$

where  $\vec{a}_s \equiv (\vec{a}_1 + \vec{a}_2)/2$  and  $\vec{a}_a \equiv (\vec{a}_1 - \vec{a}_2)/2$  are the symmetric and antisymmetric combinations of the spin vector,  $\delta m = (m_1 - m_2)/m$ , and the subscript  $\parallel$  denotes projection of the corresponding vector quantity along  $\hat{L}$ . We then see that a measurement of the individual component spins of the binary and of the final spin of the merged object can be used to infer the location of the ISCO through  $L_{\text{orb}}$ .

Let us determine what the dominant source of error in the above equation is. The individual masses and the individual dimensionless spins associated with event GW150914 were determined to be  $(m_1, m_2) = (35.7_{-3.8}^{+5.4}, 29.1_{-4.4}^{+3.8})M_{\odot}$  and  $(\chi_1, \chi_2) := (|\vec{a}_1|/m_1, |\vec{a}_2|/m_2) = (0.31_{-0.28}^{+0.48}, 0.46_{-0.42}^{+0.48})$  [65]. The LIGO/Virgo collaboration also found that the so-called effective dimensionless spin  $\chi_{\text{eff}}$ , related to the projected symmetric spin combination by  $a_{\parallel s} = m\chi_{\text{eff}}/2$ , could be extracted to  $\chi_{\text{eff}} = -0.06_{-0.18}^{+0.17}$  [65]. From the merger-ringdown phase, the final dimensionless spin was measured to be  $\chi_f := |\vec{a}_f|/m_f = 0.67_{-0.57}^{+0.2}$  [12], where we assumed the mean value to correspond to that derived from a full inspiral-merger-ringdown analysis. To apply these aLIGO measurements to Eq. (42), for simplicity, we assume  $a_{\parallel f} = |\vec{a}_f|$ , namely the final spin is aligned with the orbital angular momentum. We also neglect contributions from the second and third terms in Eq. (42)

since the former has been shown to be small from the measurement of  $\chi_{\text{eff}}$ , while the latter is suppressed by a factor of  $\delta_m \sim 0.1$ . Using the error on  $\chi_f$  from the merger-ringdown phase to estimate the error on  $L_{\text{orb}}$  in the GW150914 event, we find

$$\frac{L_{\text{orb}}(\mu, r_{\text{ISCO}}, a_f)}{m^2} \approx 0.67_{-0.57}^{+0.2}. \quad (43)$$

The above calculation suggests that GW observations can constrain the predicted orbital angular momentum of a test particle at the ISCO but a strong caveat is here needed: such a constraint is only valid provided the mapping constructed in [78] remains valid when non-GR physical mechanisms are active, i.e. if the non-GR contribution to the total angular momentum radiated during merger is negligible compared to the non-GR correction to the orbital angular momentum at ISCO and its location for a rotating BH. Whether this is the case or not depends on the particular theory in question and should be studied through numerical simulations on a case-by-case basis.

Assuming the mapping in Eq. (41) holds, we can then study the theoretical physics implications of Eq. (43) on the hypothesis that the spacetime of BHs is that of the Kerr metric. This Kerr hypothesis is violated in a large class of modified gravity theories, where the orbital angular momentum of a test particle at the equatorial ISCO can be written as

$$\begin{aligned} L_{\text{orb}}(r_{\text{ISCO}}) &= L_{\text{orb}}^{\text{Kerr}}(r_{\text{ISCO}}^{\text{Kerr}}) \\ &+ \zeta \left[ \left. \frac{\partial L_{\text{orb}}^{\text{Kerr}}}{\partial r} \right|_{r_{\text{ISCO}}^{\text{Kerr}}} \delta r_{\text{ISCO}} + \delta L_{\text{orb}}(r_{\text{ISCO}}^{\text{Kerr}}) \right] \\ &+ \mathcal{O}(\zeta^2). \end{aligned} \quad (44)$$

We have here expanded to linear order in the small deformation parameter  $\zeta$ , modeling the angular momentum of a test particle as  $L_{\text{orb}} = L_{\text{orb}}^{\text{Kerr}} + \zeta \delta L_{\text{orb}}$  and the location of the ISCO as  $r_{\text{ISCO}} = r_{\text{ISCO}}^{\text{Kerr}} + \zeta \delta r_{\text{ISCO}}$ . The GW150914 event then places a constraint on the combination

$$\frac{1}{m^2} \left( \left. \frac{\partial L_{\text{orb}}^{\text{Kerr}}}{\partial r} \right|_{r_{\text{ISCO}}^{\text{Kerr}}} \delta r_{\text{ISCO}} + \delta L_{\text{orb}}(r_{\text{ISCO}}^{\text{Kerr}}) \right) \lesssim \mathcal{O}(1), \quad (45)$$

where on the right-hand we have used that the error in Eq. (43) is of order unity. Notice that this constrains a *combination* of the modification to the angular momentum of a test-particle in a non-Kerr spacetime and a modification to the location of the ISCO. Notice also that the intrinsic error of  $\sim 3\%$  in Eq. (42) for BH binary mergers in GR (due to neglecting the radiated angular momentum at merger) does not affect our test of the Kerr hypothesis through Eq. (45) since the error on the right-hand side of this equation is much larger.

The constraint above can be refined further by specifying a parametrically deformed Kerr spacetime [80, 113, 215–225]. Only to give a concrete example, let us consider the quasi-Kerr metric [80], which is constructed to

represent a deformation to the Kerr metric through a correction in its quadrupole moment

$$Q = Q_K \left( 1 + \frac{\zeta_{\text{QK}}}{\chi^2} \right), \quad (46)$$

where  $\zeta_{\text{QK}}$  is supposed to be a small (dimensionless) deformation parameter that controls the magnitude of the Kerr deviation. One can compute the orbital angular momentum and the shift in the location of the ISCO for a test-particle in an equatorial orbit of the quasi-Kerr metric. Using these results in Eq. (43) or (45), one finds  $-2.0 \lesssim \zeta_{\text{QK}} \lesssim 5.3 \times 10^{-3}$ , which is a constraint of order unity in the deformation parameter.

A final refinement of this constraint is to consider specific modified gravity theories that violate the Kerr hypothesis, such as EdGB and dCS gravity [45, 79]. In these two theories, the location of the ISCO is modified from the GR prediction by [45, 79]

$$\delta r_{\text{ISCO}}^{\text{EdGB}} = -\frac{16297}{9720} \zeta_{\text{EdGB}} \times \left( 1 + \frac{205982\sqrt{6}}{440019} \chi - \frac{1167369773}{9702418950} \chi^2 \right), \quad (47)$$

$$\delta r_{\text{ISCO}}^{\text{CS}} = \frac{77\sqrt{6}}{5184} \zeta_{\text{CS}} \chi \left( 1 - \frac{9497219}{19559232} \chi \right), \quad (48)$$

while corrections to the orbital angular momentum can be found in Eq. (68) of [79] and Eq. (99) of [45], assuming slowly-rotating BHs to quadratic order in spin and working in the small-coupling approximation  $\zeta \ll 1$  (where recall that  $\zeta_{\text{EdGB}} \geq 0$  and  $\zeta_{\text{CS}} \geq 0$  by definition). Substituting these expressions in Eq. (43) or (45) and truncating all expressions at quadratic-order in spin, we find the constraints  $\zeta_{\text{EdGB}} \lesssim 5.2$  and  $\zeta_{\text{CS}} \lesssim 1.2 \times 10^3$ .

These bounds, however, are not compatible with the small-deformation or small-coupling approximations used to derive the above expressions. For example, the constraints on the quasi-Kerr metric, or on EdGB and dCS gravity, are only valid when  $|\zeta_{\text{QK}}| \ll 1$ ,  $\zeta_{\text{EdGB}} \ll 1$  and  $\zeta_{\text{CS}} \ll 1$ , since these approximations are heavily used to construct the spacetime and compute the corrections to the orbital angular momentum and the location of the ISCO. Thus, we conclude that the GW150914 event cannot place meaningful constraints on mechanisms that modify the orbital angular momentum of a test particle at the ISCO if such a mechanism is built as a small deformation from GR. Either the mechanism must be known to all orders in the deformation parameter, such as in Lorentz violating theories of gravity [160, 161], or we must wait for more accurate GW observations that can constrain  $a_f$  more accurately.

## B. Implications for exotic compact objects

We now consider properties that exotic matter alternatives to BHs would need to have to be consistent with the signal seen by aLIGO.

### 1. Effective Hydrodynamic Properties of Exotic Matter

We begin by treating such exotic compact objects within the framework of hydrodynamics by estimating the *effective* viscosity that would be required to explain the observed damping time,  $\tau = 4\text{ms}$  [12], assuming large amplitude matter oscillations were produced by the merger. There are numerous ways to proceed here, and the specific numbers obtained in the eventual constraints and corresponding effective physical properties they map to will depend on this model. However, we emphasize again that this does not depend on the theory or nature of the exotic compact object; it is merely a way to characterize the properties of the exotic object using a mundane object whose properties we understand.

For simplicity then, we consider our model to be a Newtonian, incompressible star with a density  $\rho$  and radius  $R$ , perturbed by a spherical harmonic mode  $Y_{\ell m}$ , for which the following relationships have been derived [226]:

$$\bar{\eta} = (\ell - 1)(2\ell + 1) \frac{\rho R^2}{\tau_{\bar{\eta}}}, \quad (49)$$

$$\bar{\zeta} = \left( \frac{5}{3} \right)^4 \frac{2(2\ell + 3)}{\ell^3} \frac{\rho R^2}{\tau_{\bar{\zeta}}}, \quad (50)$$

where  $\bar{\eta}$  and  $\bar{\zeta}$  are the shear and bulk viscosity respectively, while  $\tau_{\bar{\eta}}$  and  $\tau_{\bar{\zeta}}$  are the damping time of oscillations associated with each type of viscosity. The least damped mode is  $\ell = 2$ , and is also the dominant GW generating mode that will be present in the initial remnant following a two body, near equal mass collision. Restricting to  $\ell = 2$  then, eliminating  $\rho$  from these expressions with

$$\rho = \frac{m}{(4\pi/3)R^3}, \quad (51)$$

and scaling with a fiducial damping time  $\tau = 4\text{ms}$ , total mass  $m = 65M_{\odot}$  and radius  $R = 370\text{km}$  (twice the Schwarzschild radius of the final BH with mass  $65M_{\odot}$  or the orbital separation at the end of the inspiral  $f = f_{\text{Int}}$ ), we obtain

$$\bar{\eta}_{\text{eff}} \sim 4 \times 10^{28} \frac{\text{g}}{\text{cm} \cdot \text{s}} \left( \frac{m}{65M_{\odot}} \right) \left( \frac{370\text{km}}{R} \right) \left( \frac{4\text{ms}}{\tau_{\bar{\eta}}} \right), \quad (52)$$

$$\bar{\zeta}_{\text{eff}} \sim 3 \times 10^{30} \frac{\text{g}}{\text{cm} \cdot \text{s}} \left( \frac{m}{65M_{\odot}} \right) \left( \frac{370\text{km}}{R} \right) \left( \frac{4\text{ms}}{\tau_{\bar{\zeta}}} \right). \quad (53)$$

Before proceeding, let us make some comments about the effective viscosities derived above. First and foremost, one should realize that the above results should be interpreted as *order-of-magnitude lower limits* to the effective viscosities of the matter comprising the remnant that aLIGO observed, *assuming* the initial amplitude of the  $\ell = 2$  mode was such as to produce a GW signal close to the peak amplitude observed. For a typical material body collision, these viscosities would be a bit of an

over-estimate, as part of the decrease in the amplitude after the two bodies intermingle is simply a decrease in the reduced quadrupole moment, as compared to a binary point-particle system that described the leading-order GW generation (within GR) prior to contact. At the other extreme, if one assumes that this latter effect is entirely responsible for the damping of the signal aLIGO witnessed, one can place fairly strong (upper limit) constraints on the damping time for the leading order matter mode not to have been observed given an initial amplitude of this mode. One can then map such a constraint on the damping time to that on effective viscosities via Eqs. (52) and (53). We will estimate this in Sec. IV B 2, though first we will compare the above lower limits of Eqs. (52) and (53) to effective viscosities of a couple of known compact objects to put these numbers in context.

Let us first compute the viscosities of non-rotating BHs [227, 228] with mass  $M$ . The kinematic viscosity  $\bar{\nu}_{\text{BH}} \sim M$  can be estimated using the membrane paradigm [210, 229], and it is related to the shear viscosity by  $\bar{\eta}_{\text{BH}} = \rho_{\text{BH}} \bar{\nu}_{\text{BH}}$  and to the bulk viscosity by  $\bar{\zeta}_{\text{BH}} = -\bar{\eta}_{\text{BH}}$  [210]. Estimating the BH density as  $\rho_{\text{BH}} \sim M/[(4\pi/3)R_s^3]$  with  $R_s = 2M$  corresponding to the Schwarzschild radius, one finds

$$\bar{\eta}_{\text{BH}} = -\bar{\zeta}_{\text{BH}} \sim 1.3 \times 10^{30} \frac{\text{g}}{\text{cm} \cdot \text{s}} \left( \frac{m}{65M_{\odot}} \right)^{-1}. \quad (54)$$

The magnitude of the BH viscosities are comparable to that of the remnant in Eqs. (52) and (53). That the sign of the bulk viscosity is negative is a well-known peculiarity of the effective fluid description of event horizons<sup>18</sup>. Naive application to the Newtonian stellar fluid model used in Eq. (53) would then suggest BHs have unstable radial modes, which of course is not the case. It is unclear exactly how to interpret negative bulk viscosity in the case of BHs, and this illustrates that not all exotic compact objects may have dynamics that fits comfortably in an effective hydrodynamic framework.

Let us now compute the viscosities of non-rotating, unmagnetized NSs. The shear viscosity due to the scattering of neutrons is given by [226, 231]

$$\bar{\eta}_{\text{NS}}^{(n)} \sim 2 \times 10^{14} \rho_{15}^{9/4} T_{11}^{-2} \frac{\text{g}}{\text{cm} \cdot \text{s}}, \quad (55)$$

while the bulk viscosity is given by [232, 233]

$$\bar{\zeta}_{\text{NS}}^{(n)} \sim 2.4 \times 10^{29} \rho_{15}^2 T_{11}^6 \omega_{10}^{-2} \frac{\text{g}}{\text{cm} \cdot \text{s}}, \quad (56)$$

where  $\omega_{10}$  is the oscillation angular frequency in 10kHz,  $\rho_{15}$  is the NS density divided by  $10^{15} \text{g/cm}^3$ ,  $T_{11}$  is the NS temperature divided by  $10^{11} \text{K} \sim 10 \text{MeV}$ , with the

latter corresponding to the typical temperature of hypermassive NSs formed after NS binary mergers. Notice that although the bulk viscosity is comparable to that of the remnant in Eq. (53), the shear viscosity is smaller by many orders of magnitude. The latter would still be true even for the shear viscosity due to trapped neutrinos [234].

Let us then proceed to compute the shear viscosity of non-rotating but magnetized NSs. For a strongly-magnetized NS, this can be estimated by comparing the Alfvén timescale to the viscous timescale [235]:

$$\bar{\eta}_{\text{NS}}^{(B)} \sim 1.3 \times 10^{28} B_{16} R_{12} \sqrt{\rho_{15}} \frac{\text{g}}{\text{cm} \cdot \text{s}}, \quad (57)$$

where  $R_{12}$  is the NS radius divided by 12km, while  $B_{16}$  is the magnetic field strength divided by  $10^{16} \text{G}$ . This magnetic shear viscosity can be comparable to that in Eq. (52) for sufficiently strong magnetic fields.

The above comparisons indicate that NS-like material can mimic the rapid ringdown of BHs, provided the former have sufficiently large magnetic field strengths and high effective temperatures. If Eq. (57) can be scaled to  $65M_{\odot}$  exotic objects, Eq. (51) implies that such objects need to have a magnetic field strength of  $B \approx B_{\text{rem}} \equiv 4 \times 10^{16} \text{G}$  in order to realize the effective shear viscosity of Eq. (52). Likewise, if Eq. (56) can similarly be scaled, and using  $\omega/2\pi = 250 \text{Hz}$  relevant to GW150914, implies that such objects need to have a temperature of  $T = T_{\text{rem}} \equiv 150 \text{MeV} = 2 \times 10^{12} \text{K}$  in order to realize the effective bulk viscosity of Eq. (53). Simulations of actual NS mergers do not quite reach these levels (see e.g. [236]), and damping timescales within the hypermassive remnant are an order of magnitude or more longer than in BHs; nevertheless these numbers illustrate what would be needed for NS-like exotic compact object collisions to look similar to BH collisions.

Let us now compute the viscosities associated with boson stars. There are numerous models for boson stars [237], though typically bosonic matter has very low effective viscosity, with the leading order dissipation of self-gravitating configurations coming from GW emission [238, 239] (this is similar to ideal fluid NSs). For example, from the calculation of the QNMs of a so-called solitonic boson star [240] with radius  $R \sim 3M$  presented in [239], the damping time of the  $\ell = 2$  polar mode is  $\tau \sim 10^3 M$ . For a  $65M_{\odot}$  boson star, the damping time is then  $\tau \sim 320 \text{ms}$ , which leads to effective shear and bulk viscosities of  $\bar{\eta}_{\text{BS}} \sim 7 \times 10^{26} \text{g/cm} \cdot \text{s}$  and  $\bar{\zeta}_{\text{BS}} \sim 5 \times 10^{28} \text{g/cm} \cdot \text{s}$  via Eqs. (52) and (53) respectively, roughly 2 orders of magnitude smaller than the effective fluid model consistent with the observation. Notice however that the frequency of the  $\ell = 2$  QNM of this boson star is  $f \sim 160 \text{Hz}$ , which by itself is incompatible with the GW150914 event. Presumably, more compact boson stars would have QNMs with frequencies closer to the observed maximum frequency in GW150914, though the damping time would be more challenging to reduce to a level consistent with this observation.

<sup>18</sup> The effective fluid description of dynamical horizons or future outer trapping horizons of BHs give a positive bulk viscosity with the same magnitude as that computed with event horizons [230].

In addition to effective viscosities, one can also probe the hydrodynamic properties of the remnant by studying its effective speed of sound. The light crossing time of an object with a diameter of  $2 \times 370\text{km} = 740\text{km}$  is  $\sim 2.5\text{s}$ , which is of the same order as the damping time observed by aLIGO. This means that the effective sound speed of an exotic compact object needs to be close to the speed of light in order to explain the observed rapid decay of the oscillation mode. On top of this, such an exotic compact object should not have a light ring. Otherwise, long-lived QNMs are typically present [31], unless their amplitude is too small to be detected by aLIGO as we will discuss in the next subsection. Both of these requirements on the effective sound speed and the absence of the light ring seem difficult to be met simultaneously by exotic compact objects. One candidate might be a boson star with  $R \gtrsim 3M$ , but then, the oscillation frequency is likely to be inconsistent with the observation, as already discussed in the previous paragraph.

## 2. Oscillation Modes of Exotic Objects

Can we infer the properties of exotic compact objects by constraining the amplitude of their oscillation modes with GW150914? If the binary constituents of GW150914 are Kerr BHs and the remnant is also a Kerr BH, the dominant QNM of the latter is the  $\ell = m = 2$  mode, and the next subleading mode is likely to be the  $\ell = m = 3$  mode. The SNR, however, seems to be too low for the subdominant modes to be detectable [28]. On the other hand, if the constituents and the remnant are exotic compact objects, they typically produce matter oscillation modes that are longer lived than the  $\ell = m = 2$  mode of a Kerr BH [241] with amplitudes possibly larger than the  $\ell = m = 3$  mode. In fact, Refs. [31, 208, 209] pointed out that when an exotic compact object with a light ring is perturbed by a test particle, the dominant GW mode will resemble that of a regular BH, followed by a set of exotic compact object QNMs, which will have a smaller amplitude than the primary  $\ell = m = 2$  mode but a longer damping time. The goal of this subsection is to place constraints on one additional mode (on top of the primary  $\ell = m = 2$  mode) in terms of the new mode's oscillation frequency  $\bar{f}_{\text{RD}}$  and damping time  $\bar{\tau}$  in a manner as agnostic as possible.

We begin by explaining how we model the GW emitted during QNM ringing for Kerr BHs in GR. The IMRPhenom waveform models the GW amplitude  $A_{\text{MR}}$  of the merger-ringdown phase as a product of a Lorentzian function and an exponential decay:

$$A_{\text{MR}} = A_0 f^{-7/6} \frac{\gamma_1}{m} \frac{\gamma_3 \bar{f}_{\text{damp}}}{(f - \bar{f}_{\text{RD}})^2 + (\gamma_3 \bar{f}_{\text{damp}})^2} e^{-\frac{\gamma_2(f - \bar{f}_{\text{RD}})}{\gamma_3 \bar{f}_{\text{damp}}}}, \quad (58)$$

where  $A_0$  is an overall amplitude factor that is common to the inspiral, intermediate and merger-ringdown phases, while the coefficients  $\gamma_i$  are given by a fit in terms of

the symmetric mass ratio and spins [69]. The oscillation and the damping frequencies of the  $\ell = m = 2$  mode are  $f_{\text{RD}}$  and  $f_{\text{damp}} \equiv 1/(2\pi\tau)$ , where  $\tau$  is the mode's damping time. aLIGO measured  $f_{\text{RD}}$  and  $\tau$  from the GW150914 event to be  $f_{\text{RD}} = 251 \pm 8$  Hz and  $\tau = 4.0 \pm 0.3$  ms, using the full inspiral-merger-ringdown waveform in GR. Due to the exponential factor in Eq. (58), the amplitude peaks at a frequency that is slightly *lower* than  $f_{\text{RD}}$ , i.e. at  $f_{\text{MR}} = 222$  Hz, which also corresponds to the transition frequency between the intermediate and merger-ringdown phase.

Let us now explain how we model the GW amplitude of the exotic compact object's additional ringdown mode. For simplicity, we adopt the same model of Eq. (58), but with the replacements  $(\gamma_i, f_{\text{RD}}, f_{\text{damp}}) \rightarrow (\bar{\gamma}_i, \bar{f}_{\text{RD}}, \bar{f}_{\text{damp}})$ ; notice that this additional ringdown mode is very similar to the original ppE ringdown waveform of [66], and is also similar to the extension used in [76] to calculate projected constraints on the ringdown phase of future aLIGO observations. The choice of  $\bar{\gamma}_3$  does not affect our analysis as shifting this parameter is equivalent to redefining  $\bar{f}_{\text{damp}}$ ; in fact, even in GR,  $\gamma_3$  is completely degenerate with  $f_{\text{damp}}$  in Eq. (58). We thus set  $\bar{\gamma}_3 = \gamma_3$  so that  $\bar{\tau}$  can be directly compared to  $\tau$ . The choice of  $\bar{\gamma}_2$  is more subtle; we set it to zero,  $\bar{\gamma}_2 = 0$ , so as to avoid having an artificial exponential enhancement in the amplitude when  $f_{\text{RD}}$  is much larger than  $f$ .

With these models at hand, we carry out a Fisher analysis to estimate a bound on  $\bar{\gamma}_1$ . We inject a GR GW signal ( $\bar{\gamma}_1 = 0$ ) with the central values  $\bar{f}_{\text{RD}}$  and  $\bar{f}_{\text{damp}}$  that aLIGO measured<sup>19</sup>, which leads to an SNR of  $\sim 7$ . The parameters in our Fisher analysis are  $(\gamma_1, \gamma_2, \bar{f}_{\text{RD}}, \tau, \bar{\gamma}_1)$ , and we only use the GW signal with  $f \geq f_{\text{MR}}$  and use the prior  $\bar{f}_{\text{RD}} \geq f_{\text{MR}}$ <sup>20</sup>. Notice that other parameters in the additional mode's amplitude, such as  $\bar{f}_{\text{RD}}$  and  $\bar{\tau}$ , cannot be measured when  $\bar{\gamma}_1 = 0$  since derivatives of the amplitude with respect to such parameters vanish. Notice also that, since here we are only constraining the amplitude of the additional mode, we only consider the amplitude in the waveform and set the waveform phase to be effectively independent of the above parameters when calculating the Fisher matrix.

Figure 10 presents the upper bound on  $\bar{\gamma}_1/\gamma_1$  as a function of  $\bar{f}_{\text{RD}}$  and  $\bar{\tau}$ . Observe that the constraint on the additional mode's amplitude becomes stronger when the oscillation frequency is close to  $f_{\text{MR}}$  and when  $\bar{\tau}$  is large. In particular, the constraint is better than 10% when  $\bar{\tau} \in (100, 1000)$  ms. This is as expected since the SNR of the additional mode becomes larger in this case. On the other hand, when  $(\bar{f}_{\text{RD}}, \bar{\tau})$  are close to the frequency and

<sup>19</sup> This SNR is different from the post-inspiral SNR of  $\sim 16$  found in [12], as the latter was calculated from  $f_{\text{int}} = 132$  Hz.

<sup>20</sup> A similar analysis could be used to place limits on lower frequency modes as well. The exponential term in Eq. (58) would then need to be modified to avoid issues when  $f < f_{\text{MR}}$ . For brevity we do not do so here, focusing instead on the  $f > f_{\text{MR}}$  case as an illustrative example.

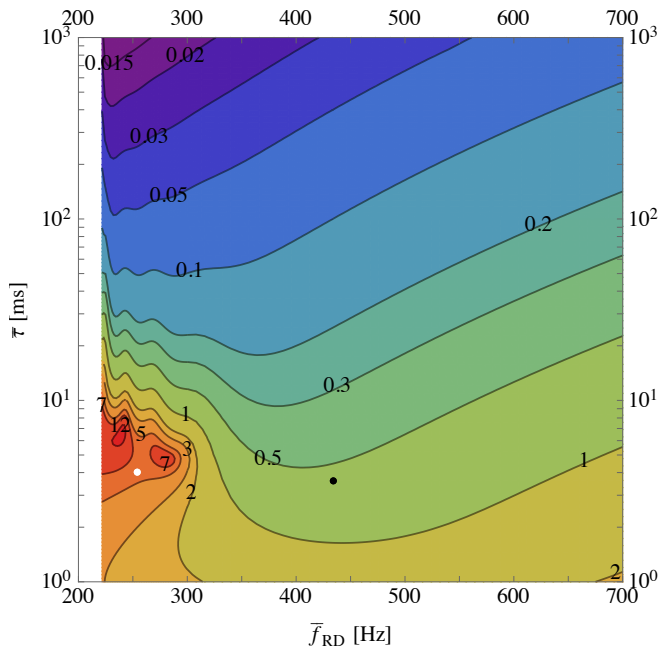


FIG. 10. (Color online) 90-% confidence upper bound on the amplitude of an additional ringdown mode  $\bar{\gamma}_1$  relative to the amplitude  $\gamma_1$  of the primary  $\ell = m = 2$  mode as a function of former's ringdown frequency  $\bar{f}_{RD}$  and damping time  $\bar{\tau}$ . Observe that  $\bar{\gamma}_1$  can be constrained to be less than  $\sim 10\%$  of the primary mode's amplitude if the damping time is larger than 100ms, which is typical for boson star QNMs. Observe also that the constraint becomes relatively weak around the white dot corresponding to the frequency and damping time of the primary  $\ell = m = 2$  mode, due to degeneracies between the primary mode and the additional mode. The black dot represents the subleading  $\ell = m = 3$  mode of a BH [27], whose amplitude is smaller than 10% [28].

damping time of the primary  $\ell = m = 2$  mode (white dot in the figure), the parameters become degenerate, which weakens the constraint. One can alternatively see Fig. 10 as showing upper bounds on  $\tau$  for a given  $\bar{\gamma}_1$  and  $\bar{f}_{RD}$ , which can be mapped to lower bounds on the viscosity via Eqs. (52) and (53). For example, when we assume  $\bar{\gamma}_1/\gamma_1 \leq 0.1$  and  $\bar{f}_{RD} = f_{RD}$ , one finds  $\tau \lesssim 50\text{ms}$ , which maps to  $\bar{\eta} \gtrsim 3 \times 10^{27}\text{g/cm/s}$  and  $\bar{\zeta} \gtrsim 2 \times 10^{29}\text{g/cm/s}$ .

Let us now discuss the implications of Fig. 10 on the properties of the compact object remnant, assuming that the remnant of GW150914 was a BH. In such a case, the remnant would have emitted subdominant modes, such as the  $\ell = m = 3$  one, whose amplitude is typically smaller than 10% of the dominant mode [28]. The frequency and damping time of such a mode can be derived from the fit in [27] to be  $f_{RD} = 434\text{ Hz}$  and  $\tau = 3.6\text{ ms}$  for a  $61.8M_\odot$  remnant BH spinning at  $\chi = 0.67$ , which is shown by the black dot in Fig. 10. The figure shows that it would be difficult for aLIGO to detect such a signal, as one can only distinguish the dominant and subdominant modes if the latter's amplitude is larger than at least  $\sim 60\%$  of the primary one. Such a finding is consistent

with [28], which found that the SNR needs to be  $\gtrsim 100$  to distinguish the first two leading BH QNMs produced by the merger of two BHs with the mass ratio of  $\sim 1.2$ .

Let us now discuss the implications of Fig. 10 on the properties of exotic compact object remnants. Reference [31] showed that exotic compact objects with a light ring can produce GWs whose dominant modes are similar to those of a Kerr BH at early times, but differ at late times through subleading modes that correspond to exotic QNMs. This conclusion was arrived at by studying how a test particle falls into an exotic object, which is quite different from the merger of comparable mass objects. Nonetheless, assuming this conclusion remains true for comparable mass mergers, then Fig. 10 implies that aLIGO can bound the amplitudes of additional, slower damped QNMs of an exotic object. For a damping time 5 times longer than the primary  $\ell = m = 2$  mode, the secondary mode amplitude must be less than  $\sim 50\%$  that of the primary mode, with the limits strengthening as the damping time of the secondary mode increases. Regarding boson star mergers, as discussed above one may expect the damping time to be  $\mathcal{O}(100\text{ms})$ . The amplitude of such a boson star QNM can then be constrained from the GW150914 measurement to be less than 10% of the primary mode's amplitude.

Let us end this subsection by discussing how a possible time delay between the primary and secondary oscillation modes may affect the constraint on the amplitude of the latter in Fig. 10. Since the above analysis assumes a damping sinusoidal waveform in the time domain for both the primary and secondary oscillation modes, we effectively assumed that the two modes were excited approximately at the same time. On the other hand, Ref. [31] showed that QNMs of exotic compact objects with a light ring are typically excited after the primary mode excitation (at merger). If the time delay between the excitation of the two modes is relatively large, one can treat them independently with the secondary one modeled by a Gaussian sinusoidal (or a sine-Gaussian) waveform. One can then easily estimate the upper bound on the amplitude of such a secondary mode relative to the primary one as a function of  $\bar{f}_{RD}$  and  $\bar{\tau}$ , requiring that the SNR of the secondary mode be smaller than a threshold SNR of  $\sim 5$ . Such a bound leads to results similar to those presented in Fig. 10, with the only exception around the white dot in the figure, where parameter degeneracies are non-negligible (such degeneracies are absent in the new analysis). To give an example on the bound comparison, we found that the upper bound on the secondary mode relative amplitude with  $\bar{f}_{RD} = f_{RD}$  and  $\bar{\tau} = 5\tau$  is 0.15, while that in Fig. 10 is 0.3. Given the similarity between the two analyses, we expect Fig. 10 to be a valid order of magnitude estimate, even if one allows for a finite time delay between the two modes, with the bound around the white dot becoming stronger as the time delay becomes larger.

## V. THEORETICAL IMPLICATIONS OF SMALLER-CONFIDENCE OBSERVATIONS

In this section, we discuss the possibility of extracting further theoretical implications from aLIGO’s recent O1 observation period, using other aLIGO triggers with a smaller confidence limit or those detected by other telescopes. We first discuss implications that could be extracted if trigger LVT151012 were interpreted as a true GW detection. We then proceed to discuss what theoretical implications one could derive if event GW150914 had a confirmed electromagnetic counterpart detected by the Fermi GBM.

### A. The LVT151012 Trigger

LVT151012 was the second most significant trigger in the aLIGO O1 observation period. This trigger had a combined SNR of 9.6, with a false-alarm rate of 1 every 2.3 years (a false alarm probability of 0.02) [83]. This false-alarm rate is sufficiently high that LIGO decided not to declare this trigger a detection, in spite of the lack of instrumental or environmental artifacts that could have caused it. If this event was a true GW detection, then the LIGO/Virgo collaboration estimated that it would have been produced by a binary BH system with (source-frame) component masses  $(m_1, m_2) = (23_{-5}^{+18}, 13_{-3}^{+4})M_\odot$  at  $1.1_{-0.5}^{+0.5}$  Gpc and an effective spin consistent with zero.

Let us then pretend that this was an actual GW observation and ask whether different theoretical physics implications can be inferred from this event. To begin with, since the component masses are so high that the event is consistent with a binary BH coalescence, such an observation would still not allow us to say anything about a large class of theories that activate GR modifications only in the presence of matter (see Sec. III A). With that caveat in mind, and assuming that this event is consistent with GR, we can then carry out a parametrized analysis of the detection, similar to that of Sec. III.

Figure 11 shows Fisher estimates of constraints on the  $\beta$  ppE parameter as a function of PN order, using a signal consistent with LVT151012 and one consistent with GW150914. Although the SNR for the former is smaller than the latter, observe that the constraints are almost identical when  $n \geq 0.5$ . This is because these constraints are mostly determined by the prior on spin, which is the same for both GW150914 and LVT151012. On the other hand, the latter leads to stronger constraints for  $n \leq -2$ . This is because this event consists of a BH binary with lower total mass, and thus, (i) the velocity of the binary constituents at a fixed frequency (e.g.  $f \sim 100$ Hz) is smaller than in the GW150904 case, and (ii) the observed frequency range is larger than in the GW150904 case. The first fact makes the negative-PN-order, ppE correction terms in the phase and the total number of GW cycles in band larger than for GW150914. This, together with the second fact above, make  $\beta$  less degen-

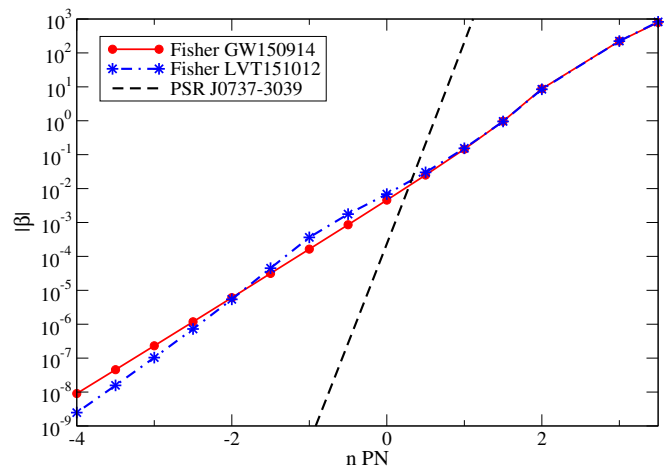


FIG. 11. (Color online) Fisher estimates of the 90%-confidence constraints one could place on the ppE amplitude coefficient  $\beta$  as a function of the PN order of the effect. The red solid line corresponds to a signal consistent with GW150914 (same as that in Fig. 4), while the blue dot-dashed line corresponds to that consistent with LVT151012. For comparison, we include again the binary pulsar constraint with PSR J0737-3039 [102]. Observe that the constraints are similar, although LVT151012 can do better at more negative PN order since the signal contains more wave cycles and the observed frequency range is larger.

erate with other binary parameters, leading to stronger constraints. Figure 11 implies that aLIGO observations of stellar-mass binaries should be significantly better at constraining negative PN order effects.

One may worry that results derived from a Fisher analysis are not trustworthy due to the low SNR of the LVT151012 trigger. Indeed, it is well-known that Fisher estimates can be an overestimate of the accuracy to which parameters can be determined when the SNR is not high relative to a Bayesian analysis [176, 181]. To estimate the accuracy of our Fisher analysis, we first compare its predicted accuracy for the extraction of the chirp mass  $\mathcal{M}$  to the posterior distribution of the chirp mass using a Bayesian analysis [65, 83]. We find that our Fisher analysis underestimates the width of the posterior by roughly a factor of 3. However, the error in a Fisher analysis relative to a Bayesian analysis is not necessarily the same for all parameters in the model. For example, when considering event GW150914, the accuracy to which  $\beta$  can be constrained with a Bayesian and a Fisher analysis agree to 15–50%, but the accuracy to which the chirp mass can be determined is still overestimated by a factor of 2 by the Fisher method. Fortunately, the robustness of our conclusions above is unaffected by such inaccuracies in the Fisher analysis (even if we allow for a 100% error in the latter), i.e. the LVT151012 trigger places a stronger bound on  $\beta$  than GW150914 for GR deformations entering first at negative PN order smaller than  $\sim -2$ PN.

A similar analysis can be carried out to constrain devi-

ations in the dispersion relation of propagating GWs with LVT151012. A Fisher analysis suggests that LVT151012 can place bounds on  $\mathbb{A}$  that are worse than those obtained with GW150914 by a factor of roughly 1.5–3. Combining these two constraints, and using Eq. (4.12d) in [59], one finds an improvement over the GW150914 bound alone of only roughly 5–20%. Thus, although the stacking of constraints will lead to improved joint constraints, this improvement is not necessarily large.

## B. Electromagnetic Counterparts to GW150914

The Fermi collaboration announced recently that the GBM in the Fermi spacecraft detected a gamma-ray signal that was coincident with event GW150914 [84] (see also [242]). This signal lasted for roughly 1 second and it started 0.4 seconds after GW150914. With a false alarm probability of roughly 0.002, this is not a high- $\sigma$  signal. Moreover, the signal was detected only in the GBM offline search [243] (not as a GBM trigger) and not in any other instrument (like the Fermi Large Area Telescope [244] or Swift [245]) or by any other particle detector (like neutrino detectors [246]). The properties of the signal make it look like a weak short GRB, but if so, it is unclear how it was generated; typically, short GRBs are expected to be produced by the merger of binary NSs or a mixed BH/NS system, and not by a binary BH merger. Some astrophysical scenarios have been proposed for the generation of such a short GRB, which include emission from a circumbinary accretion disk with possible future afterglows [87, 247].

In broad terms, electromagnetic counterparts can be classified in two groups: precursor-emission signals or prompt/delayed-emission signals. In the first scenario, the electromagnetic counterpart is produced during the inspiral phase, for example due to interactions of the binary with a circumbinary accretion disk (see e.g. [248, 249]). In this case, assuming GR is correct, the electromagnetic signal can arrive before or with the peak of the GW strain. In the second scenario, the electromagnetic signal is produced after the compact objects have merged, for example due to the production of a short GRB (see e.g. [250, 251]). In this case, the electromagnetic counterpart arrives a certain time after the peak of the detected GW. The Fermi GBM observation would fit in this second scenario (as a prompt-emission signal), if GWs travel at or slower than the speed of light. But if GWs travel at super-luminal speeds, however, then the Fermi GBM signal could have been emitted before the GW signal, with the latter arriving first due to its faster propagation speed.

Let us study then what theoretical implications one can derive if the GBM signal were indeed interpreted as an electromagnetic counterpart to GW150914. The most obvious implication is a model-independent test of the speed of gravity. In Einstein’s theory, GWs travel at the speed of light (essentially due to the characteristic

structure of the Einstein equations), which then implies that gravitons are massless. In modified gravity models, this need not be the case, especially when gravitational Lorentz violation is broken. EA theory [89, 252] breaks gravitational Lorentz invariance by introducing a vector field that couples to the metric tensor; this theory is the most generic modification to Einstein’s theory that contains a (unit timelike) vector field and (at most) quadratic combinations of its first derivative. Khronometric theory [91, 253] breaks gravitational Lorentz invariance by introducing a globally preferred frame selected by a scalar field (the “khronon”); this theory arises as the low-energy limit of the ultraviolet complete and power-counting renormalizable Hořava-Lifshitz theory [137].

A model-independent test of the speed of gravity through a coincident GW/electromagnetic observation consists of simply comparing the times of arrival of the two signals [85]. In the prompt/delayed-emission scenario, if GWs travel at the speed of light, the difference in the arrival times can, at most, be due to the intrinsic time delay in the emission of photons after the GW emission has ended. For NS mergers in the standard short GRB scenario, this time delay can be anywhere between 10 seconds and 500 seconds, with variations dependent on the particular details of the astrophysical model. The fractional difference between the speed of light and the speed of GWs,  $\delta_g = 1 - v_g/c$ , can then be bounded by [85]

$$|\delta_g| < \frac{c\Delta\tau_{\text{int}}}{D_L}, \quad (59)$$

where  $D_L$  is the luminosity distance.

Let us now investigate how strongly the GW150914 event constrains  $|\delta_g|$  if the Fermi event was a prompt/delayed counterpart to GW150914. Using that the GW inferred distance  $D_L = 410_{-180}^{+160}$  Mpc, one can place a conservative bound on the speed of gravity, but only as a function of the unknown  $\Delta\tau_{\text{int}}$ . The top (bottom) panel of Fig. 12 shows constraints in the subluminal (super-luminal) region, with the region above the curves excluded. Since the Fermi GBM time binning is 0.256s [84], we do not show constraints on  $|\delta_g|$  with  $\Delta\tau_{\text{int}} < 0.256$ s. One could also map constraints on  $|\delta_g|$  to constraints on  $\mathbb{A}$ , assuming e.g. a GW frequency of  $f \sim 100$ Hz, but such constraints are weaker than those in Fig. 9 by more than two orders of magnitude, except in the  $\alpha = 2$  case, which cannot be constrained from GW observations alone. The point of this figure is to observe that the constraint depends sensitively on the unknown intrinsic time delay parameter, without which a constraint cannot actually be placed.

Let us discuss in detail constraints on the subluminal propagation of GWs. The top panel of Fig. 12 shows the hypothetical Fermi/GW150914 constraint, together with the bound from cosmic ray observations due to the absence of gravitational Cherenkov radiation [144]:

$$\delta_g \leq 2.45 \times 10^{-15} \left( \frac{E}{10^{11} \text{GeV}} \right)^{-3/2} \left( \frac{D_L}{1 \text{Mpc}} \right)^{-1/2}, \quad (60)$$

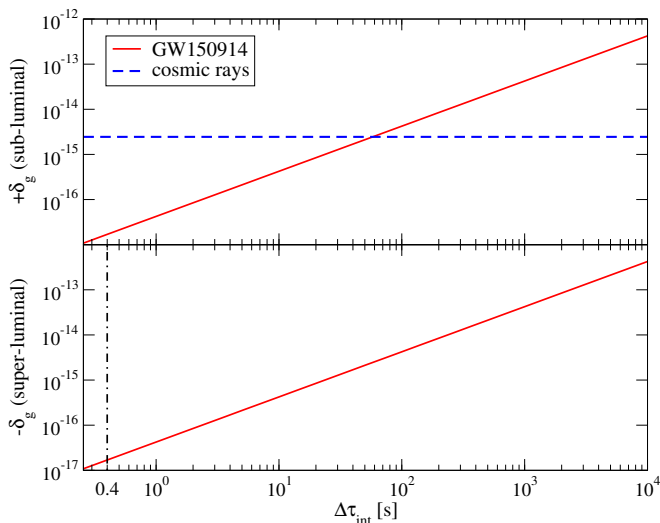


FIG. 12. (Color online) GW150914 constraints on the fractional deviation in the propagation speed of GWs away from the speed of light for the  $\delta_g > 0$  (top) and  $\delta_g < 0$  region, assuming that the event Fermi observed was associated with GW150914. We also show the cosmic ray constraints from the absence of the gravitational Cherenkov radiation in Eq. (60) in the top panel. The vertical dotted-dashed line in the bottom panel corresponds to  $\Delta\tau_{\text{int}} = 0.4$  assumed in [86, 87]. We do not show the region with  $\Delta\tau_{\text{int}} < 0.256$  s, since then the binning of the Fermi observation in time dominates the error budget over  $\Delta\tau_{\text{int}}$ .

where we conservatively assumed that cosmic ray particles with an energy  $E = 10^{11}$  GeV have traveled  $D_L = 1$  Mpc to reach Earth. Observe that the GW/Fermi coincident constraint is more stringent than the cosmic ray bound, provided that  $\Delta\tau_{\text{int}} < 60$  s. Given that there are no agreed-upon models for the electromagnetic emission detected by Fermi, it is not clear whether such an intrinsic time delay is reasonable.

Let us now discuss in detail constraints on the super-luminal propagation of GWs. The bottom panel of Fig. 12 shows the coincident Fermi/GW150914 constraint, which again depends on the intrinsic time delay  $\Delta\tau_{\text{int}}$ . If one assumes the Fermi event was a prompt/delayed scenario, the most conservative bounds on negative  $\delta_g$  is obtained when  $\Delta\tau_{\text{int}} = 0.4$  s (shown with a dotted dashed line), which gives  $\delta_g \gtrsim -10^{-17}$  [86, 87]. On the other hand, Collett et al. [88] assumed that GWs and gamma rays are emitted simultaneously at merger, which corresponds to  $\Delta\tau_{\text{int}} = 0$  and leads to  $\delta_g = -1.0^{+0.8}_{-1.9} \times 10^{-17}$ , where the errors are propagated from the Fermi timing bins and from errors in the luminosity distance measurement. Notice that the error bar does not contain  $\delta_g = 0$  in this case, which means that GWs must propagate super-luminally under the assumption that gravitons and photons were emitted simultaneously.

Assuming that our understanding of the astrophysi-

cal emission mechanism improves in the future and constraints can be placed from a coincident Fermi/GW observation, let us investigate the theoretical implications of the resultant model-independent constraint on the speed of gravity. The most obvious implication is a severe constraint on gravitational Lorentz violation [93]. In EA theory and in khronometric theory, the speed of GWs is not unity, but it is rather corrected through a fractional modification of the form

$$\delta_g^{\text{EA}} = 1 - (1 - c_+)^{-1/2}, \quad (61)$$

$$\delta_g^{\text{KG}} = 1 - (1 - \beta_{\text{KG}})^{-1/2}, \quad (62)$$

where  $c_+$  is a combination of coupling constants in EA theory, while  $\beta_{\text{KG}}$  is a coupling constant in khronometric gravity. A bound on  $\delta_g$  of order  $10^{-17}$  then implies a constraint on gravitational Lorentz violation at the level

$$c_+ \lesssim 10^{-17}, \quad (63)$$

$$\beta_{\text{KG}} \lesssim 10^{-17}. \quad (64)$$

Such a constraint is 10 orders of magnitude more stringent than any other constraint on gravitational Lorentz violation. Notice that the EA and khronometric modification to GW propagation cannot be constrained from the bound on  $\mathbb{A}$  with the Fisher analysis of Fig. 9 and only GW observations. This is because such a modification corresponds to the  $\alpha = 2$  case in Eq. (25), and thus, it is degenerate with the time of coalescence in the waveform phase, as explained in Sec. III C. On the other hand, one can apply the GW150914 bound on  $\delta_g$  from the GW arrival time delay between Hanford and Livingston detectors [64], which yields  $(c_+, \beta_{\text{KG}}) \lesssim 0.7$ , as summarized in Table I. A simultaneous measurement of GWs and gamma rays also allows us to place constraints on a more generic Lorentz-violating framework, the gravitational SME framework, in particular on non-dispersive and non-birefringent coefficients like  $k_{(V)}^{(4)}$ , as discussed in Sec. II B 3.

Another theoretical implication that could be derived from a coincident GW/electromagnetic observation is a severe constraint on gravitational parity violation [106, 108, 254]. If gravity breaks parity, then, generically, left- and right-polarized GWs will obey different propagation equations, with the amplitude of one mode suppressed and the other enhanced. To constrain this effect, a network of GW detectors would then need to separate the two GW polarization amplitudes. Due to parameter degeneracies, however, such a test also requires that a coincident short GRB observation (a) constrain the inclination angle (the angle between the orbital angular momentum of the binary and the line of sight) and (b) provide a distance measurement through galaxy identification. Event GW150914 is particularly well-suited for this test, as it was observed nearly face-on and thus the signal arrives almost entirely circularly polarized. The aLIGO detectors, however, are essentially co-aligned, so the two GW polarizations could not be separated in event

GW150914. Moreover, the GBM signal was not bright enough to allow for galaxy identification and a measurement of distance. Therefore, a test of gravitational parity invariance cannot be carried out, even if one associated the GBM signal with a counterpart to GW150914; for this, one will have to wait for a network of GW detectors to allow for the extraction of polarizations, as well as a coincident short GRB signal that is loud (and close) enough to allow for galaxy identification.

## VI. CONCLUSION

We have studied the theoretical physics implications of GW150914. The LIGO collaboration has demonstrated that this event is entirely consistent with a binary BH merger in GR, in that subtraction of the best-fit GR template from the data gives a residual consistent with noise. Our analysis has shown that more than simply verifying consistency with GR, the information contained in GW150914 allows one to place limits on many physical phenomena that various modified gravity theories predict and could have been operational in a binary merger. We have shown that event GW150914 limits theoretical mechanisms such as the strength of the activation of a scalar field and a vector field, the leakage of BH mass into extra dimensions, temporal variations of Newton's gravitational constant, the speed of gravity and the dispersion relation of GWs. Such constraints on theoretical mechanisms allow us to probe fundamental pillars of GR, including the SEP, gravitational parity and Lorentz invariance, a massless graviton and the 4D nature of space-time.

Even though some of the constraints on these physical mechanisms are not as stringent as current bounds with binary pulsars, low mass X-ray binaries, Solar System experiments, table-top experiments on Earth or cosmological observations, constraints with GW150914 are of a completely different nature: they come directly from the extreme gravity environment of merging BHs. Moreover, we can anticipate that these bounds will steadily become stronger over the years as (i) more GW observations are made (through stacking of multiple signals), (ii) different sources of GWs are observed (e.g. binary NS inspirals will constrain low-frequency mechanisms better than binary BH mergers), (iii) higher SNR events are observed (since the strength of any constraint in terms of the ppE parameter  $\beta$  scales inversely with this number), and (iv) multi-band GW observations of a GW150914-like binary with ground- and space-based interferometers may be possible [170, 255]. For example, if aLIGO detects  $N$  events that are similar to GW150914, one can statistically improve<sup>21</sup> the upper bound on  $|\beta|$  presented here

by a factor of  $\sim \sqrt{N}$ , an excellent prospect for the future considering that the expected number of highly significant events at the end of the O3 run is above 35 [257].

We also studied how GW150912 allows us to constrain properties of the dynamics of matter for exotic alternatives to a BH remnant. We first placed a generic constraint on the orbital angular momentum of a test particle at ISCO orbiting around the remnant. We then showed how such a bound can be mapped to constraints on modified gravity theories and can be used to test the Kerr hypothesis. We next studied the effective hydrodynamic properties of the remnant by deriving effective viscosities that are needed to explain the rapid decay in the post-merger signal. We showed that such viscosities are consistent with those of BHs obtained via the membrane paradigm; NS-like material needs to be hot and highly magnetized in order to explain such a rapid damping. We finally derived constraints on additional oscillation modes, i.e. in addition to the primary  $\ell = m = 2$  mode that aLIGO measured. We found that the amplitude of such a secondary mode can be constrained to be less than  $\sim 10\%$  of the primary if the damping time is larger than 100ms, which is typical for boson star remnants.

We have further explored other implications derived from events observed at smaller confidence. Some of these involve the trigger LVT151012, which though having a decent SNR of 9.6, had too large a false alarm rate with the preliminary analysis to declare it an event. However, such a trigger may be elevated to an actual event if the false alarm rate is reduced significantly by further repeating the time-shift analysis of the signals to estimate the background more accurately. If this trigger was a GW from a binary inspiral, due to its lower chirp mass and hence more of the inspiral signal being in band, we showed that more stringent constraints can be placed on physical mechanisms that dominate at lower frequencies relative to the merger/ringdown frequency. We also explored the possibility that the Fermi GBM detected a coincident short GRB to event GW150914. We found that if this were the case, then the combined detection would place extremely stringent constraints on the speed of gravity (relative to the speed of light), and thus, to gravitational Lorentz-violation. However, such a bound has a large systematic error due to uncertainties in the intrinsic time delay of photon and graviton emission.

Let us end by stressing that the true potential of GW150914 for testing GR and exotic compact objects is highly limited by the lack of knowledge of how GWs behave during the merger phase in such GR alternatives. In our ppE analysis we only included non-GR corrections to the inspiral phase of coalescence. If one were to include modifications to the merger-ringdown phase, the bounds on various theoretical GW generating mechanisms presented in the top part of Table I will become stronger. However, the physics of the actual merger may not be well-characterized, if at all, by mechanisms that affect GW generation during the inspiral. GW150914 has given us a remarkable glimpse into this regime of ex-

<sup>21</sup> As shown in [256], the improvement can be better than  $\sqrt{N}$ , since the  $N$  events will not typically have the same SNR.

treme gravity, which could in principle place very stringent constraints on modified gravity theories, were their dynamics known in this regime. GW150914 therefore calls for a more concerted effort by the gravity and high-energy communities to explore the full non-linear regime of merging compact object binaries.

### ACKNOWLEDGMENTS

We thank Neil Cornish and Vasileios Paschalidis for useful discussions and comments, and Katie Chamberlain for a code comparison. We also thank Kenta Kiuchi for sharing with us gravitational waveforms from strongly-magnetized hypermassive NSs. We further thank Enrico Barausse, Emanuele Berti, Vitor Cardoso and Paolo Pani for carefully reading the manuscript and giving us important comments. N.Y. acknowledges support from the NSF CAREER Grant PHY-1250636. K.Y. acknowledges support from JSPS Postdoctoral Fellowships for Research Abroad. F.P. acknowledges support from the NSF grant PHY-1305682 and the Simons Foundation.

### Appendix A: Noise Spectrum Fit

We construct a fit for the Hanford noise spectrum data [95] through the polynomial

$$\sqrt{S_n(f)} = \sqrt{S_0} \exp(a_0 + a_1 x + a_2 x^2 + a_3 x^3 + a_4 x^4 + a_5 x^5 + a_6 x^6), \quad (\text{A1})$$

where  $S_0 = 0.8464/\text{Hz}$ ,  $x \equiv \ln[f/(1\text{Hz})]$  and the coefficients  $a_i$  are given by Table IV. We assumed that the Livingston noise spectrum is identical to the Hanford one, for simplicity. None of the conclusions derived in this paper are affected by that assumption.

$a_0$	$47.8466 \pm 5.38$
$a_1$	$-92.1896 \pm 6.41$
$a_2$	$35.9273 \pm 3.07$
$a_3$	$-7.61447 \pm 0.759$
$a_4$	$0.916742 \pm 0.103$
$a_5$	$-0.0588089 \pm 0.00721$
$a_6$	$0.00156345 \pm 0.000206$

TABLE IV. Fitting coefficients and their standard deviation for the fitting function of Eq. (A1), which approximates the aLIGO noise spectrum during O1, and in particular, around the time of the GW150914 observation.

Although the fit provided above is good ( $r^2 = 0.99995$ ), it is by no means perfect. To see this graphically, the top panel of Fig. 13 shows the actual Hanford noise spectral density during the O1 run, together with the fit as a function of frequency in Hz. Observe that the data contains many spikes, which the fit smoothes

over. The bottom panel shows the fractional difference between the fit and the data. On average, observe that the fit accurately describes the data to  $\mathcal{O}(1\%)$  accuracy in the  $f > 10^2$  Hz region, while the fractional difference becomes  $\mathcal{O}(10\%)$  in the  $f < 60$  Hz region. We could have constructed a more accurate fit to the data, but we found that this was not necessary.

One may wonder whether the spikes in Fig. 13 affect the constraints derived in this paper. The answer is no. The spikes do affect the SNR that would be measured at Hanford and at Livingston, but we have here chosen the waveform amplitude such that the SNR with the fitted noise curve is exactly what LIGO measured. With the SNR properly adjusted, we have checked that the difference between the fit and the data only affects the constraints on  $|\beta|$  at  $-1\text{PN}$  order by 3%–6% at most relative to what we quote in this paper.

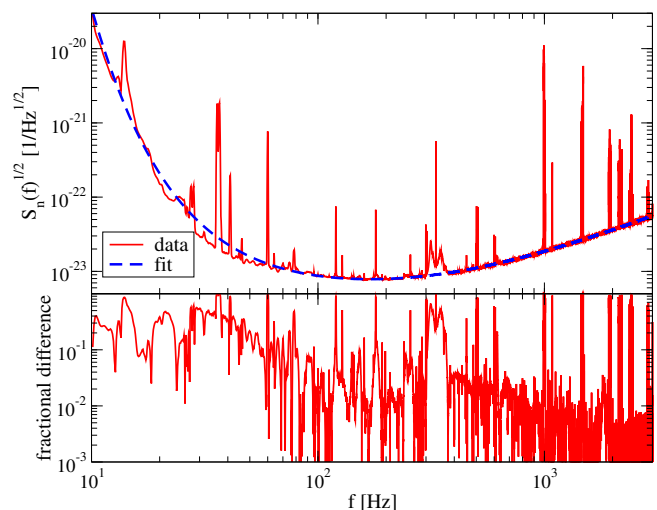


FIG. 13. (Color online) (Top) Square-root of the noise spectral density as a function of frequency (in Hz) for the Hanford detector during the O1 (red solid) and using the fitted function of Eq. (A1) (blue dashed). (Bottom) The relative fractional difference between the data and the fit. Observe that the data contains spikes that are absent from the fit, but we have checked that these spikes do not significantly affect the constraints quoted in this paper, if the SNR is fixed.

### Appendix B: Constraining GR Modifications with PhenomB and PhenomD Waveforms

In this appendix, we compare constraints on the ppE parameter  $\beta$  using PhenomB [67] and PhenomD [69, 96] waveforms. Although we only used the latter for parameter estimation, it is still interesting to see whether the constraints we found are affected by the GR waveform model employed (especially given that GW150914 is in a regime where some of the approximations used to create these models become questionable.)

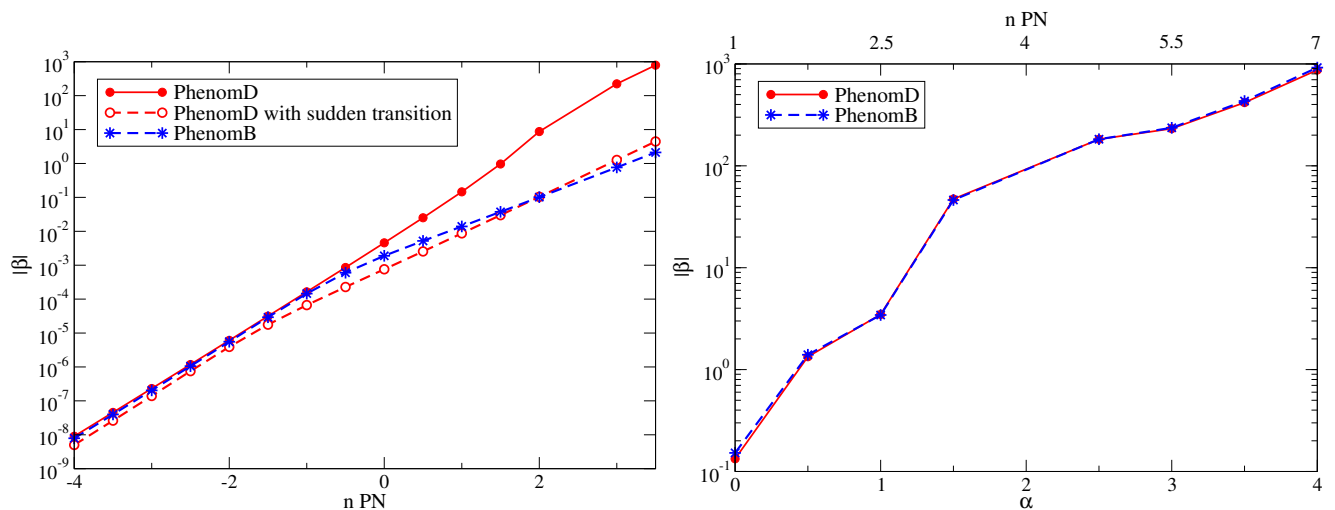


FIG. 14. (Color online) Comparison of 90%-confidence GW150914 constraints on  $|\beta|$  with PhenomD and PhenomB waveforms for modified generation (left) and propagation (right) effects on GWs. We also show the PhenomD result with a sudden transition of the non-GR effect at  $f = f_{\text{Int}}$  like PhenomB, which corresponds to the sudden deactivation of the scalar field with a transition at  $f_* = f_{\text{Int}}$  in Sec. III B 3 (but for arbitrary  $b$ ).

Let us then begin by reviewing the similarities and differences of these two waveform models. The PhenomB waveform was obtained by first constructing hybrid PN and numerical relativity waveforms in the time domain over the mass ratio range  $1 \leq q \leq 10$  and the spin range  $-0.85 \leq \chi_A \leq 0.85$ , and then Fourier transforming them into the frequency domain. Each part of the waveform (inspiral, merger and ringdown) was then fitted by polynomials of the form of Eq. (1), with  $\Phi_i = \Phi_{\text{EI}}$  in Eq. (3). On the other hand, the PhenomD waveform was obtained by constructing hybrid waveforms directly in the frequency domain in a larger sector of parameter space:  $1 \leq q \leq 18$  and  $-0.95 \leq \chi_A \leq 0.95$ . Moreover, the PhenomD waveform amplitude and phase in each segment (described in Sec. II B 1) are matched together to ensure continuity and differentiability at the interfaces.

These phenomenological waveforms in GR can be extended to capture non-GR effects by adding a ppE correction term in Eq. (12) in the waveform phase. We include such a term only in the inspiral phase when investigating modified GW generation mechanisms. However, such a correction propagates to the intermediate and merger-ringdown phases in PhenomD due to the continuity and differentiability requirements at interface frequencies. This does not occur in the modified PhenomB model, and thus, the model is discontinuous at the interface between the inspiral and merger phases when  $\beta \neq 0$ . When studying modified GW propagation effects, we include the ppE correction term in all phases, which renders both the modified PhenomB and PhenomD models continuous and differentiable at the interfaces.

Figure 14 compares the upper bound on  $|\beta|$  as a function of the leading PN order of the ppE correction using the ppE-modified PhenomB and PhenomD models.

The left and right panels show the bound on modified generation and propagation mechanisms. Observe that the two models give almost identical bounds at any PN order in the propagation case but only when  $n \leq -1$  in the generation case, with larger differences arising at positive PN order. This is because the generation-modified PhenomB model only has a correction in the inspiral phase, with the correction shutting off suddenly at the inspiral-merger interface, while the propagation-modified model is always continuous and differentiable as the Phenom D model is. This non-smooth feature of the generation-modified PhenomB model makes such a correction unique, allowing  $\beta$  to be less degenerate with other parameters relative to the PhenomD case. In order to check this, we also constructed a modified PhenomD waveform by adding Eq. (3) in the inspiral phase but not imposing continuity and differentiability at the interface frequency in the non-GR part of the phase. Thus, such a waveform suddenly changes to the GR model in the post-inspiral phases, which is similar to what occurs in the scalar field deactivation waveform with a transition frequency of  $f_* = f_{\text{Int}}$  (see Sec. III B 3) but an arbitrary  $b$  instead of  $b = -7/3$ . As we expect, the bound on  $|\beta|$  shown by the red dashed curve in the left panel of Fig. 14 gives a similar bound compared to the PhenomB one even for positive PN corrections.

This result allows us to draw several conclusions. First, if one wishes to obtain an accurate constraint on a possible deviation from GR using GW data, one should use the ppE-modified PhenomD model (or a model as accurate as this one), as this guarantees smoothness at the transition frequencies. Indeed, one does not expect that GR deviations will lead to non-smooth GWs; even when there is a sudden activation or de-activation of scalar dipole radi-

tion, this ought to occur smoothly (even though such a transition has sometimes been modeled with a Heaviside function in the literature [76, 184–186]). Second, if one is carrying out a *science case* study to predict e.g. how different detector configurations will affect our ability to test GR, then one can use the ppE-modified PhenomB model if the modifications one is interested in occur at  $-1$ PN order or lower. Ultimately, once data with new, advanced detectors is obtained, one would re-do the analysis with a ppE-modified model extended from the most accurate GR waveform model available at that point; this is likely to be different from PhenomD, given that GR waveform models are likely to become more accurate in the future.

### Appendix C: Constraining EdGB Gravity with GW150914

We here study in detail whether the GW150914 observation by aLIGO allows us to place constraints on EdGB gravity from the absence of scalar dipolar radiation. As shown in Fig. 4, such an observation places a bound on the ppE parameter  $|\beta|$  at  $-1$ PN of  $|\beta| \leq 1.7 \times 10^{-4}$ . One can map this constraint to that on the coupling constant  $\alpha_{\text{EdGB}}$  using Eq. (19). Assuming the injected values of spins ( $\chi_1 = 0 = \chi_2$ ) and masses that we used to derive the bound on  $|\beta|$  via a Fisher analysis, one finds  $\sqrt{|\alpha_{\text{EdGB}}|} \leq 22\text{km}$ . However, to be as conservative as possible, one needs to study how such a bound depends on the injected values of binary parameters such as individual spins  $\chi_A$ , as the latter are only weakly constrained ( $|\chi_1| \leq 0.79$  and  $|\chi_2| \leq 0.94$  [83]), even when the effective spin parameter is better constrained  $\chi_{\text{eff}} = -0.06^{+0.17}_{-0.18}$  [65].

Figure 15 presents the upper bound on  $\sqrt{|\alpha_{\text{EdGB}}|}$  in km obtained by mapping the bound on  $|\beta|$  but varying  $\chi_1$  and  $\chi_2$  within their allowed range mentioned above. Observe that the bound weakens rapidly as one approaches spins that shut off dipole radiation completely (shown by white curves). These bounds are obtained within the small coupling approximation ( $16\pi\alpha_{\text{EdGB}}^2/r_{\text{H}}^4 \ll 1$  with

$r_{\text{H}}$  corresponding to the horizon size of the smaller BH), which is only valid within the region enclosed by horizontal yellow curves. In fact, the  $(\chi_1, \chi_2)$  region allowed by the aLIGO measurement of  $\chi_{\text{eff}}$  (within the orange dashed lines) contains values of the spin that are outside the regime of validity of the small coupling approximation. This then implies that GW150914 cannot place any meaningful constraints on EdGB gravity within such an approximation. The figure, however, also shows that if aLIGO were to detect GWs from a similar source in the future with a better mass and spin measurement with the secondary spin parameter determined to be  $|\chi_2| \lesssim 0.6$ , then one could indeed place a bound on EdGB dipole radiation of  $\sqrt{|\alpha_{\text{EdGB}}|} \lesssim 27\text{km}$ , as predicted in Eq. (32).

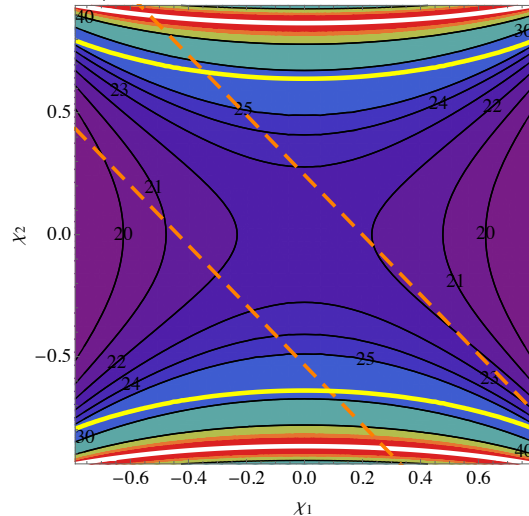


FIG. 15. (Color online) GW150914 upper bound on  $\sqrt{|\alpha_{\text{EdGB}}|}$  in km derived by mapping the constraint on  $\beta$  at  $-1$ PN order with each  $(\chi_1, \chi_2)$  allowed from the aLIGO measurement. Orange dashed lines show the allowed region from the effective spin  $\chi_{\text{eff}}$  measurement, while white curves show spins that shut off dipole radiation completely. However, note that the small coupling approximation used to derive these bounds is only valid within the region between the yellow curves.

- 
- [1] B. P. Abbott *et al.* (Virgo, LIGO Scientific), *Phys. Rev. Lett.* **116**, 061102 (2016), arXiv:1602.03837 [gr-qc].
  - [2] K. Popper, *The Logic of Scientific Discovery* (Mohr Siebeck, Germany, 1934).
  - [3] C. M. Will, *Living Reviews in Relativity* **9** (2006), arXiv:gr-qc/0510072.
  - [4] I. H. Stairs, *Living Rev. Rel.* **6**, 5 (2003), arXiv:astro-ph/0307536 [astro-ph].
  - [5] N. Wex, (2014), arXiv:1402.5594 [gr-qc].
  - [6] B. Jain and J. Khoury, *Annals Phys.* **325**, 1479 (2010), arXiv:1004.3294 [astro-ph.CO].
  - [7] T. Clifton, P. G. Ferreira, A. Padilla, and C. Skoldis, *Phys. Rept.* **513**, 1 (2012), arXiv:1106.2476 [astro-ph.CO].
  - [8] A. Joyce, B. Jain, J. Khoury, and M. Trodden, *Phys. Rept.* **568**, 1 (2015), arXiv:1407.0059 [astro-ph.CO].
  - [9] K. Koyama, *Rept. Prog. Phys.* **79**, 046902 (2016), arXiv:1504.04623 [astro-ph.CO].
  - [10] V. Salvatelli, F. Piazza, and C. Marinoni, (2016), arXiv:1602.08283 [astro-ph.CO].
  - [11] N. Yunes and X. Siemens, *Living Reviews in Relativity* **16** (2013), 10.12942/lrr-2013-9, arXiv:1304.3473 [gr-qc].
  - [12] B. P. Abbott *et al.* (Virgo, LIGO Scientific), (2016), arXiv:1602.03841 [gr-qc].

- [13] J. R. Gair, M. Vallisneri, S. L. Larson, and J. G. Baker, *Living Rev. Rel.* **16**, 7 (2013), arXiv:1212.5575 [gr-qc].
- [14] E. Berti *et al.*, *Class. Quant. Grav.* **32**, 243001 (2015), arXiv:1501.07274 [gr-qc].
- [15] K. Yagi and L. C. Stein, *Class. Quant. Grav.* **33**, 054001 (2016), arXiv:1602.02413 [gr-qc].
- [16] S. B. Giddings, (2016), arXiv:1602.03622 [gr-qc].
- [17] E. Barausse, C. Palenzuela, M. Ponce, and L. Lehner, *Phys.Rev.* **D87**, 081506 (2013), arXiv:1212.5053 [gr-qc].
- [18] C. Palenzuela, E. Barausse, M. Ponce, and L. Lehner, *Phys. Rev.* **D89**, 044024 (2014), arXiv:1310.4481 [gr-qc].
- [19] M. Shibata, K. Taniguchi, H. Okawa, and A. Buonanno, *Phys. Rev.* **D89**, 084005 (2014), arXiv:1310.0627 [gr-qc].
- [20] J. Healy, T. Bode, R. Haas, E. Pazos, P. Laguna, D. M. Shoemaker, and N. Yunes, *Class. Quant. Grav.* **29**, 232002 (2012), arXiv:1112.3928 [gr-qc].
- [21] E. Berti, V. Cardoso, L. Gualtieri, M. Horbatsch, and U. Sperhake, *Phys. Rev.* **D87**, 124020 (2013), arXiv:1304.2836 [gr-qc].
- [22] D. Psaltis, *Living Reviews in Relativity* **11** (2008), arXiv:0806.1531 [astro-ph].
- [23] C. Bambi, (2015), arXiv:1509.03884 [gr-qc].
- [24] T. Johannsen, (2015), arXiv:1512.03818 [astro-ph.GA].
- [25] T. Johannsen, (2016), arXiv:1602.07694 [astro-ph.HE].
- [26] S. Doleman, E. Agol, D. Backer, F. Baganoff, G. C. Bower, A. Broderick, A. Fabian, V. Fish, C. Gammie, P. Ho, M. Honman, T. Krichbaum, A. Loeb, D. Marrone, M. Reid, A. Rogers, I. Shapiro, P. Strittmatter, R. Tilanus, J. Weintroub, A. Whitney, M. Wright, and L. Ziurys, in *astro2010: The Astronomy and Astrophysics Decadal Survey*, Astronomy, Vol. 2010 (2009) arXiv:0906.3899 [astro-ph.CO].
- [27] E. Berti, V. Cardoso, and C. M. Will, *Phys. Rev. D* **73**, 064030 (2006), gr-qc/0512160.
- [28] E. Berti, J. Cardoso, V. Cardoso, and M. Cavaglia, *Phys. Rev.* **D76**, 104044 (2007), arXiv:0707.1202 [gr-qc].
- [29] M. Dafermos, G. Holzegel, and I. Rodnianski, (2016), arXiv:1601.06467 [gr-qc].
- [30] C. Chirenti and L. Rezzolla, (2016), arXiv:1602.08759 [gr-qc].
- [31] V. Cardoso, E. Franzin, and P. Pani, (2016), arXiv:1602.07309 [gr-qc].
- [32] L. Lehner, S. L. Liebling, C. Palenzuela, O. L. Caballero, E. O'Connor, M. Anderson, and D. Neilsen, (2016), arXiv:1603.00501 [gr-qc].
- [33] D. Radice, F. Galeazzi, J. Lippuner, L. F. Roberts, C. D. Ott, and L. Rezzolla, (2016), arXiv:1601.02426 [astro-ph.HE].
- [34] K. Hotokezaka, K. Kyutoku, Y.-i. Sekiguchi, and M. Shibata, (2016), arXiv:1603.01286 [gr-qc].
- [35] T. Dietrich, N. Moldenhauer, N. K. Johnson-McDaniel, S. Bernuzzi, C. M. Markakis, B. Bruggmann, and W. Tichy, *Phys. Rev.* **D92**, 124007 (2015), arXiv:1507.07100 [gr-qc].
- [36] F. Foucart, R. Haas, M. D. Duez, E. O'Connor, C. D. Ott, L. Roberts, L. E. Kidder, J. Lippuner, H. P. Pfeiffer, and M. A. Scheel, *Phys. Rev.* **D93**, 044019 (2016), arXiv:1510.06398 [astro-ph.HE].
- [37] W. E. East, V. Paschalidis, F. Pretorius, and S. L. Shapiro, *Phys. Rev.* **D93**, 024011 (2016), arXiv:1511.01093 [astro-ph.HE].
- [38] J. A. Clark, A. Bauswein, N. Stergioulas, and D. Shoemaker, *Class. Quant. Grav.* **33**, 085003 (2016), arXiv:1509.08522 [astro-ph.HE].
- [39] L. Amendola, C. Charmousis, and S. C. Davis, *JCAP* **0710**, 004 (2007), arXiv:0704.0175 [astro-ph].
- [40] P. Kanti, N. Mavromatos, J. Rizos, K. Tamvakis, and E. Winstanley, *Phys.Rev.* **D54**, 5049 (1996), arXiv:hep-th/9511071 [hep-th].
- [41] K. Yagi, *Phys.Rev.* **D86**, 081504 (2012), arXiv:1204.4524 [gr-qc].
- [42] P. Pani and V. Cardoso, *Phys.Rev.* **D79**, 084031 (2009), arXiv:0902.1569 [gr-qc].
- [43] M. W. Horbatsch and C. P. Burgess, *JCAP* **1205**, 010 (2012), arXiv:1111.4009 [gr-qc].
- [44] Y. Ali-Haïmoud and Y. Chen, *Phys.Rev.* **D84**, 124033 (2011), arXiv:1110.5329 [astro-ph.HE].
- [45] K. Yagi, N. Yunes, and T. Tanaka, *Phys.Rev.* **D86**, 044037 (2012), arXiv:1206.6130 [gr-qc].
- [46] K. Yagi, D. Blas, N. Yunes, and E. Barausse, *Phys. Rev. Lett.* **112**, 161101 (2014), arXiv:1307.6219 [gr-qc].
- [47] K. Yagi, D. Blas, E. Barausse, and N. Yunes, *Phys.Rev.* **D89**, 084067 (2014), arXiv:1311.7144 [gr-qc].
- [48] T. Johannsen, D. Psaltis, and J. E. McClintock, *Astrophys. J.* **691**, 997 (2009), arXiv:0803.1835 [astro-ph].
- [49] T. Johannsen, *Astron. and Astrophys.* **507**, 617 (2009), arXiv:0812.0809.
- [50] E. G. Adelberger, B. R. Heckel, S. A. Hoedl, C. D. Hoyle, D. J. Kapner, and A. Upadhye, *Phys. Rev. Lett.* **98**, 131104 (2007), arXiv:hep-ph/0611223 [hep-ph].
- [51] D. Psaltis, *Phys. Rev. Lett.* **98**, 181101 (2007), arXiv:astro-ph/0612611.
- [52] O. Y. Gnedin, T. J. Maccarone, D. Psaltis, and S. E. Zepf, *Astrophys. J.* **705**, L168 (2009), arXiv:0906.5351 [astro-ph.CO].
- [53] R. N. Manchester, *Int. J. Mod. Phys.* **D24**, 1530018 (2015), arXiv:1502.05474 [gr-qc].
- [54] A. S. Konopliv, S. W. Asmar, W. M. Folkner, Ö. Karatekin, D. C. Nunes, S. E. Smrekar, C. F. Yoder, and M. T. Zuber, *Icarus* **211**, 401 (2011).
- [55] F. Hofmann, J. Müller, and L. Biskupek, *Astron. and Astrophys.* **522**, L5 (2010).
- [56] C. J. Copi, A. N. Davis, and L. M. Krauss, *Phys. Rev. Lett.* **92**, 171301 (2004), arXiv:astro-ph/0311334 [astro-ph].
- [57] C. Bambi, M. Giannotti, and F. L. Villante, *Phys. Rev.* **D71**, 123524 (2005), arXiv:astro-ph/0503502 [astro-ph].
- [58] C. Talmadge, J. P. Berthias, R. W. Hellings, and E. M. Standish, *Phys. Rev. Lett.* **61**, 1159 (1988).
- [59] L. S. Finn and P. J. Sutton, *Phys. Rev.* **D65**, 044022 (2002), arXiv:gr-qc/0109049.
- [60] A. S. Goldhaber and M. M. Nieto, *Phys. Rev.* **D9**, 1119 (1974).
- [61] M. G. Hare, *Can. J. Phys.* **51**, 431 (1973).
- [62] R. Brito, V. Cardoso, and P. Pani, *Phys. Rev.* **D88**, 023514 (2013), arXiv:1304.6725 [gr-qc].
- [63] S. Kiyota and K. Yamamoto, *Phys. Rev.* **D92**, 104036 (2015), arXiv:1509.00610 [gr-qc].
- [64] D. Blas, M. M. Ivanov, I. Sawicki, and S. Sibiryakov, (2016), arXiv:1602.04188 [gr-qc].
- [65] B. P. Abbott *et al.* (Virgo, LIGO Scientific), (2016), arXiv:1602.03840 [gr-qc].
- [66] N. Yunes and F. Pretorius, *Phys.Rev.* **D80**, 122003 (2009), arXiv:0909.3328 [gr-qc].

- [67] P. Ajith *et al.*, *Phys. Rev. Lett.* **106**, 241101 (2011), [arXiv:0909.2867 \[gr-qc\]](#).
- [68] L. Santamaria *et al.*, *Phys. Rev.* **D82**, 064016 (2010), [arXiv:1005.3306 \[gr-qc\]](#).
- [69] S. Khan, S. Husa, M. Hannam, F. Ohme, M. Purrer, X. J. Forteza, and A. Bohe, *Phys. Rev.* **D93**, 044007 (2016), [*Phys. Rev.*D93,044007(2016)], [arXiv:1508.07253 \[gr-qc\]](#).
- [70] M. Fierz, *Helv. Phys. Acta* **29**, 128 (1956).
- [71] P. Jordan, *Z. Phys.* **157**, 112 (1959).
- [72] C. Brans and R. H. Dicke, *Phys. Rev.* **124**, 925 (1961).
- [73] C. M. Will and H. W. Zaglauer, *Astrophys. J.* **346**, 366 (1989).
- [74] N. Yunes, P. Pani, and V. Cardoso, *Phys. Rev.* **D85**, 102003 (2012), [arXiv:1112.3351 \[gr-qc\]](#).
- [75] S. Mirshekari and C. M. Will, *Phys. Rev.* **D87**, 084070 (2013), [arXiv:1301.4680 \[gr-qc\]](#).
- [76] L. Sampson, N. Cornish, and N. Yunes, *Phys. Rev.* **D89**, 064037 (2014), [arXiv:1311.4898 \[gr-qc\]](#).
- [77] S. A. Hughes and K. Menou, *Astrophys. J.* **623**, 689 (2005), [arXiv:astro-ph/0410148 \[astro-ph\]](#).
- [78] A. Buonanno, L. E. Kidder, and L. Lehner, *Phys. Rev.* **D77**, 026004 (2008), [arXiv:0709.3839 \[astro-ph\]](#).
- [79] D. Ayzenberg, K. Yagi, and N. Yunes, (2016), [arXiv:1601.06088 \[astro-ph.HE\]](#).
- [80] K. Glampedakis and S. Babak, *Class. Quant. Grav.* **23**, 4167 (2006), [arXiv:gr-qc/0510057](#).
- [81] C. A. R. Herdeiro and E. Radu, *Phys.Rev.Lett.* **112**, 221101 (2014), [arXiv:1403.2757 \[gr-qc\]](#).
- [82] C. Herdeiro, E. Radu, and H. Runarsson, (2016), [arXiv:1603.02687 \[gr-qc\]](#).
- [83] B. P. Abbott *et al.* (Virgo, LIGO Scientific), (2016), [arXiv:1602.03839 \[gr-qc\]](#).
- [84] V. Connaughton *et al.*, (2016), [arXiv:1602.03920 \[astro-ph.HE\]](#).
- [85] A. Nishizawa and T. Nakamura, *Phys. Rev.* **D90**, 044048 (2014), [arXiv:1406.5544 \[gr-qc\]](#).
- [86] J. Ellis, N. E. Mavromatos, and D. V. Nanopoulos, (2016), [arXiv:1602.04764 \[gr-qc\]](#).
- [87] X. Li, F.-W. Zhang, Q. Yuan, Z.-P. Jin, Y.-Z. Fan, S.-M. Liu, and D.-M. Wei, (2016), [arXiv:1602.04460 \[astro-ph.HE\]](#).
- [88] T. E. Collett and D. Bacon, (2016), [arXiv:1602.05882 \[astro-ph.HE\]](#).
- [89] T. Jacobson and D. Mattingly, *Phys.Rev.* **D64**, 024028 (2001), [arXiv:gr-qc/0007031 \[gr-qc\]](#).
- [90] T. Jacobson, *PoS QG-PH*, 020 (2007), [arXiv:0801.1547 \[gr-qc\]](#).
- [91] D. Blas, O. Pujolas, and S. Sibiryakov, *Phys.Rev.Lett.* **104**, 181302 (2010), [arXiv:0909.3525 \[hep-th\]](#).
- [92] D. Blas, O. Pujolas, and S. Sibiryakov, *JHEP* **1104**, 018 (2011), [arXiv:1007.3503 \[hep-th\]](#).
- [93] D. Hansen, N. Yunes, and K. Yagi, *Phys. Rev.* **D91**, 082003 (2015), [arXiv:1412.4132 \[gr-qc\]](#).
- [94] C. W. Misner, K. Thorne, and J. A. Wheeler, *Gravitation* (W. H. Freeman & Co., San Francisco, 1973).
- [95] <https://dcc.ligo.org/LIGO-T1600030/public>.
- [96] S. Husa, S. Khan, M. Hannam, M. Purrer, F. Ohme, X. J. Forteza, and A. Bohe, *Phys. Rev.* **D93**, 044006 (2016), [*Phys. Rev.*D93,044006(2016)], [arXiv:1508.07250 \[gr-qc\]](#).
- [97] L. Blanchet, *Living Rev. Rel.* **9**, 4 (2006).
- [98] T. Baker, D. Psaltis, and C. Skordis, *Astrophys. J.* **802**, 63 (2015), [arXiv:1412.3455 \[astro-ph.CO\]](#).
- [99] I. Ciufolini and E. C. Pavlis, *Nature* **431**, 958 (2004).
- [100] J. G. Williams, S. G. Turyshev, and D. H. Boggs, *Phys. Rev. Lett.* **93**, 261101 (2004), [arXiv:gr-qc/0411113 \[gr-qc\]](#).
- [101] G. Hobbs *et al.*, *Gravitational waves. Proceedings, 8th Edoardo Amaldi Conference, Amaldi 8, New York, USA, June 22-26, 2009, Class. Quant. Grav.* **27**, 084013 (2010), [arXiv:0911.5206 \[astro-ph.SR\]](#).
- [102] A. G. Lyne, M. Burgay, M. Kramer, A. Possenti, R. N. Manchester, F. Camilo, M. A. McLaughlin, D. R. Lorimer, N. D'Amico, B. C. Joshi, J. Reynolds, and P. C. C. Freire, *Science* **303**, 1153 (2004), [arXiv:astro-ph/0401086](#).
- [103] P. Schmidt, M. Hannam, and S. Husa, *Phys. Rev.* **D86**, 104063 (2012), [arXiv:1207.3088 \[gr-qc\]](#).
- [104] L. Sampson, N. Cornish, and N. Yunes, *Phys. Rev.* **D87**, 102001 (2013), [arXiv:1303.1185 \[gr-qc\]](#).
- [105] P. Ajith *et al.*, *Phys. Rev.* **D77**, 104017 (2008), [Erratum: *Phys. Rev.*D79,129901(2009)], [arXiv:0710.2335 \[gr-qc\]](#).
- [106] S. Alexander, L. S. Finn, and N. Yunes, *Phys. Rev.* **D78**, 066005 (2008), [arXiv:0712.2542 \[gr-qc\]](#).
- [107] N. Yunes, F. Pretorius, and D. Spergel, *Phys. Rev.* **D81**, 064018 (2010), [arXiv:0912.2724 \[gr-qc\]](#).
- [108] N. Yunes, R. O'Shaughnessy, B. J. Owen, and S. Alexander, *Phys.Rev.* **D82**, 064017 (2010), [arXiv:1005.3310 \[gr-qc\]](#).
- [109] N. Cornish, L. Sampson, N. Yunes, and F. Pretorius, *Phys.Rev.* **D84**, 062003 (2011), [arXiv:1105.2088 \[gr-qc\]](#).
- [110] K. Yagi, L. C. Stein, N. Yunes, and T. Tanaka, *Phys.Rev.* **D85**, 064022 (2012), [arXiv:1110.5950 \[gr-qc\]](#).
- [111] K. Yagi, N. Tanahashi, and T. Tanaka, *Phys. Rev.* **D83**, 084036 (2011), [arXiv:1101.4997 \[gr-qc\]](#).
- [112] N. Yunes and L. C. Stein, *Phys. Rev.* **D83**, 104002 (2011), [arXiv:1101.2921 \[gr-qc\]](#).
- [113] S. Vigeland, N. Yunes, and L. Stein, *Phys. Rev.* **D83**, 104027 (2011), [arXiv:1102.3706 \[gr-qc\]](#).
- [114] K. Chatziioannou, N. Yunes, and N. Cornish, *Phys.Rev.* **D86**, 022004 (2012), [arXiv:1204.2585 \[gr-qc\]](#).
- [115] S. Mirshekari, N. Yunes, and C. M. Will, *Phys.Rev.* **D85**, 024041 (2012), [arXiv:1110.2720 \[gr-qc\]](#).
- [116] K. Yagi, N. Yunes, and T. Tanaka, *Phys.Rev.Lett.* **109**, 251105 (2012), [arXiv:1208.5102 \[gr-qc\]](#).
- [117] L. Sampson, N. Yunes, and N. Cornish, *Phys. Rev.* **D88**, 064056 (2013), [Erratum: *Phys. Rev.*D88,no.8,089902(2013)], [arXiv:1307.8144 \[gr-qc\]](#).
- [118] L. Sampson, N. Yunes, N. Cornish, M. Ponce, E. Barausse, A. Klein, C. Palenzuela, and L. Lehner, *Phys. Rev.* **D90**, 124091 (2014), [arXiv:1407.7038 \[gr-qc\]](#).
- [119] K. Yagi, L. C. Stein, and N. Yunes, *Phys. Rev.* **D93**, 024010 (2016), [arXiv:1510.02152 \[gr-qc\]](#).
- [120] R. R. Metsaev and A. A. Tseytlin, *Nucl. Phys.* **B293**, 385 (1987).
- [121] K.-i. Maeda, N. Ohta, and Y. Sasagawa, *Phys. Rev.* **D80**, 104032 (2009), [arXiv:0908.4151 \[hep-th\]](#).
- [122] T. Jacobson, *Phys. Rev. Lett.* **83**, 2699 (1999), [arXiv:astro-ph/9905303 \[astro-ph\]](#).
- [123] L. Randall and R. Sundrum, *Phys. Rev. Lett.* **83**, 3370 (1999), [arXiv:hep-ph/9905221 \[hep-ph\]](#).
- [124] L. Randall and R. Sundrum, *Phys. Rev. Lett.* **83**, 4690 (1999), [arXiv:hep-th/9906064 \[hep-th\]](#).
- [125] P. A. M. Dirac, *Nature (London)* **139**, 323 (1937).
- [126] S. Alexander and N. Yunes, *Phys. Rept.* **480**, 1 (2009),

- arXiv:0907.2562 [hep-th].
- [127] C. M. Will, *Phys. Rev.* **D57**, 2061 (1998), arXiv:gr-qc/9709011 [gr-qc].
- [128] V. A. Rubakov and P. G. Tinyakov, *Phys. Usp.* **51**, 759 (2008), arXiv:0802.4379 [hep-th].
- [129] K. Hinterbichler, *Rev. Mod. Phys.* **84**, 671 (2012), arXiv:1105.3735 [hep-th].
- [130] C. de Rham, *Living Rev. Rel.* **17**, 7 (2014), arXiv:1401.4173 [hep-th].
- [131] G. Amelino-Camelia, *Phys. Lett.* **B510**, 255 (2001), arXiv:hep-th/0012238 [hep-th].
- [132] J. Magueijo and L. Smolin, *Phys. Rev. Lett.* **88**, 190403 (2002), arXiv:hep-th/0112090 [hep-th].
- [133] G. Amelino-Camelia, *Nature* **418**, 34 (2002), arXiv:gr-qc/0207049 [gr-qc].
- [134] G. Amelino-Camelia, *Symmetry* **2**, 230 (2010), arXiv:1003.3942 [gr-qc].
- [135] A. S. Sefiedgar, K. Nozari, and H. R. Sepangi, *Phys. Lett.* **B696**, 119 (2011), arXiv:1012.1406 [gr-qc].
- [136] P. Horava, *JHEP* **03**, 020 (2009), arXiv:0812.4287 [hep-th].
- [137] P. Horava, *Phys.Rev.* **D79**, 084008 (2009), arXiv:0901.3775 [hep-th].
- [138] S. I. Vacaru, *Gen. Rel. Grav.* **44**, 1015 (2012), arXiv:1010.5457 [math-ph].
- [139] E. Barausse, L. C. Stein, and K. Yagi, (in preparation).
- [140] M. Bojowald and G. M. Hossain, *Phys. Rev. D* **77**, 023508 (2008), arXiv:0709.2365 [gr-qc].
- [141] P. R. Chouha and R. H. Brandenberger, (2005), arXiv:hep-th/0508119.
- [142] R. J. Szabo, *General Relativity and Gravitation* **42**, 1 (2010), arXiv:0906.2913 [hep-th].
- [143] C. M. Caves, *Annals Phys.* **125**, 35 (1980).
- [144] G. D. Moore and A. E. Nelson, *JHEP* **09**, 023 (2001), arXiv:hep-ph/0106220 [hep-ph].
- [145] D. Blas and H. Sanctuary, *Phys.Rev.* **D84**, 064004 (2011), arXiv:1105.5149 [gr-qc].
- [146] A. Kostelecky and M. Mewes, (2016), arXiv:1602.04782 [gr-qc].
- [147] J. Collins, A. Perez, D. Sudarsky, L. Urrutia, and H. Vucetich, *Physical Review Letters* **93**, 191301 (2004), arXiv:gr-qc/0403053.
- [148] J. Collins, A. Perez, and D. Sudarsky, (2006), arXiv:hep-th/0603002.
- [149] R. Gambini, S. Rastgoo, and J. Pullin, *Class. Quant. Grav.* **28**, 155005 (2011), arXiv:1106.1417 [gr-qc].
- [150] C. Cutler and É. E. Flanagan, *Phys. Rev. D* **49**, 2658 (1994), arXiv:gr-qc/9402014.
- [151] E. Poisson and C. M. Will, *Phys. Rev.* **D52**, 848 (1995), arXiv:gr-qc/9502040 [gr-qc].
- [152] E. Berti, A. Buonanno, and C. M. Will, *Phys. Rev.* **D71**, 084025 (2005), arXiv:gr-qc/0411129.
- [153] M. Banados and P. G. Ferreira, *Phys. Rev. Lett.* **105**, 011101 (2010), [Erratum: *Phys. Rev. Lett.*113,no.11,119901(2014)], arXiv:1006.1769 [astro-ph.CO].
- [154] E. Barausse, T. P. Sotiriou, and J. C. Miller, *Class. Quant. Grav.* **25**, 062001 (2008), arXiv:gr-qc/0703132 [GR-QC].
- [155] E. Barausse, T. P. Sotiriou, and J. C. Miller, *Class. Quant. Grav.* **25**, 105008 (2008), arXiv:0712.1141 [gr-qc].
- [156] P. Pani, T. P. Sotiriou, and D. Vernieri, *Phys. Rev.* **D88**, 121502 (2013), arXiv:1306.1835 [gr-qc].
- [157] T. Damour and G. Esposito-Farese, *Classical and Quantum Gravity* **9**, 2093 (1992).
- [158] T. Damour and G. Esposito-Farese, *Phys. Rev. Lett.* **70**, 2220 (1993).
- [159] T. P. Sotiriou and V. Faraoni, *Rev. Mod. Phys.* **82**, 451 (2010), arXiv:0805.1726 [gr-qc].
- [160] E. Barausse, T. Jacobson, and T. P. Sotiriou, *Phys.Rev.* **D83**, 124043 (2011), arXiv:1104.2889 [gr-qc].
- [161] E. Barausse and T. P. Sotiriou, *Class. Quant. Grav.* **30**, 244010 (2013), arXiv:1307.3359 [gr-qc].
- [162] E. Barausse and T. P. Sotiriou, *Phys.Rev.Lett.* **109**, 181101 (2012), erratum-ibid. **110**, 039902 (2013), arXiv:1207.6370 [gr-qc].
- [163] E. Barausse and T. P. Sotiriou, *Phys.Rev.* **D87**, 087504 (2013), arXiv:1212.1334 [gr-qc].
- [164] E. Barausse, T. P. Sotiriou, and I. Vega, *Phys. Rev.* **D93**, 044044 (2016), arXiv:1512.05894 [gr-qc].
- [165] R. Brito, V. Cardoso, and P. Pani, *Phys. Rev.* **D88**, 064006 (2013), arXiv:1309.0818 [gr-qc].
- [166] E. Babichev and R. Brito, *Class. Quant. Grav.* **32**, 154001 (2015), arXiv:1503.07529 [gr-qc].
- [167] R. P. Woodard, *Lect. Notes Phys.* **720**, 403 (2007), arXiv:astro-ph/0601672.
- [168] T. Delsate, D. Hilditch, and H. Witek, *Phys. Rev.* **D91**, 024027 (2015), arXiv:1407.6727 [gr-qc].
- [169] R. Jackiw and S. Y. Pi, *Phys. Rev.* **D68**, 104012 (2003), arXiv:gr-qc/0308071.
- [170] E. Barausse, N. Yunes, and K. Chamberlain, (2016), arXiv:1603.04075 [gr-qc].
- [171] P. Pani, E. Berti, V. Cardoso, and J. Read, (2011), \* Temporary entry \*, arXiv:1109.0928 [gr-qc].
- [172] T. Johannsen, D. Psaltis, and J. E. McClintock, *Astrophys. J.* **691**, 997 (2009), arXiv:0803.1835 [astro-ph].
- [173] N. Yunes and S. A. Hughes, *Phys. Rev.* **D82**, 082002 (2010), arXiv:1007.1995 [gr-qc].
- [174] L. S. Finn and D. F. Chernoff, *Phys. Rev.* **D47**, 2198 (1993), arXiv:gr-qc/9301003 [gr-qc].
- [175] D. F. Chernoff and L. S. Finn, *Astrophys. J.* **411**, L5 (1993), arXiv:gr-qc/9304020 [gr-qc].
- [176] M. Vallisneri, *Phys. Rev.* **D77**, 042001 (2008), arXiv:gr-qc/0703086 [GR-QC].
- [177] P. Pani, V. Cardoso, and L. Gualtieri, *Phys. Rev.* **D83**, 104048 (2011), arXiv:1104.1183 [gr-qc].
- [178] R. Emparan, A. Fabbri, and N. Kaloper, *JHEP* **08**, 043 (2002), arXiv:hep-th/0206155.
- [179] T. Tanaka, *Prog. Theor. Phys. Suppl.* **148**, 307 (2003), arXiv:gr-qc/0203082.
- [180] E. E. Flanagan and T. Hinderer, *Phys.Rev.* **D77**, 021502 (2008), arXiv:0709.1915 [astro-ph].
- [181] M. Vallisneri and N. Yunes, *Phys. Rev.* **D87**, 102002 (2013), arXiv:1301.2627 [gr-qc].
- [182] K. Taniguchi, M. Shibata, and A. Buonanno, *Phys. Rev.* **D91**, 024033 (2015), arXiv:1410.0738 [gr-qc].
- [183] N. Sennett and A. Buonanno, (2016), arXiv:1603.03300 [gr-qc].
- [184] V. Cardoso, S. Chakrabarti, P. Pani, E. Berti, and L. Gualtieri, *Phys. Rev. Lett.* **107**, 241101 (2011), arXiv:1109.6021 [gr-qc].
- [185] J. Alsing, E. Berti, C. M. Will, and H. Zaglauer, *Phys. Rev.* **D85**, 064041 (2012), arXiv:1112.4903 [gr-qc].
- [186] E. Berti, L. Gualtieri, M. Horbatsch, and J. Alsing, *Phys. Rev.* **D85**, 122005 (2012), arXiv:1204.4340 [gr-qc].

- [187] C. M. O’Neill, *Phys. Rev.* **D50**, 865 (1994), [arXiv:hep-th/9311022 \[hep-th\]](#).
- [188] C. Herdeiro and E. Radu, *Class. Quant. Grav.* **32**, 144001 (2015), [arXiv:1501.04319 \[gr-qc\]](#).
- [189] C. A. R. Herdeiro, E. Radu, and H. Runarsson, *Phys. Rev.* **D92**, 084059 (2015), [arXiv:1509.02923 \[gr-qc\]](#).
- [190] C. A. R. Herdeiro and E. Radu, *Proceedings, 7th Black Holes Workshop 2014*, *Int. J. Mod. Phys.* **D24**, 1542014 (2015), [arXiv:1504.08209 \[gr-qc\]](#).
- [191] B. Kleihaus, J. Kunz, and S. Yazadjiev, *Phys. Lett.* **B744**, 406 (2015), [arXiv:1503.01672 \[gr-qc\]](#).
- [192] X.-F. Wu, H. Gao, J.-J. Wei, X.-L. Fan, P. Meszaros, B. Zhang, Z.-G. Dai, S.-N. Zhang, and Z.-H. Zhu, (2016), [arXiv:1602.01566 \[astro-ph.HE\]](#).
- [193] E. O. Kahya and S. Desai, (2016), [arXiv:1602.04779 \[gr-qc\]](#).
- [194] P. Bicudo, (2016), [arXiv:1602.04337 \[gr-qc\]](#).
- [195] M. Fierz and W. Pauli, *Proc. Roy. Soc. Lond.* **A173**, 211 (1939).
- [196] V. A. Rubakov, (2004), [arXiv:hep-th/0407104 \[hep-th\]](#).
- [197] S. L. Dubovsky, *JHEP* **10**, 076 (2004), [arXiv:hep-th/0409124 \[hep-th\]](#).
- [198] D. G. Boulware and S. Deser, *Phys. Rev.* **D6**, 3368 (1972).
- [199] P. Creminelli, A. Nicolis, M. Papucci, and E. Trincherini, *JHEP* **09**, 003 (2005), [arXiv:hep-th/0505147 \[hep-th\]](#).
- [200] D. Blas and S. Sibiryakov, *Zh. Eksp. Teor. Fiz.* **147**, 578 (2015), [*J. Exp. Theor. Phys.*120,no.3,509(2015)], [arXiv:1410.2408 \[hep-th\]](#).
- [201] S. F. Hassan and R. A. Rosen, *JHEP* **02**, 126 (2012), [arXiv:1109.3515 \[hep-th\]](#).
- [202] A. De Felice, T. Nakamura, and T. Tanaka, *PTEP* **2014**, 043E01 (2014), [arXiv:1304.3920 \[gr-qc\]](#).
- [203] T. Narikawa, K. Ueno, H. Tagoshi, T. Tanaka, N. Kanda, and T. Nakamura, *Phys. Rev.* **D91**, 062007 (2015), [arXiv:1412.8074 \[gr-qc\]](#).
- [204] V. A. Kostelecky and J. D. Tasson, *Phys. Lett.* **B749**, 551 (2015), [arXiv:1508.07007 \[gr-qc\]](#).
- [205] R. Konoplya and A. Zhidenko, (2016), [arXiv:1602.04738 \[gr-qc\]](#).
- [206] V. Cardoso, P. Pani, M. Cadoni, and M. Cavaglia, *Phys. Rev.* **D77**, 124044 (2008), [arXiv:0709.0532 \[gr-qc\]](#).
- [207] P. Pani, E. Barausse, E. Berti, and V. Cardoso, *Phys. Rev.* **D82**, 044009 (2010), [arXiv:1006.1863 \[gr-qc\]](#).
- [208] E. Barausse, V. Cardoso, and P. Pani, *Phys. Rev.* **D89**, 104059 (2014), [arXiv:1404.7149 \[gr-qc\]](#).
- [209] V. Cardoso, L. C. Crispino, C. F. Macedo, H. Okawa, and P. Pani, *Phys. Rev.* **D90**, 044069 (2014), [arXiv:1406.5510 \[gr-qc\]](#).
- [210] K. S. Thorne, R. H. Price, and D. A. MacDonald, *Black Holes: The Membrane Paradigm* (Yale University Press, 1986).
- [211] J. Healy, C. O. Lousto, and Y. Zlochower, *Phys. Rev.* **D90**, 104004 (2014), [arXiv:1406.7295 \[gr-qc\]](#).
- [212] E. Barausse and L. Rezzolla, *Astrophys. J.* **704**, L40 (2009), [arXiv:0904.2577 \[gr-qc\]](#).
- [213] H. Nakano, T. Tanaka, and T. Nakamura, *Phys. Rev.* **D92**, 064003 (2015), [arXiv:1506.00560 \[astro-ph.HE\]](#).
- [214] A. Ghosh *et al.*, (2016), [arXiv:1602.02453 \[gr-qc\]](#).
- [215] V. S. Manko and I. D. Novikov, *Classical and Quantum Gravity* **9**, 2477 (1992).
- [216] N. A. Collins and S. A. Hughes, *Phys. Rev.* **D69**, 124022 (2004), [arXiv:gr-qc/0402063](#).
- [217] S. J. Vigeland and S. A. Hughes, *Phys. Rev.* **D81**, 024030 (2010), [arXiv:0911.1756 \[gr-qc\]](#).
- [218] S. J. Vigeland, *Phys. Rev.* **D82**, 104041 (2010), [arXiv:1008.1278 \[gr-qc\]](#).
- [219] T. Johannsen and D. Psaltis, *Phys. Rev.* **D83**, 124015 (2011), [arXiv:1105.3191 \[gr-qc\]](#).
- [220] T. Johannsen, *Phys. Rev.* **D87**, 124017 (2013), [arXiv:1304.7786 \[gr-qc\]](#).
- [221] V. Cardoso, P. Pani, and J. Rico, *Phys. Rev.* **D89**, 064007 (2014), [arXiv:1401.0528 \[gr-qc\]](#).
- [222] L. Rezzolla and A. Zhidenko, *Phys. Rev.* **D90**, 084009 (2014), [arXiv:1407.3086 \[gr-qc\]](#).
- [223] T. Johannsen, *Phys. Rev.* **D88**, 044002 (2013), [arXiv:1501.02809 \[gr-qc\]](#).
- [224] N. Lin, N. Tsukamoto, M. Ghasemi-Nodehi, and C. Bambi, *Eur. Phys. J.* **C75**, 599 (2015), [arXiv:1512.00724 \[gr-qc\]](#).
- [225] R. Konoplya, L. Rezzolla, and A. Zhidenko, (2016), [arXiv:1602.02378 \[gr-qc\]](#).
- [226] C. Cutler and L. Lindblom, *Astrophys. J.* **314**, 234 (1987).
- [227] S. W. Hawking and J. B. Hartle, *Commun. Math. Phys.* **27**, 283 (1972).
- [228] J. B. Hartle, *Phys. Rev.* **D8**, 1010 (1973).
- [229] K. Glampedakis, S. J. Kapadia, and D. Kennefick, *Phys. Rev.* **D89**, 024007 (2014), [arXiv:1312.1912 \[gr-qc\]](#).
- [230] E.ourgoulhon and J. L. Jaramillo, *New Astron. Rev.* **51**, 791 (2008), [arXiv:0803.2944 \[astro-ph\]](#).
- [231] E. Flowers and N. Itoh, *Astrophys. J.* **230**, 847 (1979).
- [232] R. F. Sawyer, *Phys. Rev. D* **39**, 3804 (1989).
- [233] C. Cutler, L. Lindblom, and R. J. Splinter, *Astrophys. J.* **363**, 603 (1990).
- [234] E. E. Kolomeitsev and D. N. Voskresensky, *Phys. Rev.* **C91**, 025805 (2015), [arXiv:1412.0314 \[nucl-th\]](#).
- [235] S. L. Shapiro, *Astrophys. J.* **544**, 397 (2000), [arXiv:astro-ph/0010493 \[astro-ph\]](#).
- [236] K. Kiuchi, P. Cerda-Duran, K. Kyutoku, Y. Sekiguchi, and M. Shibata, *Phys. Rev.* **D92**, 124034 (2015), [arXiv:1509.09205 \[astro-ph.HE\]](#).
- [237] S. L. Liebling and C. Palenzuela, *Living Rev. Rel.* **15**, 6 (2012), [arXiv:1202.5809 \[gr-qc\]](#).
- [238] E. Berti and V. Cardoso, *Int. J. Mod. Phys.* **D15**, 2209 (2006), [arXiv:gr-qc/0605101 \[gr-qc\]](#).
- [239] C. F. B. Macedo, P. Pani, V. Cardoso, and L. C. B. Crispino, *Phys. Rev.* **D88**, 064046 (2013), [arXiv:1307.4812 \[gr-qc\]](#).
- [240] R. Friedberg, T. D. Lee, and Y. Pang, *Phys. Rev.* **D35**, 3658 (1987), [73(1986)].
- [241] M. A. Abramowicz, M. Bruni, S. Sonogo, N. Andersson, and P. Ghosh, *Class. Quant. Grav.* **14**, L189 (1997).
- [242] Z. Bagoly, D. Szecsi, L. G. Balazs, I. Csabai, I. Horvath, L. Dobos, J. Lichtenberger, and L. V. Toth, (2016), [arXiv:1603.06611 \[astro-ph.HE\]](#).
- [243] B. P. Abbott *et al.* (Intermediate Palomar Transient Factory (iPTF), InterPlanetary Network, INTEGRAL, Australian Square Kilometer Array Pathfinder (ASKAP), MWA, Fermi-LAT, J-GEM, La Silla-QUEST Survey, Pi of the Sky, Fermi GBM, MASTER, Dark Energy Survey, Swift, Dark Energy Camera, VISTA, SkyMapper, PESSTO, TOROS, Pan-STARRS, Virgo, GRAvitational Wave Inaf TeAm (GRAWITA), Liverpool Telescope, BOOTES, LIGO Scientific, LOFAR, C2PU, MAXI), (2016), [arXiv:1602.08492 \[astro-](#)

- ph.HE].
- [244] M. Ackermann *et al.* (Fermi-LAT), (2016), [arXiv:1602.04488 \[astro-ph.HE\]](#).
- [245] P. A. Evans *et al.* (Swift), (2016), [arXiv:1602.03868 \[astro-ph.HE\]](#).
- [246] S. Adrian-Martinez *et al.* (Virgo, IceCube, ANTARES, LIGO Scientific), (2016), [arXiv:1602.05411 \[astro-ph.HE\]](#).
- [247] A. Loeb, (2016), [arXiv:1602.04735 \[astro-ph.HE\]](#).
- [248] T. Bode, R. Haas, T. Bogdanovic, P. Laguna, and D. Shoemaker, *Astrophys. J.* **715**, 1117 (2010), [arXiv:0912.0087 \[gr-qc\]](#).
- [249] T. Bogdanovic, T. Bode, R. Haas, P. Laguna, and D. Shoemaker, *Laser interferometer space antenna. Proceedings, 8th International LISA Symposium, Stanford, USA, June 28-July 2, 2010*, *Class. Quant. Grav.* **28**, 094020 (2011), [arXiv:1010.2496 \[astro-ph.CO\]](#).
- [250] B. Zhang and P. Meszaros, *Int. J. Mod. Phys. A* **19**, 2385 (2004), [arXiv:astro-ph/0311321 \[astro-ph\]](#).
- [251] S. Capozziello, M. De Laurentis, I. De Martino, and M. Formisano, *Astrophys. Space Sci.* **332**, 31 (2011), [arXiv:1004.4818 \[astro-ph.CO\]](#).
- [252] C. Eling, T. Jacobson, and D. Mattingly, (2004), [gr-qc/0410001](#).
- [253] D. Blas, O. Pujolas, and S. Sibiryakov, *JHEP* **0910**, 029 (2009), [arXiv:0906.3046 \[hep-th\]](#).
- [254] N. Yunes and L. S. Finn, *Laser Interferometer Space Antenna. Proceedings, 7th international LISA Symposium, Barcelona, Spain, June 16-20, 2008*, *J. Phys. Conf. Ser.* **154**, 012041 (2009), [arXiv:0811.0181 \[gr-qc\]](#).
- [255] A. Sesana, (2016), [arXiv:1602.06951 \[gr-qc\]](#).
- [256] E. Berti, J. Gair, and A. Sesana, *Phys. Rev.* **D84**, 101501 (2011), [arXiv:1107.3528 \[gr-qc\]](#).
- [257] B. P. Abbott *et al.* (Virgo, LIGO Scientific), (2016), [arXiv:1602.03842 \[astro-ph.HE\]](#).